The Use of Microseismic Monitoring as a Guide for Gas Production

Rizgar Rassul Maolod

Submitted in accordance with the requirements for the degree of Doctor of Philosophy

The University of Leeds

School of Civil Engineering

September 2016

The candidate confirms that the work submitted is his own, and that appropriate credit has been given within the thesis where reference has been made to the work of others.

Acknowledgment

The author is grateful to the following for their contributions towards the completion of this work: my principal supervisor Dr Yong Sheng for his great support, advice and ideas, my co-supervisor Dr Dongmin Yang for his assistance and help. Furthermore, I would like to thank Dr. Yaser Ismael, Dr. Kenneth Ishiet, Dr. Tariq, my wife and my mother for their guidance and moral support.

Abstract

Numerical modelling makes it possible to consider studying microseismic events resulted from hydraulic fracturing through a synthetic model, too give us rational understandings for generation of the events and the efficiency of the fracturing process itself.

The research presented in this thesis uses Discrete Element Method (DEM) approach to simulate the acoustic emissions within rock samples in order to achieve the computational modelling of the micro seismic events during hydraulic fracturing process. In terms of its relation to the fracture properties and its uses in determining the successfulness of the fracturing operation. (DEM), is used in three dimensions to create model to simulate the acoustic emission from a rock sample under stress and from an injection tests on two rock sample too.

The model modifies a method that was originally developed before. The developed model was validated by comparing with the results from an experiment on Springwell sandstone under a triaxial stresses. In addition, comparison with two injection tests was performed. The program is further improved using a novel changing combination factor of event to enhance the modelling results, and to expand the application of the microseismic monitoring.

The developed model offers control on the number of seismic events and the statistical distribution of the events. In addition, the source of the event predictions were similar to the real one which can lead to realistic prediction

regarding the type of fracture. Furthermore, it was possible to extend the program application to predict the pore collapse sources of the acoustic emissions and the aperture of the resulted fractures. In addition, the model can predict the aperture of the fractures and the expected permeability of the fractured model. The validated model could therefore help to assess the effectiveness of a hydraulic fracturing project.

Contents

List of figures

List of tables

Nomenclature

Abbreviation	Description
AE	Acoustic emissions
b_value	Slope of straight part of the Gutenberg-Richter
α	Damping value
a	The aperture of the pipe
αp	Is proportionality coefficients 0.125
com_fac	Combination factor
DEM	Discrete Element Method
E_c^-	Parallel-bond young modulus
f	The contact force
h	Sample height
h_f	Height of the cloud
k	Permeability
K_f	The bulk density of water
K_{inv}	The in-situ permeability calculated by inversion method
k_n/k_s	Particle stiffness ratio
k_n^-/k_s^-	Parallel-bond stiffness ratio
Len	The length of the fracture
m^2	Square metre
Mag	Magnitude of the seismic event
mm	Millimetre
md	Millidarcies
md_ravg	Average particle radius
n	Number of pipes connected to the domain
P	The density
p_e	External pressure in *Ps*
p_b	Particles or ball density
PFC	Particle flow code by Itasca
P-wave	Compressional waves
Q	The attenuation
Qr	The injection rate
Ra	Ruptured area in the fracture in km square.

r	Minimum particle radius
Re	External radius
R_j	Is the jth component of the distance between the contact point and the event centroid
S-wave	Shear waves
s	The surface enclosing the event.
S_f	Is the safety factor
$\bar{t_c}$	Particles bond shear strength Mean and Standard deviation
U	The constant of displacement
UCS	Uniaxial compression strength
u	Viscosity
μ	Particle friction coefficient
V_p	Pore volume.
V_d	The domain volume
P_r	Bulk density of the reservoir rock.
α_{us}	Relation between the seismic cloud dimensions
$\bar{\gamma}$	Parallel-bond radius multiplier
$\bar{\sigma_c}$	Particle bond tensile strength Mean and standard deviation
W	Peak strain energy during the cycle
	Parallel-bond radius multiplier
φ	Porosity, fraction.
Δf_i	is the ith component of the change in contact force
ΔW	Dissipated energy in one wavelength
Δp	The pressure of the injected fluids
s	The surface enclosing the event.
$\sum_{Nt} i$	Is the summation of all the pipe radiuses in the sample.
$\sum_{\mathrm{b}} \mathrm{R}^2$	The square of the radius of the balls in the model
$\sum_{\mathrm{p}} \mathrm{La}^3$	Cubic summation of the length of the pipes

Chapter 1 Introduction

1.1 Introduction

It is clear to the observer that the conventional hydrocarbon will be depleted. Global oil suppliers across the entire world, except countries in the Middle East, will reach the peak of their production within 20-30 years, as is clear from the figure below Figure 1-1. In addition, even the Middle Eastern countries have limited production and ability to satisfy the global thirst of oil. It is clear that these so-called conventional oil and gas reservoirs will be depleted in future.

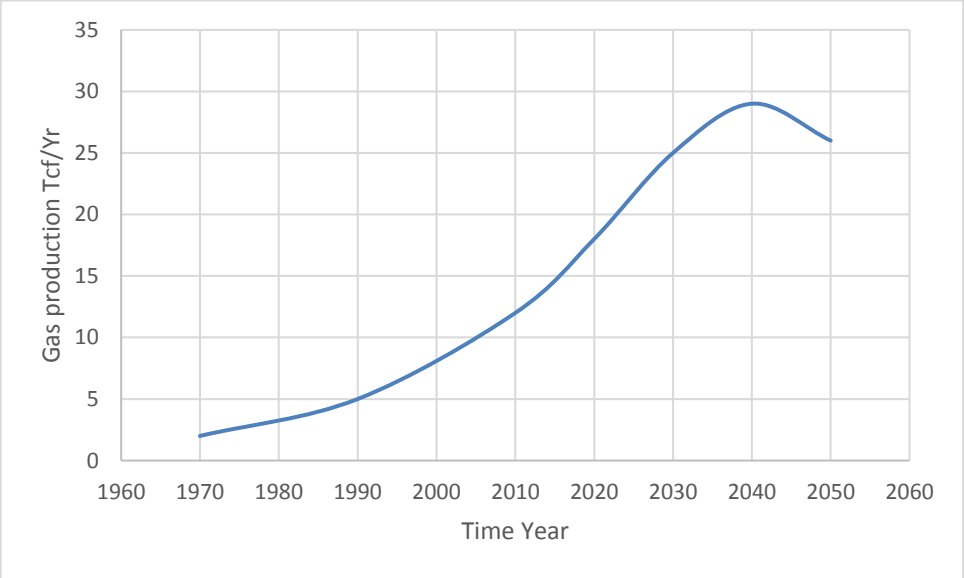

Figure 1-1 The Middle Eastern region's natural gas production model (Al-Fattah and Startzman, 2000)

Any way since there are new sources of energy that is called unconventional resources. The production rate of these unconventional resources has been increased dramatically as explained in Figure (1-2). Which shows the production of unconventional gas and oil is extending and the world does need to develop

these new resources, which are in great demand (Holditch and Madani, 2010). It is very important to add that, besides being a cheap source of energy, they cause less air pollution and are widely available (Holditch and Madani, 2010).

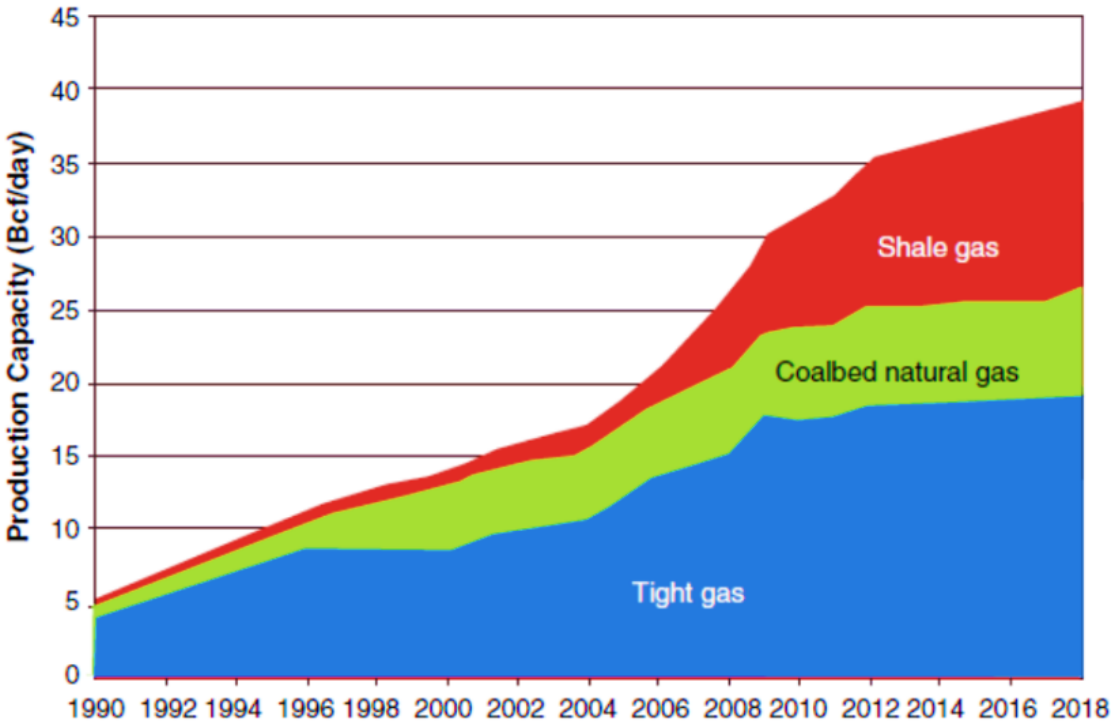

Figure 1-2 Forecast of shale growth in meeting energy demand. (Holditch and Madani, 2010)

Although some observers have their doubts about these unconventional gas reservoirs. The fact that these unconventional resources are economically available and less polluting means that they cannot be ignored. Anyway, in order to meet the global demand for oil and gas for the time being, it is clear that gas and oil are needed from unconventional resources, at least for the time being and in the near future too. Additionally, this means that more studies and more instruments are needed to find an effective way to improve and accelerate gas recovery from tight reservoirs via hydraulic fracturing stimulation.

Furthermore, the method that can increase production from the unconventional reservoirs is hydraulic fracturing (Li et al., 2015; Tiab and Donaldson, 2004). It can also improve the permeability of unconventional reservoirs, as proved by Wang et al. (2014b) during a study that included modelling the effect of fracturing on gas production from coal seams in west Henan, China. They concluded that water injection can extend the damage of the crack and improve the efficiency by about 100 times. In addition, increasing the life of the wells and increasing the production too (Bazan et al., 2012; Biglarbigi et al., 2007). But the hydraulic fracturing is linked with certain phenomena, such as pollution and induced microseismicity, that might cause small earthquake hazards (Busetti et al., 2014; Rutqvist et al., 2013).

In order to achieve more production in a more efficient way and predict the potential of the associated seismicity, there is a need to create models that have the capability to predict the future effects of hydraulic fracturing on the reservoir's associated phenomena, such as earthquake hazards and success of the fracturing operations. Moreover, the only way to predict such phenomena is by modelling the fracturing operations and the resulted microseismicity from the fracturing operations. This will help in the field of monitoring and production estimates, plus their use in the field of earthquake hazard prediction. Moreover, microseismic models could be used to study the relationship between microseismicity and the fracturing process, with its components like injection pressure (Raziperchikolaee et al., 2014; Zhang and Bian, 2015; Zhao, 2010). It is possible to use accurate models to develop a more useful relationship between microseismic events and reservoir characteristics or fracture properties. That

could be used to develop our understanding of the relationship between microseismicity and hydraulic fracturing efficiency, which will increase production efficiency.

1.2 Rock properties

There are some rock properties that control the fluid movement and the amount of fluid content in the voids of the rock's solid mass. These properties are essential in any modelling or hydraulic fracturing process. In addition, determining their value is crucial for understanding and interpreting any geological and geophysical data (Tiab and Donaldson, 2004).

1.2.1 Porosity

The amount of voids in the rock solid mass can be calculated by dividing the volume of the spaces within the rock mas by the total rock mass, according to this definition, The porosity of porous materials could have any value, but the porosity of most sedimentary rock is generally lower than 50%.

$$\varphi = {}^{V_P}/_{V_b} \quad (1)$$

Where,

$\varphi =$ Porosity, fraction.

V_p= bulk volume of the reservoir rock.

$V_b =$ Pore volume.

1.2.2 Permeability

Permeability means the connectivity of the voids in the rock mass. This is affected by the rock grain size, grain shape, grain size distribution (sorting), grain packing, and the degree of consolidation and cementation. The type of clay or cementing material between sand grains also affects the permeability, especially where fresh water is present. This parameter is very important because it controls the amount of fluid that can be extracted from the rock mass. Permeability is usually measured by unit called a Darcy but one Darcy is a relatively high permeability unit which is bigger than most natural rocks. The permeability of most petroleum reservoir rocks is less than one Darcy. Thus a smaller unit of permeability is used, the millidarcies (md), which is widely used in the oil and gas industry. In the SI unit system, the square metre (m^2) is used instead of the Darcy. The permeability of most petroleum reservoir rocks may range between (1000-0.1)md.

Furthermore, any rock that has low-porosity (<10%) and low-permeability (<0.00001 md) will be hard to extract oil and gas from it using conventional methods, and that is why the resources with low permeability that it is hard to extract gas and oil from using conventional methods are called unconventional resources. Because they need unconventional methods like horizontal drilling and hydraulic fracturing. The permeability could be measured either by laboratory methods, or by using geophysical methods see 1.7.1.

1.2.3 Density

Density is a property of a material that is equal to the object's mass divided by its volume. It could be identified either by a lab test or the degree of sonic wave velocity in the rock mass, which could be used to identify other elastic parameters.

In addition, there are several other mechanical properties and these could be identified by conducting a uniaxial test or biaxial test on the rock sample. The parameters that could be determined by these tests include the Young modulus, Position ratio, and unconfined compressive strength (UCS).

Furthermore, it is possible to measure the dynamic mechanical properties of the rock, like the dynamic Young modulus, and dynamic Position ratio, by measuring the speed of the mechanical waves, compressional waves (P-wave) or Shear waves (S-wave). These dynamic properties could differ from the lab tests, but it is possible sometimes to detect a relationship between these two types of properties (Tiab and Donaldson, 2004). Furthermore, certain factors affects the rock's mechanical properties, such as the texture, micro fractures, plains grain boundaries, mineral cleavage, and anisotropy.

Furthermore, this rock will suffer from a change in volume, shape or both according to the elasticity, rigidity, pressure and temperature of the rock mass and the fluids in its pores, which will affect the rock properties too. Since all of the variables mentioned above contribute to a certain degree to rock's mechanical properties, it is not easy to predict the rock attitude towards external

changes like pressure and fluid with drawl without having a specific idea about most of them (Tiab and Donaldson, 2004).

Moreover, there is another character that affects the rock's mechanical properties, that is total carbon content (TCC) and Kerogen maturation to a certain degree too. These two are very important in the petroleum industry because (TCC and Kerogen maturation) controls to a certain degree whether the rock is considered a resource rock or not; in other words, whether it is possible to extract gas and oil from it or not (Zargari et al., 2011).

1.3 Types of oil and gas reservoirs

There are two main types of resources in the world that supply the world with the needed oil and gas for its energy, as mentioned in 1.1.

1.3.1 Conventional reservoirs

This type of reservoir has high permeability, and consists mainly of carbonate or sandstone rocks. It is possible to extract oil and gas from these two types without the need for unconventional methods such as horizontal drilling and hydraulic fracturing. It is possible to say that these types are not considered source rocks, so these types lie outside the range of this study.

1.3.2 Unconventional reservoirs

These types of reservoir include reservoirs with very low permeability and these types needs unconventional methods like hydraulic fracturing and horizontal drilling to extract gas or sometimes oil from them. With these types, microseismic

monitoring plays a major part in monitoring the process of fracturing. This type is divided into three types.

1.3.2.1 Tight Gas reservoir

In this type, the formation is composed of sandstone and carbonate, and in order to extract the gas, horizontal drilling and hydraulic fracturing are required to stimulate the reservoir and so obtain more production.

1.3.2.2 Coal bed natural gas

This type of reservoir is composed of coal beds with low porosity and low permeability, so to produce oil from the wells in this type of reservoir there is need for hydraulic fracturing too. It is possible through the use of hydraulic fracturing to extract gas from coal bed formations, although some additional processes may be needed to enhance the production of hydrocarbons.

1.3.2.3 Shale formation

In this type, the reservoir consists of shale rock, which is a high porosity and low permeability rock, and needs horizontal wells and hydraulic fracturing in order to extract gas from it. In this type, it is important to have the degree of total organic carbon (TOC), thermal maturity, and Kerogen analysis. Knowing these factors, it will be possible to predict whether the formation has the ability to produce gas or not.

In these types of unconventional reservoirs, one of the best of ways to extract oil and gas is hydraulic fracturing which will increase the permeability of the reservoir. Furthermore, each type has its own features and treatment fluids that can be used as fracturing fluid or even proppant. In addition, each type of

reservoir has its own pressure schemes that give the best results (Zargari et al., 2011).

1.4 Hydraulic fracturing

Hydraulic fracturing is the operation of increasing permeability and hence the conductivity of the low permeable formations that contain gas or oil. This is done by creating synthesized fractures through injecting fluids into the formation under huge pressure. The fluids are composed primarily of water with other components and some proppants, mainly sand or ceramic. This will lead to the creation of fractures around the drilled hole and the proppant should hold the induced fractures, to stay open after completing the fracturing. This will allow the hydrocarbons to flow through the fracture into the production well (Arop, 2013; Aslam, 2011).

1.4.1 Hydraulic fracturing design

Any hydraulic fracturing will be based on the petrophysical properties of the reservoir's rock properties. The fracturing procedure contains the injection of fluids, mainly water, with other ingredients under high pressure into the previous, drilled and cemented well. In order to protect the surface water from pollution,. Finally, the installation or the so-called fracturing tree and again a new pumping test will take place. After passing all of these tests, the perforation of the horizontal well will starts at the end of the well.

The perforating and fracturing portions of the horizontal wellbore starts with the far end to maintain sufficient pressure for the hydraulic fracturing for the rest of

the well, and to gain good control of the entire operations. This will provide an opportunity to adapt the design because of the changes in the geological conditions that control the treated length. The length of the treated stages can vary between 300-500 feet. The water consumption is about (2.4-7.8) millions of gallons of water for a single well, and more or less water may be used according to the changes in the condition of the well. The pumping rate could be 1.260-3000 gallons per day (Cheng, 2010; Morrill and Miskimins, 2012). Regarding the hydraulic fracturing fluids, fracturing fluids is composed mainly from water with other additives to increase or to decrease fracturing fluids properties such as viscosity . This fluid should cause no problems like the movement of fines, swelling of clay and can carry on the proppant, and has to be easily removable from the reservoir. Additionally, it has to be cost-effective and chemically stable (Aslam, 2011). After conducting the actual fracturing process under the monitoring of microseismic or Tiltmetere that could give indications about the successfulness of the fracturing process. It is possible to change the design again for example changing the pressure or changing the fluids properties. This process is a continuous process for improving the design through gathering new data in the new areas.

1.5 Monitoring the hydraulic fracturing process

There are several methods that might be used to monitor the hydraulic fracturing process Table 1-1. These methods include the Tiltmetere monitoring that is an instrument that measures the change in the surface deformation gradient caused by the evolution of the hydraulic fracturing. The other method is microseismic

event monitoring. These microseismic events are small earthquakes that occur in the fractured area due to the effect of hydraulic fracturing, which can be used to gain data during fracturing operations. In addition, to these methods, there are other methods like radioactive tracer, temperature logging, well testing and production data, which are used to gain data in the post fracturing phase. Furthermore, it is possible to gain data from all of these methods to create a model that explains and predicts the behaviour of the reservoir.

Among all of these methods, the microseismic method can be used during the post fracturing process to monitor hydraulic fracturing effectiveness, to provide information about the success of the fracturing process, the characteristics of the induced reservoir (rock layer), location of the resulting fracture, the length and the height of fracture, and the growth of the fracture during and after fracturing, as stated by (Silas et al., 2000; Simiyu, 2009).

It is a fact that microseismic events were used, firstly, to determine the geothermal reservoir characters, by using microseismic events associated with the geothermal activities. For example, by using S-wave splitting, it was possible to determine a fractured area, and by using the change in P-wave velocity to S-wave velocity VP/Vs ratio, it was possible to determine the phase changes and fluid flow as well, In addition, it was possible to determine the source of the microseismic events associated with the geothermal activities through the use of P-waves and S-waves with the determination of changes in the pore pressure in the geothermal reservoir. It is well known that the same principle was used during the monitoring of hydraulic fracturing (Simiyu, 2009).

Table 1-1 Capabilities and limitations of the fracture diagnostic methods used in the field of monitoring hydraulic fracturing. (Cipolla and Wright, 2000a)

Technique	Azimuth	Height	Length	Asymmetry	Width	Dip	Range
Microseismic	Yes	Yes	Yes	May		May	Far field
Tiltmetere (Downhole)	May	Yes	Yes	May	May		Far field
Tiltmetere (Surface)	Yes	May	May	May		Yes	Far field
Production analyses			May		May		Far field
Well testing			May		May		Far field

1.5.1 Tiltmetere monitoring

Tiltmetere is a method that is used in the monitoring of hydraulic fracturing operations, using spatially accurate instruments to monitor the earth's surface or well side deformations, because hydraulic fracturing causes some small but measurable deformation in the area around the fracturing operation. It is used either to measure the surface of the earth's deformation to determine the fracture orientation, or downhole Tiltmetere monitoring is used to measure wellbores deformation to identify the fracture geometry.

The number of Tiltmetere tools on the surface of the earth are around 12-16. With the radial distance of a few hundred radians, to get a full picture of the earth's deformation, the magnitude of the change in the earth's elevation is about (0.00001 inch) at the point of placing the instruments, so it is possible to say that this titling operation provides a map of the deformation or changes in the surface

elevations of the earth's surface above the fracture. By studying this map, it is possible to get the fracture's azimuth, dip, depth to fracture centre and total fracture volume, although it must be added here that what is actually measured is the gradient of the displacement or the tilt field Figure 1-3. The Tiltmetere is extremely sensitive and it can measure 10e-6 radians. The old telemeters used two bubbles to measures the change in the gradient of the displacement, but the new ones uses electronic equipment to do the same thing (Arop, 2013; Castillo et al., 1997; Cipolla and Wright, 2000b; Evans and Columbia, 1983; Warpinskil et al., 1997).

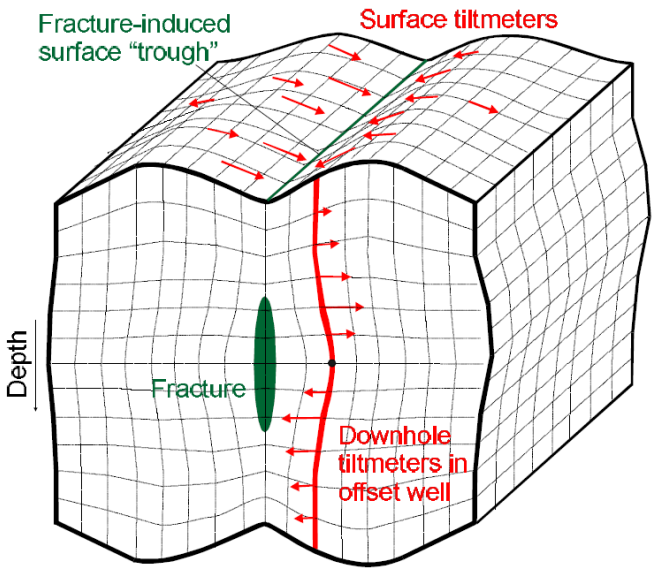

Figure 1-3 The deformation of the surface of the earth caused by hydraulic fracturing (Cipolla and Wright, 2000b)

1.5.2 Microseismic monitoring

It is possible to say that microseismic events monitoring in any hydraulic fracturing operations are merely recording and studying the small earthquakes resulting from hydraulic fracturing, as mentioned previously. Microseismic monitoring can be used to gain data during the fracturing process and could be used to map fractures by detecting microseismic events or micro-earthquakes that are triggered by shear slippage on bedding planes or natural fractures adjacent to the hydraulic fracture see Figure 1-4 and Figure 1-5. The location of these microseismic events is obtained using a downhole receiver or surface receivers called geophones, which are buried at a certain depth on the surface or in one or more offset wellbores. When a fracturing process begins, the events starts. This induced earthquake energy, emitted in the form of vibrations, reaches the geophones and will be recorded and analysed, These data are gathered and processed with a surface data acquisition system, and these events are located using techniques based on P-waves and S-waves accompanied by any release of earthquakes, using the same method that is used to locate earthquake centres (Cipolla and Wright, 2000b).

Furthermore, the microseismic method can be used during and in the post fracturing process to monitor hydraulic fracturing's effectiveness, to give information about the success of the process, the characteristics of the induced reservoir (rock layer), location of the resulting fracture, length and height of the fracture, and the growth of the fracture during and after fracturing which will have lots of application, as it will discussed later (Cipolla et al., 2011; Cipolla et al., 2012; Cipolla and Wright, 2000b; Hummel and Muller, 2009)

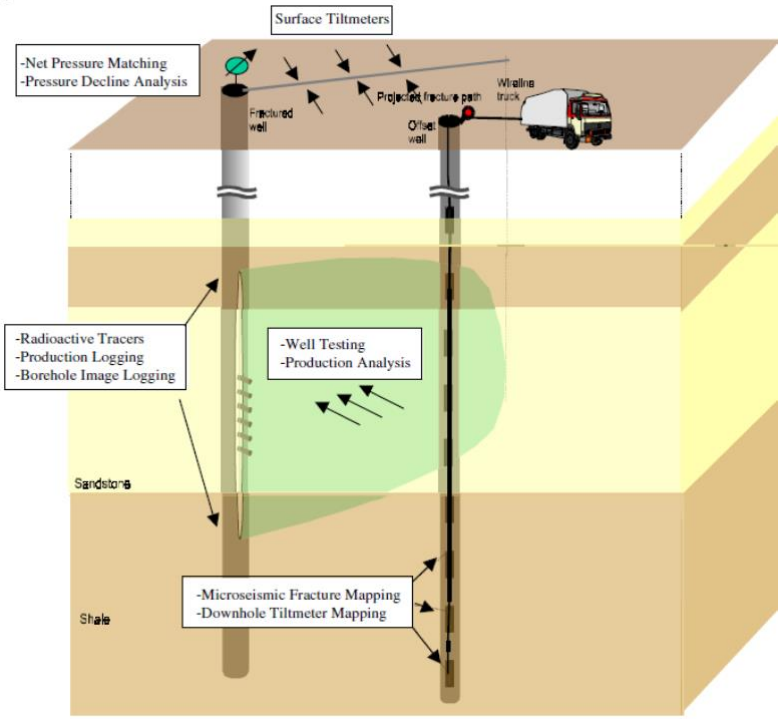

Figure 1-4 Diagram representing hydraulic fracturing and microseismic monitoring (Cipolla and Wright, 2000b)

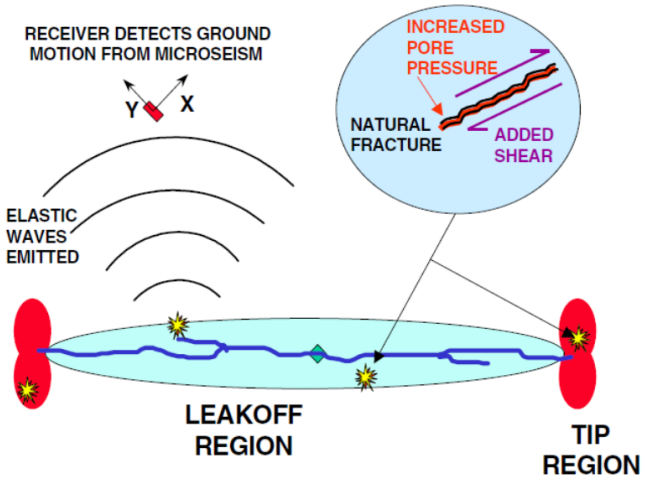

Figure 1-5 Capabilities & Limitations of Fracture Diagnostics (Cipolla and Wright, 2000a)

1.5.2.1 Magnitude and the moment of microseismic events

Magnitude is a measure of the size or intensity of a seismic event. It is usually based on the event amplitude over a particular frequency range. First, Richter (1935) developed a scale called the Richter scale. Richter (1935) developed this scale for describing the relative strengths of earthquakes in California, and related the amplitude of a waveform recorded with a particular instrument (a Wood-Anderson seismograph) at a given distance from an event, but the main problem with Richter's magnitude scale is that the Wood-Anderson seismograph is no longer in use, and cannot record magnitudes greater than 6.8.

Therefore, another scale is used to measure seismic energy that is the moment magnitude (Mag) which was invented by seismologists to measure the size of earthquakes in terms of the energy released. The scale was developed in the 1970s to succeed the Richter magnitude scale (ML). Even though the formulae are different, the new scale can provide similar results to the old one. It must be mentioned here that this is measured by instruments called seismograph but in hydraulic fracturing geophones is used instead. Additionally, these measured earthquake magnitudes provide a measure of the size of the fault that caused the earthquake.

In order to parameterize the earthquake's size, however a measure was invented, called the moment of the earthquake, where the moment is a measure of the earthquake's rupture size related to a couple of forces across the area of the fault, according to Aki (1967), who was the first to estimate the seismic moment through a systematic analysis of seismic data. The success of Aki's procedure, in which the data are fit by assuming exact prior knowledge of the

source mechanism, has led to its wide application in microseismic studies to estimate source parameters through an equation that relates the seismic moment to the average displacement, the area of the fault, then the Shear modulus of the fractured rock.

$$M_o = \mu\, d\, A \tag{2}$$

Where,

μ is the shear modulus of the rocks involved in the earthquake (in Pa).

A is the area of the rupture along the geologic fault where the earthquake occurred (m^2), and

d is the average displacement in *m*

With M_o as the moment of the seismic event, thus M_o has dimensions of energy in Newton. Meters.

It is possible to estimate the source area of the fracture slip, through measuring the moment of the event. The seismic moment of an earthquake is usually estimated from ground motion recordings of earthquakes known as seismograms although, for monitoring fracturing processes, geophones are used to recode the waves and then to estimate the moment. Earthquakes that occurred prior to the invention of modern instruments may be estimated from geologic data using the size of the fault rupture and the displacement, assuming that the shear modulus of the rocks involved in the earthquake is known.

It is possible to measure another parameter called the moment magnitude (Mag) of any earthquake based on the seismic moment.

$$Mag = \frac{2}{3}\log M_o - 6 \tag{3}$$

Where.

(2/3) is a constant that was used for the conversion purpose that has been suggested by (Hanks and Kanamori, 1979) .

From now on, the seismic moment will be referred to as the moment and the moment magnitude will be referred to as the magnitude only (Abercrombie, 1995; Hanks and Kanamori, 1979; Lee et al., 2002; Silver and Jordan, 1982).

1.6 Fracture induced acoustic emission

According to the frequency, the magnitude and fracture dimensions of events can be called either microseismic events, acoustic emissions or earthquakes. It is crucial to mention here that, although they are similar in size distribution, stress drop and source characteristics (Lei and Ma, 2014; McLaskey et al., 2014), their main differences are their magnitude, frequencies and fracture dimensions (see Figure 1-6). Most modelling studies were tested first on models for acoustic emissions resulting from laboratory tests and then on microseismic events induced in the fieldwork, using equations that were initially developed for earthquakes (Lei and Ma, 2014). The only disadvantage of the acoustic emission research is that it is not sensitive to ductile deformation. Therefore, it is applicable only in brittle regimes; other than that, it shares most of the other features (Lei and Ma, 2014) and, since acoustic emissions are easy to produce and monitor in laboratory tests, it was decided in this study to create a model for acoustic emissions that could be used later to study microseismic events caused by hydraulic fracturing.

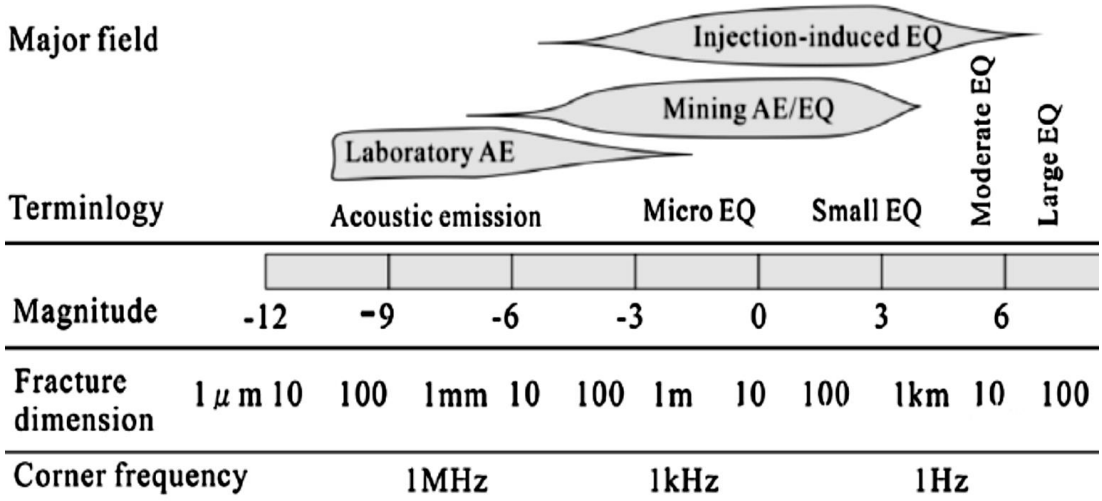

Figure 1-6 The differences between acoustic emission microseismic events and earthquakes in terms of the frequency fracture dimensions magnitudes (Lei and Ma, 2014)

Moreover, there are a few techniques used to interpret and study acoustic emission events either in a model or in a lab test. These techniques includes the number of events, the shape of the seismic cloud, the source types, the frequency-magnitude or Gutenberg-Richter relationship between moments and the cumulative ascending number of event moments (b_value), position of the events and seismic moment tensor inversion. In addition, many other techniques were not used in this research because, in comparing our model results with those from the laboratory tests (see chapter 4). We used the same methods that were used to study the acoustic emissions in these tests (Chang and Lee, 2004; Gutenberg and Richter, 1956; Hazzard, 1998; Pettitt, 1998; Wuestefeld et al., 2012).

1.6.1 The frequency-magnitude relationship (b_value)

The well-known Gutenberg-Richter relationship (1954) relates the frequency of the earthquake, microseismic or acoustic emission occurrence to the earthquake's magnitudes or moments by;

$$Log\ N = a - b\ Mag \tag{4}$$

Where,

N is the number of events used to draw the curve

a is a constant that could be concluded from the graph

Mag is the magnitude of events used in the graph

$b - value$ is the constants that represent the slope of the straight part of the curve .

This relationship represents a power law distribution where *b* or the $b - value$, which is the slope of straight part of the curve, can be used to determine the characteristics of the distribution of earthquake magnitudes. It is also related to the pore pressure in the hydraulic fracturing operation where a decrease of b-values is associated with an increasing distance of the injection point which is probably caused by a decrease in pore-pressure.

In addition, the Gutenberg-Richter relationship has been used to study damage in concrete beams, where a higher *b* indicates a larger proportion of small earthquakes, and a lower *b-value* indicates a smaller proportion of small earthquakes (Bachmann et al., 2012; Cipolla et al., 2012; Colombo et al., 2003; Gutenberg and Richter, 1956; Maxwell, 2012).

On the other hand, Scholz (1968) stated that stress depends on the b_value in laboratory tests and in earthquakes. Furthermore, the b_value does not have any correlation with the stress history, nor between the b-values and the spatial migration of seismicity, and aseismic slips is the main reason why the relation between the b_value and deformation is unclear which implies that, when changes in the b_value is used for earthquake prediction, the prediction may be inaccurate (Volant et al., 1992).

Additionally, Nuannin (2006) pointed out in his research that b-value mapping is a good instrument that can display variation in stress accumulation in large areas, and that small earthquakes will take place in high b_value areas. Moreover, Kwiatek et al. (2014) compared the inter-slip and pre slip periods, with respect to the differences in frequency magnitude distributions of acoustic emissions, and differences in the changes in moment tensor properties. During an experiment on granite, they found that acoustic emission characteristics could be used to study micromechanical operations, that they can reflect the deformation of the material under stress, and that the acoustic properties correlate well with the fracture's topography and roughness.

On the other hand, the change in the b_value during the fracturing process could be used to make an estimation of the development of the fracturing process. The b-value was found to be a function of grain size, so finer grain size could lead to a higher b-value (Lei and Ma, 2014).

1.6.2 Studying the source mechanism of the events

Identifying the source mechanism is of great importance because, by determining the source mechanism of the fracture that caused the recorded seismic event as proven by Sasaki (1998) during a study in the geothermal field, it is possible to determine the type of fracture that caused that event; such as, whether it is due to the activation of an old fault of not.

There are three main source mechanisms of fracture-induced seismicity in nature in the field of analysing the event source of a seismic events: a pure isotropic mechanism that corresponds to an implosion or explosion, that is then compensated for by a linear vector dipole; the (double couple) force DC shows the extent to which the source follows a conventional shear mechanism, and the amount of CLVD (Compensated Linear Vector Dipole) corresponds to a mechanism associated with the fracture closing or opening (Pettitt, 1998) .

Additionally, by determining the source mechanism, it will be possible to determine what causes this event: is it old fault, a new fracture tensile or a shear. This makes source plots helpful in analysing a large number of events that resulted from the fracturing operations, because, in studying microseismicity, it is very common to deal with tens or hundreds of events at the same time, so plotting them onto the same surface and analysing them to get there fracture mechanism makes it possible to obtain a large amount of information on the cracking mechanisms through studying a huge number of events at the same time and on the same plotting surface.

Among the methods for studying source mechanisms of induced events is the T.K. plot (Hudson et al., 1989). This can be done by calculating two parameters *T* and *k* values and plotting them on a T-k plot. *T* is related to the deviatoric component, and is a measure of the deviatoric component of the source, ranging from a pure positive CLVD at -1 to a pure negative CLVD at +1 and passing through a pure double couple at the origin. On the other hand, *K* is related to the isotropic component, is a measure of the isotropic component of the source and varies from a pure explosion at +1 to a pure implosion at -1 (see Figure 1 7). The equations required to calculate the *T* and *K* are listed below (Pettitt, 1998).

$$\begin{cases} k = \frac{(1/3)tr(M_E)}{|(1/3)tr(M_E)| - m_1^*} & when\ m_2^* \geq 0 \quad (5) \\ k = \frac{(1/3)tr(M_E)}{|(1/3)tr(M_E)| + m_3^*} & when\ m_2^* \leq 0 \quad (6) \end{cases}$$

$$\begin{cases} T = \frac{-2m_2^*}{m_1^*} & when\ m_2^* > 0 \quad (7) \\ T = 0 & when\ m_2^* = 0 \quad (8) \\ T = \frac{2m_2^*}{m_3^*} & when\ m_2^* < 0 \quad (9) \end{cases}$$

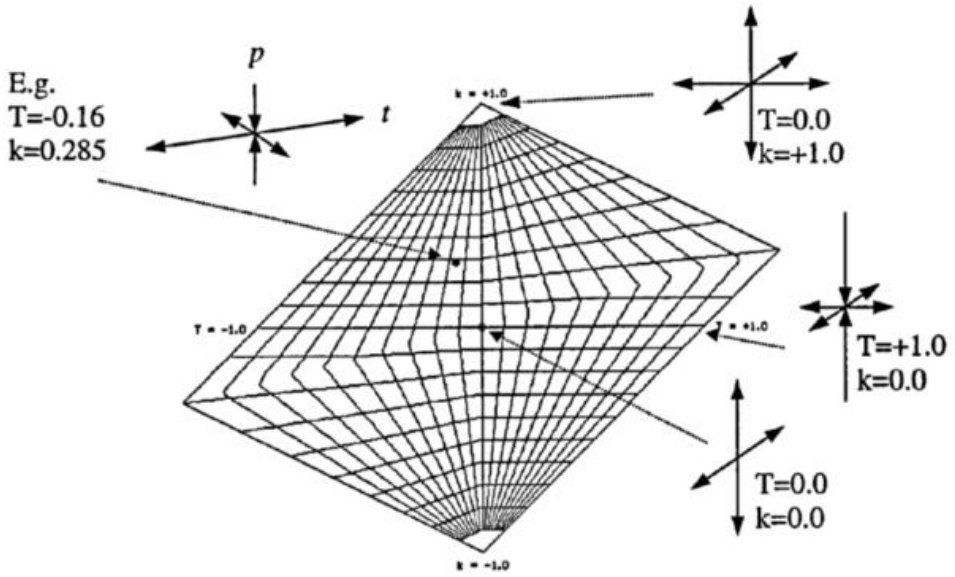

Figure 1-7 The T.K. plot and fracture mechanisms on it (Hudson et al., 1989)

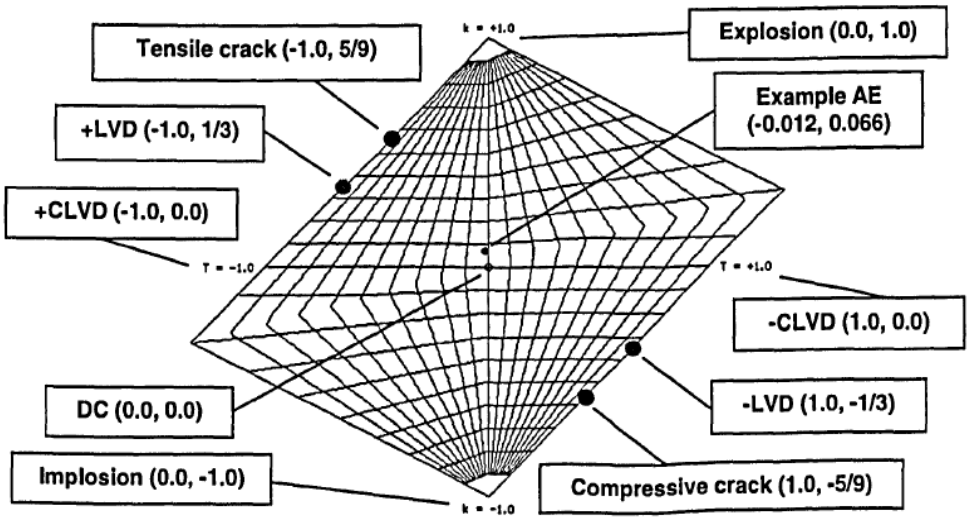

Figure 1-8 The Tk. plot and the position of the type of cracks plotted on it (Hazzard, 1998)

Figure 1.8 shows an example of a T-k plot. The deviator T value is plotted along the horizontal axis. The isotropic k value is plotted up the vertical axis. The grid lines are at 0.1 increments in either T or k. The theoretical positions of a tensile crack and a compressive crack are shown as well. Knowing these two parameters makes it possible to describe completely any possible source type.

1.7 Modelling hydraulic fracturing and associated seismicity

One of the methods that could be used for studying microseismic event generation and source type, and that helps in the process of interpreting the seismic data recorded while monitoring the hydraulic fracturing is modelling the events and their causes, like hydraulic fracturing, which will increase our understanding of the microseismic emissions properties and their causes.

Furthermore, modelling hydraulic fracturing and the resulting microseismic events could be used to predict the activation of faults, the fracture mechanism,

the effectiveness of fracturing process, the fracture spacing, and the behaviour of the proppant through comparing different hypotheses of the model results with the field results, to provide different field development scenarios for different hypothetical cases too. (Gil, 2005; Hazzard and Young, 2004; Potyondy, 2012; Rutqvist et al., 2013; Sarmadivaleh, 2012 ; Tomac, 2014; Wilson and Durlofsky, 2013), although we must emphasize here that some of the modelling experiments were tested first on models, in laboratory scale tests, then were used to study the microseismic events caused by hydraulic fracturing. Moreover, in most cases, the equations that were used were developed to study earthquakes, as mentioned earlier in 1.6.2.

1.8 The chosen methodology

As mentioned earlier, the DEM/PFC has the capability, to be used to study the hydraulic fracturing process, with the associated microseismic events. To achieve this aim, the PFC program by Itasca will be used to create a model in order to study the induced microseismic events caused by hydraulic fracturing because, by creating a valid computer model, any experiment can be repeated many times with different parameters to draw different conclusions and be used in different cases with different scenarios. Moreover, it is possible to use these models to study and to increase our understanding about the fracturing process, In addition, it is possible to use these models to create a better interpretation of the microseismic data

1.9 Aim and objectives

Predicting the efficiency of hydraulic fracturing in a certain environment is crucial in the field of hydraulic fracturing. Furthermore, predicting the pattern and characteristics of the induced seismic cloud will make the interpretation of the real seismic cloud easier and more accurate. Moreover, this information can be helpful in the field of predicting the seismic hazard in areas where hydraulic fracturing will take place. These applications are possible only through the use of computer modelling, so the aim of the thesis will be to create or develop a program that has the ability to predict the microseismic events produced by the hydraulic fracturing process. This program should have the ability to reproduce a synthetic seismic cloud, the microseismic event resulting from a synthetic hydraulic fracturing test.

The developed model should overcome some of the deficiencies that have been pointed out in 2.10. Then, the model can be validated by comparing it with real fracturing tests in different cases and environments. After creating the model and validating it on an actual model, the next step is to conduct several hypothetical injection tests, with different scenarios, to enhance our understanding of hydraulic fracturing and the associated microseismic events.

1.10 Thesis layout

The first chapter will cover the basic concepts, ideas, and applications in the field of microseismic events induced by hydraulic fracturing, while the second chapter will focus on the literature review and determining the gap in the knowledge in

the field of induced microseismicity. Furthermore, the third chapter will focus on the program used in this thesis. The fourth chapter will discuss the preliminary simple models and validating procedure. This will include simulating the acoustic emission experiments on a rock sample under a triaxial test, then modelling the resulting acoustic emission by fluid injection. Moreover, the fifth chapter will focus on modelling a more complicated model, then conducting a few hypothetical models to study the effect of changing different parameters on acoustic emission events and on the acoustic emission cloud distribution, studying the seismic events and the seismic cloud. Finally, the sixth chapter will present the conclusions and recommendations for further studies.

1.11 Summary

It is possible to increase permeability of the low permeable reservoir and hence increasing the oil and gas production, through using a process known as hydraulic fracturing. This includes pumping fluids contains proppants under huge pressure. The hydraulic fracturing is monitored by using induced earthquakes called microseismic events, that could be used to determine the successfulness of the fracturing operations. In addition, to many other applications. Modelling hydraulic fracturing and it associated microseismic events will increase our understanding towards the fracturing operations.

Chapter 2 Literature review of the existing work

2.1 Introduction

Sometimes, the fracturing process can fail to achieve its goal. The reason may be fracture mechanics and an inappropriate reservoir's geomechanical reaction. Regarding the first reason, fracture growth in the reservoir depends on the rock mechanical properties and the in-situ stresses of the formation whereas other fracture properties, such as fracture height, fracture propagation and fracture orientation, are controlled by fracture mechanics while, in the case of inappropriate reservoir properties, sufficient reservoir pressure is required to drive the hydrocarbons from the formation to the wellbore. In addition, it is possible to add that one of the problems that can arise during the fracturing process is the activation of faults and fractures that could induce seismic hazards. Additionally, there are other problems that accompany the hydraulic fracturing process, such as penetrating other layers surrounding the water reservoirs by the fracture resulting from hydraulic fracturing, which may cause pollution (Aslam, 2011; Rutqvist et al., 2013; Sarmadivaleh, 2012 ; Willis et al., 2005).

It is possible to use the induced microseismic monitoring, to study the fracturing process and to help to solve most of the problems mentioned above, as pointed out in the first chapter. Besides that, it is used in the field of studying the fracture mechanism and the activation of faults as well, in addition to the many other applications mentioned in the first chapter.

As mentioned one of the methods that could be used for studying and analysing microseismic events, and could be used in the process of interpreting, understanding and analysing the microseismic events is simulating the hydraulic fracturing and induced semi city. This could be done by using computer programs. Additionally, simulating the hydraulic fracturing and induced microseismic events could be used determine the effectiveness of fracturing process schemes, the efficiency of the fracturing fluids, and predicting the seismic hazards in different hypothetical cases too. (Gil, 2005; Hazzard and Young, 2004; Potyondy, 2012; Rutqvist et al., 2013; Sarmadivaleh, 2012 ; Tomac, 2014; Wilson and Durlofsky, 2013).

2.2 Simple review of seismic events

One of the older scales used to study earthquakes was presented by Richter (1935), who introduced a scale for quantifying the relative strength of earthquakes in California, and related their strength to the amplitude of a waveform recorded with a tool that was used at that time (a Wood-Anderson seismograph), but it was Gutenberg and Richter (1956) who discovered a relation between the ascending cumulative frequency of earthquake occurrence and earthquake magnitude. See Equation 4 1.5.1. In which This relationship is a power law distribution in which b is called the b-value, which is the slope of the straight part of the curve.

In addition, it was Aki (1967) who created an equation that relates the surface of the slip, the Shear modulus of the medium and the seismic moment together. He did that by conducting a systematic analysis of seismic data and studying the

known properties of sources in certain earthquakes. In addition, Wong (1982) proved that the local grain scale heterogeneities, elastic anisotropy and the mineral composition of the particles in the rock sample all control the shape of the fractures. The importance of this study arises from the fact that it shows the role of the mechanical properties of particles in controlling the shape of the fractures. On the other hand, Hudson et al. (1989) created a plot called the Hudson plot or T.K. plot, which is a very popular plot for displaying the source mechanisms of multiple events. Unfortunately, in his original paper, there were no practical example or comparisons with real cases.

Furthermore, Sasaki (1998) pointed out that studying and plotting the source of the fracture mechanism is important in the field of geothermal studies, when he proved the benefits of focal mechanism studies to the field scale microseismic tests. During a study at the Hijiori hot dry rock geothermal site in Japan, he found that the direction of P-axes deduced from the fault planes, obtained during the fluid circulation tests in a previously fractured well, were compatible with the direction of fracture the planes, deduced by studying the induced microseismic events during hydraulic fracturing. He also noticed that the induced seismicity rate is correlated with the injection flow rate of fluids into the well. Although (Chang and Lee, 2004) pointed out that “The moment tensor analysis should be considered as representing a microscopic failure mechanism rather than a macroscopic mechanism. The macroscopic failure mechanism, and failure planes especially, could be estimated by considering the relative crack volume obtained from the moment tensor analysis as a damage index”.

Moreover, one of the main elements in any earthquake study is studying the velocity of the rupturing of the earthquake. (Lei et al., 2003) described the rupture process in an under stressed rock sample in a lab test and stated that the rupture speed of the source of the earthquakes is not constant, but rather increases in an ascending way, with a value of 0.5-0.9 of Vs where Vs is the velocity of the shear wave velocity. He added that there is no accurate way to calculate the actual rupture velocity in the test, that the rate of the acoustic emission differs during the period of the test, and that in the last stages of the test, it was hard to separate events from each other.

Schubnel et al. (2007), in a lab injection test on a rock sample, stated that, in the initiation of the nucleation patch, the slip accelerated up to speeds of 296 mm/s. Then the rupture was propagated in less than 0.25 s at 297 speeds between 0.1–4 m/s, which will lead to the conclusion that that rupture speed is changeable and the rate of the induced events are changeable or cannot be recognised by the sensors, especially in the last stages of the fracturing. It is noticed that the resolution of events by the geophones or sensors were not studied, and the effect of recoding more than one event in the last stages based on the measured rupture speed were not accounted for either.

Additionally, Nuannin (2006), during a study on variations of b-values in time, stated that b-value plotting in a map is a good tool for predicting earthquakes, that can be used to display variations in stress accumulation in big scale areas, and that high b_value areas are an indication that small earthquakes will take place in the studied area. Additionally, Crampin and Gao (2015) supported the

conclusion that the b_value could be used in stress forecasting for earthquake areas.

2.2.1 Microseismic clusters

Among the techniques that have been applied to analyse microseismic events is a technique called clusters studying. In this method, the events are dealt with as if they were groups related together. It is possible to create seismic clusters, based on the assumption that microseismic events occur on fractures that existed before, as well as the assumption that the events are related to one another through the rock mass joint and induced stress (Hazzard et al., 1998; Tezuka and Niitsuma, 2000). It is possible to create clusters through their frequency or using statistical methods to analyse these frequencies and to cluster seismic events accordingly (Likrama, 2008).

There are many applications for creating seismic clusters. It was possible to use this technique to estimate the in situ stress state within the Hijiori hot dry rock geothermal reservoir, based on focal mechanism analysis, supplemented with microseismic seismic clusters, created by analysing microseismic clusters induced by hydraulic fracturing injections. It was possible to obtain good results regarding the geology of the reservoir. The results were consistent with other estimates obtained by using other methods (Tezuka and Niitsuma, 2000).

Identifying individual subsurface faults in a larger fault system is important in order to characterise and understand the relationship between microseismicity and the subsurface processes. This information can potentially help to drive reservoir management and mitigate the risks of natural or induced seismicity.

The clustering method was applied in the field of petroleum industry with good results. This is clear from the study of Arop (2013), who presented a method for statistically clustering power spectra from microseismic events associated with an enhanced oil recovery operations. In which seismic data were collected using a geophone array, between March 2008 and March 2009. Based on the 3800 events recorded, this work suggests that spectral clustering may help to predefine subsets of hypocentres, which in turn can then be relocated via double-difference techniques. Hypocentre maps provide information on the style of the generated fractures. Narrow bi-wing fractures contrast with shorter, broader hypocentre clouds, indicative of greater fracture network complexity. Sometimes, but not always, the clouds suggest details of the fracture geometry, particularly in areas where the horizontal anisotropy is not large.

2.2.2 The rupture speed

In real earthquakes, the rupture velocity of the fault is decreased in an ascending way from 0.1 of the shear wave velocity to about 1.2 of the shear wave velocity in super shear earthquakes, but in the lab tests under stress, it varies between 0.1-0.9 of the shear wave (Lei et al., 2003) but in some cases the rupture could propagated in less than 0.25 s at 297 speeds between 0.1–4 m/s. In other cases, this change may be related to the size of the sample or the type of the rock (Schubnel et al., 2007). Furthermore, the rupture speed in field induced seismicity is about an average of 0.6 of the shear wave. The differences could be related to the size and scale of the rupture.

The main conclusion here is that the rupture speed is not constant, and that the values differ from one case to another, while other studies stated that the terminal

rupture speed is 0.9-1.1 of the S-wave's velocity (Harris and Day, 1997) regarding the effect of stress on the slow slip earthquakes rupture speed and this depends on the initial stress profiles. The average rupture velocities may increase with an increase in the pre-rupture stresses, and the angle of the slope in the slip-weakening is an affecting factor that controls the rupture speed. Additionally, it was found that the crack length in 3-D heterogeneous rupture models decreases as the rupture propagates far from the crack centre (Schmedes et al., 2010) and there are correlations between the local rupture velocities with local interfacial stresses. In addition, they pointed out that local pre-stress can control rupture behaviour in earthquakes in some cases.

Moreover, Walter et al. (2015) find that off-fault plasticity does not qualitatively alter the range of rupture styles in elastic media, as peak slip velocity and rupture speed are connected by a non-linear relation. Moreover, Schmedes et al. (2010) created a model to study the relation between the source and the rupture velocity, and stated that the rupture accelerates as it propagates away from the nucleation zone. They also pointed out that the rupture velocity is not a good function for total slip amplitude.

2.3 Applications of the seismic cloud characteristics

The shape of the entire recorded seismic events in a certain place is called the seismic cloud. The seismic cloud properties, the medium and the injected fluid properties could be used in the determination of the formation permeability from the recorded and plotted microseismic data that resulted from certain fluid injection cases. There are two methods that can use the seismic cloud properties

to determine the formation permeability after the injection test: the r-t method and the inversion approach (Grechka et al., 2010). The last technique was chosen to be applied in this study, because the measured permeability obtained during the laboratory experiment was better than the other method (Moreno, 2011).

2.3.1 Inversion approach to permeability estimation

The inversion approach is used to determine the effective permeability based on the seismic cloud properties and was proven to be more accurate and give good results through a study on the acoustic emission induced by fluid injection on a laboratory test conducted by Moreno (2011). Where he used equation 10 to determine in-situ permeability based on (Grechka et al., 2010);

$$K_{inv} = \frac{u\ \alpha_{us}\ Q_i}{4h_f\ \Delta p} \tag{10}$$

Where,

K_{inv} is the in-situ permeability of the fractured sample in *Darcy*

α_{us} is ratio between the seismic cloud dimensions between width and length of the cloud

Q_i is the fluid injection rate

u is the fluid viscosity *Pa.Sec*

h_f is the height of the cloud In *m*

Δp is the pressure differencse Pa

In equation 10 the K_{inv} i in-situ formation permeability according to the inversion approach. Through the use of this equation, it is possible to determine the

formation permeability during the injection process by using the resulting acoustic emission or microseismic events cloud shape. Note that, in either fluid solution, we are not recovering the intrinsic permeability but an “effective” permeability which may locally reflect the natural fracture.

2.4 Predicting the fracture aperture

Predicting the aperture of the resulted fractures from hydraulic fracturing, is important in the hydraulic fracturing planning, for choosing the proper proppant type, concentration, size, and to obtain best results from hydraulic fracturing operations (Palmer et al., 2012). Therefore it was decided in this study to use microseismic data information, to predict fracture aperture from magnitude of the seismic event that is usually easy to get in the model form converting moments to magnitudes see 3.9.3.

At first Wells and Coppersmith (1994a) during a study that included the data for 421 historical earthquakes. Established an imperial relation between the magnitude of the earthquakes and the raptured area of the fault surface, equation (11).

$$Mag = 4.07 + 0.98\ log\ (Ra) \tag{11}$$

Where,

Ra Ruptured area in the fracture in km square.

Mag The magnitude of the event

Moreover, based on the studies of Olson (2003) on the relation between of fracture length and fracture aperture. Klimczak et al. (2010) concluded an

imperial relation between the aperture and the length of the fracture equation (12)

$$Len = (16 * Ra\text{^}2)/(3.148 * ap) \quad (12)$$

Where,

Len The length of the fracture

Ra is the radius of the fracture

αp Is proportionality coefficients for opening-mode fracture and it is varied. Therefore it was decide to take the average value which will be 0.125.

Now if we assumed that the resulted fracture is circular, then it will be possible calculate the length of the fracture for the circular surface from knowing the magnitude of the seismic events only. And then calculating the aperture of the fracture from the length of the fault. In this procedure it is possible to get the area of the fractured area too which is important in the geothermal studies as stated by Hofmann (2015)

2.5 Application of microseismic events to study reservoirs characters and fracture properties

The basic equations and theoretical foundation of seismicity were first invented and developed to be applied in the field of earthquakes. They have been used continuously over the past 50 years in the field of mining, where the primary task of microseismic monitoring was to determine the source position, the source type (tensile or shear), the origin time and source strength of the earthquakes.

Microseismic monitoring of hydraulic fracturing could be used to study the reservoir properties and the induced fractures parameters too. Some of these parameters are very important in the petroleum industry. The first and most important is the use of microseismic events to determine the location of fractures caused by the hydraulic fracturing process, as stated by Pearson (1981) and Talebi and Cornet (1987) when they used microseismic events to determine the location, and the focal mechanism in an fracturing experiment on granite rock mass injection at depths of 443 m, although it is possible to say that their results were not verified by an independent method.

Additionally, microseismic events could be used to study the areal extent of the fractures, and it is possible to see the relation between the areal extent of the fractures and their distribution, and hence the production of gas and the size of proppant used, which makes it possible to change the size of the proppant used during the hydraulic fracturing operations to improve productivity. It is obvious that this procedure will increase the efficiency of the hydraulic fracturing process. Additionally, microseismic events monitoring could be used to study the reservoir's pore pressure, because it was noticed that the pore pressure diffuses from nearby the hydraulic fracture position by the same width as that of the zone where the seismic activity occurred, and it was concluded that these microseismic events may be caused by the high pore pressures (Pearson, 1981).

Furthermore, (Simiyu, 2009; Simiyu and Malin 2000) studied the use of microseismic events to determine the geothermal reservoir's character. The reservoir temperature and the flow channels were investigated. By using the ratio of compressional wave velocity P-waves to shear waves velocity S-wave

(Vp/Vs) ratio and S-wave attenuation, it was possible to identify the heat source areas directly beneath the Olkaria geothermal field and the Casa Diablo volcanic centre but, by using S-wave splitting, it was possible to determine the fractured area, and the change in (Vp/Vs) wave was a good tool for determining phase changes and fluid flow as well. This clearly indicates that we can determine the fractured area, the phase change and the fluid flow. In addition, microseismic monitoring was used and developed further in the field of geothermal reservoir analyses too (Goertz-Allmann et al., 2011; Phillips et al., 2002; Silas et al., 2000). Regarding the application of S-wave splitting, it must be clear that S-wave splitting sometimes may not be very accurate because of the anisotropy of the rock material or velocity variations (Warpinski et al., 2009).

Maxwell et al. (2008) studied the ratio between fluid injection energy and the fracture energy, which was about 15 % of the injection energy. They stated that much of the deformation will take place in aseismic way, and that it is possible to predict seismic efficiency and seismic deformation for a specific design, taking into account that this ratio is higher in pre-existing fractured areas. However, in the study, there was no mention of the difference between the hydraulic fracturing design which took place in the high seismic injection efficiency places within the reservoir, and the one that took place in low seismic injection efficiency. Furthermore, much of the fracturing energy goes into the creation of fracture and the deformation of the rocks surrounding the fractured area not the seismic emissions which may limit the information gained from studying microseismic events' energy, as pointed out by (Warpinski, 2014). Which may limit the accuracy of the results.

(Coulson, 2009), based on an analogy to laboratory testing on sample studies that included microseismic events measurements during failure, concluded that microseismicity can be used to study fractures and the steps of fracture development, in the pre-peak and post-peak stage. In addition, microseismic monitoring was used to monitor the co2 storage. An example is Verdon (2010). During a study on the microseismic emissions on Weyburn reservoir after the injection of co2, it was discovered that the microseismic events observed were not caused by fluid migration or co2 injection but by stress transfer through the rock frame. Additionally, he stated that both fluids (water and CO2) have similar styles of induced seismicity despite the fact that they are different in terms of compressibility and viscosity. Moreover, he used shear-wave splitting measurements to explore the aligned fractures sets. The results matched previously identified fractures in the core samples and a model was developed to predict induced microseismicity, although other modelling studies found differences between induced fractures (not seismicity) from co2 injection and water injection (Zhou and Burbey, 2014).

(Williams-Stroud and Billingsley, 2010) stated that microseismic monitoring could be interpreted and used side by side with geological information background to create a model for the fractures existing in the cap rock formation.

The estimation of the fracture length, and the fracture system in the cap rock and the field were also proven to be possible, through using microseismic monitoring, as shown by Al-Harrasi et al. (2011), who used microseismic events to conclude the fracture length in the reservoir and the reservoir cap. For that purpose, they used a pyroclastic model, which accounts for fluid communication in the pore

spaces and macroscale scale fractures that causes the anisotropy in the frequency of the microseismic waves. The results from the inversion suggested that anisotropy is caused by microscale cracks in the shale cap rocks and clearly showed the potential for characterising fracture systems using observations of frequency dependent anisotropy.

Additionally, there were other parameters that were deduced from these induced events. An example of this is seismic energy, in which the magnitude of the energy indicates that the size of the fracture and the duration of the pulse were found to related to the brittleness and homogeneity of the rock (Qin et al., 2012), although Warpinski (2013) cast doubt on the accuracy of using seismic energy as an indication of fracture size, claiming that this energy is too small if compared to the total fracturing energy.

Moreover, it is possible to determine the direction of natural fractures and their extent in the reservoir through studying the focal mechanism and comparing the data with geological data (Barker, 2009; Busetti et al., 2014). Not only that, but it is possible to determine if natural faults were induced by the fracturing process, through the analysis of the failure mechanisms of the microseismic sources, as did (Talebi and Cornet, 1987 ; Williams-Stroud et al., 2012), although (Warpinski et al., 2012a) raised questions about the reliability of using microseismicity in these applications if it was not supported by geological data.

Ali (2011) showed that seismic wave propagation properties and the well production data could be used to complement each other, because it is clear that there is a relation between the fracture properties, fracture density and the production data from the wells, which may help in finding fracture apertures and

the effective permeability tensor, because production data are more sensitive to the fracture aperture than the seismic data. Additionally, he stated that the fracture aperture could be considered one of the most controlling factors regarding fluid flow, and the pressure changes can have an impact on the aperture of the fractures.

Besides the arguments mentioned above, microseismic monitoring is used to determine the effectiveness of different types of fracturing fluids, and the effect on fracturing patterns, as noticed from microseismic monitoring in Canada (Duhault, 2012). In other words, it is possible to use microseismic data to determine which fluid or pressure scheme will cause the type of fracture desired.

Adejuyigbe (2013) conducted a study of the effect of slurry on fracture volume using microseismic cloud distribution, because a large micro-seismic event (cloud) structure must be approximately equivalent to the actual fracture network size. He stated that the volume occupied by the fractures increased with an increasing volume of slurry and that was because of increasing the crack density increases. Additionally, a relationship between the volume of the fractures created by the fracking operation, the volume of the slurry, and the crack density were created. Additionally, Wang et al. (2015) stated that it could be used to determine the fracture distribution, fracture volumes and sizes, depending on real data from oil fields during the microseismic monitoring of fracturing operations, but it is obvious that not all fractures are seismically active and not all events were recoded due to attestation, so is it possible to say that the volume mentioned is the recoded microseismic volumes only.

It must be added here that the acoustic emission is not sensitive to ductile deformation. Therefore, it is applicable in brittle regimes only (Lei and Ma, 2014).

2.6 The laboratory tests on acoustic emissions

In order to understand microseismic or seismic events, many laboratory studies have been carried out. Although the emissions in these studies can be considered acoustic emissions, depending on the size of the fractures and the frequencies, they are similar in size distribution, stress drop and source characteristics (Lei and Ma, 2014; McLaskey et al., 2014).

Majer and Doe (1986) used the acoustic emission method to study induced fractures in salt blocks of 30 x 30 x 45 cm under triaxial stress, as well as small field cases in granite. The AE events were recorded either in the place of the induced fracture or near the discontinuities in the rock sample, while the observed cracks were of the asymmetric type. It was noticed that, in the salt blocks, only tensile events were reported, but both tensile and shear events were noticed in the field case. Additionally, Satoh et al. (1990) conducted a laboratory triaxial test on Oshima granite, and studied the failure mechanism based on the recoded seismic signals. It was noticed that a weaker sub-fracture developed perpendicular to the main fracture. Furthermore, that acoustic emission clusters gathered around the fracture plane before failure. An analysis of the focal mechanism of fractures clustered around the sub-fracture plane revealed that the majority of events were shear events.

Furthermore, Solberg et al. (1980) studied the effect of the injection rate on the permeability of the induced fractures, and the induced fracture mechanisms too,

using induced Acoustic emission motoring, for cylindrical Westerly granite samples of 76.2 x 190.5 mm under thermal conditions. The results indicated that high injection rates will cause the tensile fracture type, whereas low injection rates will cause the generation of shear events. On the other hand, in the case of the intermediate injection rates, accompanied by elevated differential stress, the results were fewer events but the permeability was higher than that observed in the other two cases.

Furthermore, Falls et al. (1992) conducted a hydraulic fracturing experiment on two unloaded Lac du Bonnet granite cores. They stated that the anisotropy of the mechanical wave velocities could be caused by the presence of a microcrack in the rock sample, and also with changes in the saturation levels. In the test, the distribution of the acoustic emission event after breakdown indicated that the two parallel fractures were controlled by the presence of pre-existing cracks. The study of the focal mechanism indicated the predominance of the double-couple mechanism in both samples. Additionally, (Pettitt, 1998) used a cubic sandstone sample under triaxial stress to measure the emitted acoustic activity, then plotted the b_value and the T.K. plot to study the source mechanisms and he calculated the number of events too.

Likewise, (Ishida, 2001), during a study on fluid injection into different types of rocks, noticed that the shear fractures are dominant in the specimens with larger grains, whereas the tensile fractures is dominant in those with smaller grains. Shear fractures are dominant during water injection and the tensile fractures are dominant during oil injection.

Moreover, (Moreno, 2011) conducted an injection experiment on three types of cylindrical under stress rocks samples and calculated the resulting permeability using the microseismic cloud. He concluded that the inversion method is more accurate than the rt method. Additionally, Stanchits et al. (2011) conducted an experimental test on water injection while monitoring the induced acoustic emission, under stress rock of 50 mm diameter and 105–125 mm length sandstone. The permeability was calculated using the position of the fluid front at the time after injection. The results showed that there is permeability anisotropy in the sample, and that increasing the pore pressure will increase the number of tensile events at the beginning of the test but at the end of the test, near failure, both shear acoustic events and pore collapse became dominant. Microstructural analysis of the rock sample after injections showed agreement between the location of the acoustic emission hypocentre and the fractures. It is noticed in this study that the number of steps are much more in other studies.

Additionally, Aker et al. (2014) conducted a study to relate the acoustic emission rate to the observations of the sandstone sample deformation, under triaxial stress. The sample contained a horizontal borehole. In addition, the events near the horizontal borehole showed complex focal mechanisms because of the complex stress field.

2.7 DEM/ PFC in rock modelling

Potyondy et al. (1996) described the use of DEM/PFC code to reproduce the fracturing process of a rock sample under stress, and to model elastic deformation. He also pointed out that this code could be used to capture the

mechanical characteristic properties of Lac du Bonnet granite, such as elasticity, failure, cracking and peak stress. Hazzard (1998) created a synthetic rock sample to simulate the release of the acoustic emission, under triaxial stress on Springwell sandstone. The T.K. plot and the b_value when using internal monitoring were inaccurate, but the other results patched the actual test. On the other hand, (Cho et al., 2004) developed a methodology for modelling dilation using the particle flow code (PFC) and stated that the programme captures many of the observations reported in conventional laboratory test results and that the most important factors in controlling dilation and the strength ratio are the geometrical factors, rather than the micro-contact parameters. The other interesting result is that the rotation of particles in assemblage has a significant effect on material strength, although it was noticed that, tests were performed using a synthetic rock mass rather than a real lab tests, which may affect his results. Additionally, he stated that, in PFC, the tensile strength to compressive strength ratio is higher than that measured in the laboratory, although other studies showed that it is possible to obtain accurate tensile strength; for example (Zhao, 2010).

Park (2006) conducted a test on Berea sandstone to measure the fracture toughness and subcritical index. Additionally, it is noticed that the radius multiplier factors were used to study the effect of cementing volume between particles on the rock properties. Additionally, he concluded that the fracture toughness decreased in a linear way with the area of bonds between particles, then provided a method for determining the fracture toughness of very weakly cemented sandstone using modelling results.

Moreover, Potyondy (2012) extended the idea and applications of the PFC code to include the bonded-particle model, that consists of connected breakable and deformable contacts at particle-particle, which will have a much wider application in future, although this research did not mention what the effect of clumped on the calculation time is going to be, because PFC already needs a fast computer, especially when using small particles.

2.8 Modelling hydraulic fracturing

Gil (2005) created an injection model to simulate the fluid injection in Antler Sandstone using PFC 3D. He concluded that the dominant failure mechanism in the hydraulic fracturing operation in poorly consolidated rocks is shear rather than tensile. Additionally, Ivars (2010) studied and presented the theory behind the rock mass model and its generation, using DEM PFC. Then the fractures and joints were studied extensively, using the Smooth-Joint Contact Model (SJM) to model the joints network. He stated that it is possible to model the peak strength, and prepack the post peak behaviour of the rock material and the jointed rock material. In addition, he confirmed the capability of the programme to predict the effect of rock scale on the rock properties and that the type of fractures could be studied in any rock mass too. It is noticed that the model was not compared with an actual sample for the injection test, and he used the same particle size distribution but he used a bigger particle size, which might affect the results.

Moreover, Gong et al. (2011) created a model of (DFM) approach to represent large-scale fractures. The geo-mechanical impact on the micro-fracture system is modelled, in which the rock permeability is sensitive to the stress changes

induced by hydraulic fracturing and pressure draw-down. Simulations have been performed based on the detailed modelling of an actual shale gas reservoir, considering various mechanisms including adsorption/desorption, matrix-fracture transfer, and non-Darcy effects. Sensitivity studies were conducted by varying the production rate, pressure and hydraulic fracture parameters to provide guidance on optimising the stimulation and production designs.

In addition, Shimizu et al. (2011) created a synthetic rock sample and conducted an injection experiment on 12 cases of hydraulic fracturing simulations with different rock properties and different fluid viscosity. His results were comparable with previous lab tests. It was concluded from his study that the shear cracks ratio to tensile cracks were low when fluids with low viscosity were used in the injection test. Additionally, the crack initiation pressure was higher with lower viscosity fluids in the fracturing test because of the infiltration of fluids into the pores near the borehole, that causes additional pore pressure near the borehole. This pore pressure minimises the effect of stresses on the sample.

Furthermore, Sarmadivaleh (2012) conducted a simulation of hydraulic fracturing experiments using a cubic shaped sample containing artificial fractures, then studied the relation between fracturing operation and natural fractures. He also created a PFC 2D model to simulate the injection. The simulation results showed that there is a threshold for the angle of approach below which a hydraulic fracture propagation direction will tend to be directed by the natural fractures regardless of the value of changing the sample's parameters under study.

Marina et al. (2014) created a synthetic model to represent an injection model in the laboratory related to hydraulic fracturing. She performed a test on a hollow cylindrical limestone, and the general parameters for the sample was used in this study, but it is noticed that she used the general rock properties of the limestone not the prices rock sample used in the tests, which must greatly affect the results.

(Tomac, 2014) created a Discrete Element Method using 2D PFC combined coupled with Computational Fluid Dynamics, to understand the nature and properties of fracture propagation in the geothermal system, and found that it was possible to combine both thermal and fluid flow in the code to create the model. The results proved the capability of the code to model the effect temperature in the hydraulic fracturing process.

Moreover, Wang et al. (2014a) created a model of the fracturing process on a coal rock, using PFC2D. This model was then used to explore the relationship between the macroscopic mechanical parameters and the microscopic parameters. It was found that macroscopic mechanical characteristics influence the nucleation and size of the produced cracks too. Then, an imperial formula was tested to determine the breakdown pressure and fracture radius. Further, they stated that the Poisson ratio has a primary effect on the fracture radius, and also has a positive nonlinear correlation with it. Additionally, according to the study, the injection rate and injection time have a positive relationship with the fracture radius. Finally, they concluded that PFC 2D could be used to study the process of hydraulic fracturing and crack propagation. Fatahi and Hossain (2015) Prepared a simulation of both fluid injection (radial fluid) and Darcy flow from side to side (linear flow), then determined the application of their procedure in the field

of modelling reservoirs, although it was noticed that, in the validation process, the results were not compared with real laboratory sample.

(Hofmann, 2015) conducted a study using different hydraulic fracturing scenarios, and used several programmes, including PFC code, using low viscosity, high viscosity, high pressure as fracturing fluids, low pressure, high slurry radius, and low slurry radius. He stated that higher viscosity fluids can create wide fractures with a smaller fracture area. On the other hand, he stated that lower viscosity fluids can create thin fractures with a large fracture area. Because this research was based on a geothermal system, he concentrated on the area of the resulting fracture. In his study, the conclusion was that a large area of the resulting fracture is more important than wide fractures to develop large heat exchange areas but, when higher flow rates are modelled, the results show an increase in fracture aperture with higher flow rates. Furthermore, the equation that was used to determine the aperture of the resulting fractures was derived based on the relation between the aperture and permeability in the Darcy equation.

Kim and Moridis (2015), through using the coupled simulator model studied the fracturing propagation caused by hydraulic fracturing, concluded that, when the injection rate increases, the fracturing rate becomes faster in a nearly linear relation, and when the Young's modulus is high, the aperture of the fracture is low. Additionally, they stated that low tensile strength indices more horizontal fractures of the rock, and that fracturing by gas may generate quicker fractures in shale gas reservoirs than water injection because of the high mobility of gas. In addition, he stated that the volume estimation of fractures by estimating the

injected volume can produce incorrect results because of the presence of gas and water in the reservoir.

2.9 Modelling microseismic events as a result of hydraulic fracturing

Hazzard and Young (2004) created a model to simulate the acoustic emissions from a 2D mine-by tunnel excavation. Comparing the results from the model and the seismic signals from the mine, it appeared that the magnitudes, locations, and focal mechanisms match in an acceptable way the magnitudes, locations, and focal mechanisms of the seismic signals. Then he proved that it is possible to study the mechanisms of the recorded seismicity from “direct observations of particle forces and motions at the seismic sources”. (Hazzard, 1998; Hazzard and Young, 2004).

Al-Busaidi et al. (2005) used the Hazzard code without any development of the model itself to simulate a produced acoustic emission in a granite sample resulting from fluid injection. The model was successful in creating synthetic events similar to the real ones from the lab test. (Diederichs, 2000) conducted confined test studies on a synthetic rock sample using a modified DEM/ PFC 2D from Itasca, and concluded that, although the model cannot simulate unstable crack propagation, it exhibits the same key stages of failure as identified by other authors too. In addition, he noticed the cracks in the post-peak, which dissipate or disperse from the main macro fracture .

Regarding the deformation and its relation to acoustic emissions, Hart (2003) gives a short discerption about the ability of the DEM/PFC code to model the

Kaiser effect, stating that the PFC3D models were used to mimic the various stages of excavating the rock cores, and also that the numerical models showed great potential to increase our understanding about the effect of rock fracturing on the state of stress. He added that these simulation experiments could be used to gain information about the in situ stress distribution in lab tests and field applications too, during reloading and coring, Furthermore, he concluded that, since the impact of the geologic structures and the influence of microseismic activities are 3 dimensional, therefore three dimensional models may produce better results regarding the evaluation of these effects on the stress state. On the other hand, he showed that the use of 3D explicit, dynamic-solution DEM models could be numerically expensive.

Hunt et al. (2003) created a model to simulate 6 centimetre diameter coarse-grained sandstone behaviour under stress to confirm the relation between acoustic emissions and the deformation rate of the rock sample. He stated that, in the simulation, the number of cracks in the PFC model depends on the number of particles constituting the model and that the cumulative number of fractures in the DEM Model is analogous to the cumulative number of the acoustic emissions during a compression test on a real specimen. Although the micro-cracks between the particle bonds in a numerical sample cannot be directly associated with acoustic emissions. Additionally they confirmed that it is possible to mimic rock sample distraction on the macro scale level.

Cai et al. (2007) used PFC code but combined it with another program called FLAC by Itasca to save calculation time. Additionally, Wanne and Young (2007) used Hazzard's code to model the seismic emissions from a PFC cluster

resulting from thermal effects. Furthermore, the code was used to model the acoustic emissions in a rock sample, then used in a bigger model to represent a field case. The only development here was developing the domain creation and the injection code, rather than the seismic code itself (Zhao, 2010; Zhao et al., 2012; Zhao and Young, 2009).

The PFC programme was used by Zang et al. (2013) to study injections in naturally fractured rocks, in order to analyse the scenario of high-pressure fluid injection (hydraulic fracturing) at depth and the associated induced seismicity too. In this model, the calculation of the seismic energy was possible and it was concluded that the cyclic stimulation is safer than the regular stimulation technique. Likewise Jung et al. (2014), studied four kinds of fluid with different viscosities that were injected at various flow rates. Through using PFC code modelling capabilities, it was concluded that the low viscosity fluids infiltrate the pores easily which causes the pore pressure to increase, which will cause a reduction in the effect of stress near the injection pipe but, when the injection rate is high, the fluid cannot penetrate the pores, and then the fractures actually happen before the fluids are reached, and then the fractures will propagate, forming brunches. When exactly the sample reaches break down pressure, tensile cracks are generated around the borehole rapidly. In the process of the growth of existing cracks, the shear cracks occurred. As the existing cracks connect to each other, this connection between the fractures produces tensile fractures.

Likewise, Raziperchikolaee et al. (2014) created a model of a synthetic Berea rock sample and the induced microseismicity resulting from the injection test.

The permeability changes resulting from the deformation of the sample were studied using different network sizes to test their effect on the permeability of the intact Berea sample. Moreover, they stated that the roughness of the fracture may produce tensile forces in the source, leading the source mechanism of the micro-cracks towards tensile opening and increasing the permeability of the rock sample. Additionally, they proved that tensile cracks may occur during failure under low confining pressure, causing an increase in the permeability of the fractures. Anyway, it is noticed that the T.K plot from Hazzard was used which, as shown in chapter three, is not entirely accurate.

Although (Fischer and Guest, 2011) showed through seismological analyses that the presence of the tensile component in the source of microseismic events is related to the differential stress along the pre-existing cracks, the deformation caused by the cracks can have a tensile component in the tensile-shear mode, and that tensile-shear mode events showed smaller seismic magnitudes than shear events.

2.10 The gap in the existing knowledge

It is concluded from see previous section, that since Hazzard (1998) developed his code, the code was not developed much and there is a shortage of studies that tried to develop the code itself. Additionally, there are deficiencies in the model's capability to predict the fracture properties. Added to that, the programme can predict shear and tensile sources of acoustic emissions, but not other types of acoustic emission sources; for example, the pore collapse sources of acoustic emissions. in order to make the code that was developed by Hazzard

(1998) more accurate and give better results these deficiencies has to be addressed and fixed.

Furthermore, there is a shortage of studies related to the relations between the microseismic events properties and the fracture characteristics on the one hand and, on the other hand, there are not enough studies on the relation of the components of the seismic cloud itself and the type of events with their relation to the fracture parameters and resulting permeability after injection, which implies that there is need for an experiment that contains all of these parameters, or a model that makes it easier to study the relation between all of these parameters together.

2.11 Summary

It is possible to monitor and use microseismic monitoring to study the reservoir, and the reservoir fractures caused by hydraulic fracturing. The parameters that can be concluded from microseismic monitoring are the relative position of the fractures, the extent of the fractures, their network connections, the length of the fractures, the permeability of the reservoir. In addition to many more applications, although some results may be over-interpreted.

Using DEM/PFC code in the modelling of a rock samples was successful in capturing the main features of the rock behaviour, and the resulting fracture under stress. Furthermore, the programme can simulate in an acceptable way the resulting seismicity from rocks under stress, in terms of the number of events and the shape of the seismic cloud.

The programme can be used to model the fluid flow and hydraulic fracturing, and reproduce the fractures resulting from the fracturing operations, as well as reproducing synthetic acoustic emissions from synthetic injections into the rock sample or, in the field cases, in terms of magnitude, relative location and determining the source mechanism type. Moreover, it was used to study the focal mechanisms through plotting or observing the forces acting on particles or observing the particles motion, although it may still need development, to be more accurate and to give better results.

Chapter 3 Particle flow code

3.1 Introduction to PFC modelling capabilities

Numerical modelling of the hydraulic fracturing operations, is the process that includes solving all equations that controls the fluid movement in the pores of the rock. And its interactions with surrounding mass. Because of, the very high pressure. The hydraulic fracturing begins, when the failure parameters of the rock mass is full filled in any point of the grid. This happens when the elastic modulus collapse as a result of fluid injection pressure. In addition, the entire system is in interaction with the reservoir fluid's movements. So, there is need for a program to solve all hydraulic fracturing equations to simulate the fracturing process. Then to simulate the induced microseismic activities too, with its sonic properties. As it was concluded from the second chapter.

This means actually, creating a synthetic rock mas by a program which could be used to study, identify rock mass failure and the acoustic emissions that happened during the failure process. In addition, using the program to model fractures in the synthetic rock sample. With, the acoustic emission produced from it, and predicting the mechanism of failure in the case of fluid injection or compression test. It is better to perform dynamic simulations in the model. This means that waves can propagate across the rock sample at a speed that depends on the mass, stiffness and other properties of the model.

The chosen program for that purpose was the distinct element program known as Particle flow code (PFC) by Itasca. In this code, it is possible to create a synthetic rock mass, that can have the same mechanical properties as any

chosen rock sample. The wave propagation is simulated not by using the wave equation. But by more realistic method. Which is recoding the displacement of particles in the model when a force applied to another part of the model. (Itasca Consulting Group, 2005). Furthermore, particles can also be bonded together and when the bonds breaks under stress, the strain energy is released. These bond breakages can be considered as fractures and as sources of the seismic events. The magnitude and the nature of these events could be calculated using seismological equations and seismological theories (Hazzard and Young 2001; Hazzard and Young, 2004). Moreover, the PFC program has been used successfully in the simulation of hydraulic fracturing process. In addition to, many more applications such as fragmentation of rocks, blasting and ground collapse too (Caia et al., 2001; Jing, 2003). For more details about the application of DEM see chapter two. There are two ways to extract seismic information from bond breakage in PFC, then calculate the conversion of energy resulting in the breakage of the bonds between particles into seismic energy, then the moment will be calculated and from moment it is possible to calculate seismic magnitude later on.

3.2 Simulating acoustic emission source

As it was explained previously there two ways to model the acoustic emissions. The first way is to calculate the magnitude of seismic events based on the kinetic energy of each crack between two particles involved, calculating the moment tensor from the force at the contact at the time of bond breakage. This method generally yields magnitudes that are too large. The second method is the one

employed in this research. In this way, the moment tensor can simply be calculated by summing the relevant components of the force at each contact times the distance of the contact from the crack location when a bond breaks (Hazzard et al., 1998; Hazzard and Young 2002).

3.2.1 Calculating the moment tensor.

This method calculates the moment tensor by summing the different components of moment in each crack. This includes the contact force times the distance from the centroid of the balls forming the model, at the contacts around the broken bond. The seismic moment can be calculated from the elements of the moment tensor. "The two particles on either side of the crack (the source particles) will move and contacts surrounding the source particles will suffer some deformation. There will be a force change at the surrounding contacts due to the formation of the crack. We can then perform a integration around the contacts surrounding the crack to calculate components of the moment tensor from the contact locations and force changes. For a discrete medium, the integration is a summation, so the moment tensor can be calculated" (Hazzard, 1998);

$$M_{ij} = \sum_s \Delta f_i \; R_j \tag{13}$$

Where,

Δf_i is the ith component of the change in contact force

R_j is the jth component of the distance between the contact point and the event centroid s the surface S enclosing the event.

The hypocentre of seismic events will be, here, the centre of the crack then after calculating. The scalar moment can be calculated from the elements of the moment tensor matrix;

$$M_o = \left(\frac{\sum_{j=1}^{3} m_j^2}{2}\right)^{1/2} \quad (14)$$

Where,

m_j^2 is the jth eigenvalue of the moment tensor to power 2 (Hazzard, 1998)

3.2.2 Calculating the moment magnitude.

After calculating the seismic moment of the resulting crack, it is easy to calculate the moment magnitude, from the relation between the seismic moment magnitude and the event moment (Hanks and Kanamori, 1979), see equation 3. And 1.4.1.

The duration of the event is determined by assuming that a shear fracture propagates at about half the shear wave velocity of the rock (Madariaga, 1976). This means that the moment tensor and hence the magnitude is calculated in each time step from the recorded time of the bond breakage to double the time. That means if another crack is formed near to the active crack in the double time period mentioned above, then the source areas will be considered as one event, and if the crack happens after that time, it will not be considered as one event. So, by this method, the acoustic events of multiple cracks can be found and more realistic magnitude distributions results will be produced. To test this technique, a model was created of Springwell sandstone made of particles sized about 0.75 to maximum 1.124 millimetre. The model was very successful in representing the acoustic emissions in terms of distribution and number of events (Hazzard,

1998) but the TK plot and the b_value were not accurate enough see chapter four. In this research it was thought using changed combination factor instead of fixed one (the shear wave velocity) and then extending the idea of calibration to include the value of the combination factor, to match the sensor's resolution power will lead to much more accurate results.

3.2.3 Clustering technique

Clustering means studying or collecting a number of seismic events together as if they were one seismic event. In DEM modelling, it will be any series of cracks or bond breakages that could conceivably be part of the same rupturing, shearing or opening episode. This is probably a realistic approach, as it is known that most seismic events in the field are made up of many smaller scale ruptures and shearing of asperities. This was noticed specially in the lab test by (Schubnel et al., 2007) who noticed that, in the last stages of the test, the number of events are so big that it is computationally expensive to separate them and it was stated that it is better to study them as one bigger event. It is also known that events occur over some finite amount of time and that the acoustic emissions are more in number and hardly distinguishable in the last stages of the test. (Bizzarri, 2012; Geller, 1976; Lei et al., 2000).

Another consideration is that, if two cracks occur virtually simultaneously and very close together in space, then the cracks could not technically be considered part of the same rupturing event but would seismically be considered one crack. This mainly depends on the resolution power of events and the position of the sensors to the events.

3.2.4 Comment on the Hazzard code

It is clear that there are some mistakes in the Hazzard model. Firstly, the TK plot is not accurate regarding the internal recoding of events in a quasi-static environment, as shown in Figure 3-4. Secondly the b_ value in the internal recoding was about 4.2 but, in the real lab test, it was about 2.36. Regarding the velocity of rupturing, although the average velocity in the case of real earthquakes is about 0.5-0.7, in reality, the rupture speed is not fixed and is changing continuously in an ascending way. Furthermore, studies have shown that the velocity is not fixed and may vary depending on the size of the sample or type of rocks.

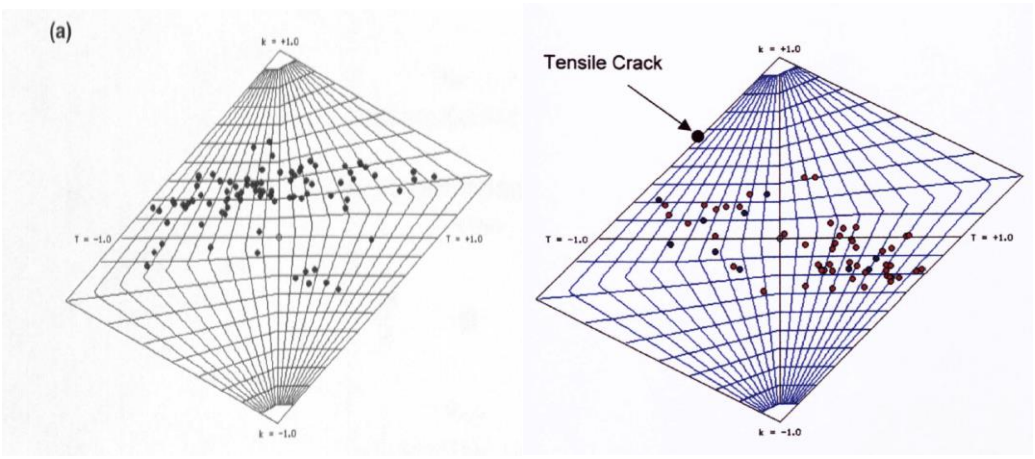

Figure 3-1 A The T.K. plot in the PFC code be Hazzard and B the T.K. plot in the real sample real sample on wright (Hazzard, 1998; Pettitt, 1998)

3.3 Distinct Element Method

First we must differentiate between the discontinuous and continuous models. In the first one medium is distinguished from the other, by having contacts or interfaces between the discrete bodies. The contacts between the discrete

bodies are through bonds, in the case of PFC it is balls. Furthermore, the distinct element method (DEM) is a numerical method used to describe the mechanical behaviour of discontinuous bodies. PFC is a simplified implementation of it. Because, it uses balls in the case of 3D to simplify contact detection and contact changes between elements for faster solutions (Itasca Consulting Group, 2005).

3.4 Cycling in DEM and PFC

This is a dynamic operation or the speed of propagation of mechanical changes depends on the physical properties, of the discontinuous medium. By assuming that the velocities and accelerations are constant within each time step. The dynamic behaviour is represented numerically, using a time-stepping algorithm. “The solution scheme is identical to that used by the explicit finite-difference method for continuum analysis. The DEM is based upon the idea that the time step chosen may be so small that during a single time step, disturbances cannot propagate further from any particle than its immediate neighbours. Then the forces acting on any particle are determined exclusively at all times by its interaction with the particles with which it is in contact. Since the speed at which a disturbance can propagate is a function of the physical properties of the discrete system, a time step can be calculated to satisfy this constraint. The use of an explicit, in contrast to an implicit, numerical scheme makes it possible to simulate the nonlinear interaction of a large number of particles without excessive memory requirements or the need for an iterative procedure. The calculations performed in the DEM alternate between the application of Newton’s second law to the particles and a force-displacement law at the contacts.

Newton’s second law is used to determine the motion of each particle arising from the contact and body forces acting upon it, while the force-displacement law is used to update the contact forces arising from the relative motion at each contact. The presence of walls in PFC requires only that the force-displacement law account for ball-wall contacts. Newton’s second law is not applied to walls, since the wall motion is specified by the user."

In any cycling, there are repeated calculation of the law of motion to each particle and force-displacement law to each contact with a constant updating of the wall positions and contacts, which may exist or not and the contacts could be formed and broken during a simulation. Moreover, it is possible to say that The DEM name is used to a program that only allows the (discrete bodies) or the balls rotations. That has finite movement with complete detachment, and the ability to recognizes new contacts automatically during the progresses of the calculation. The term “distinct element method” was appointed to refer to the particular DEM. That uses an explicit time-domain solution of the original equations of motion and deformable contacts (Cundall and Starck, 1979) see Figure 3-2.

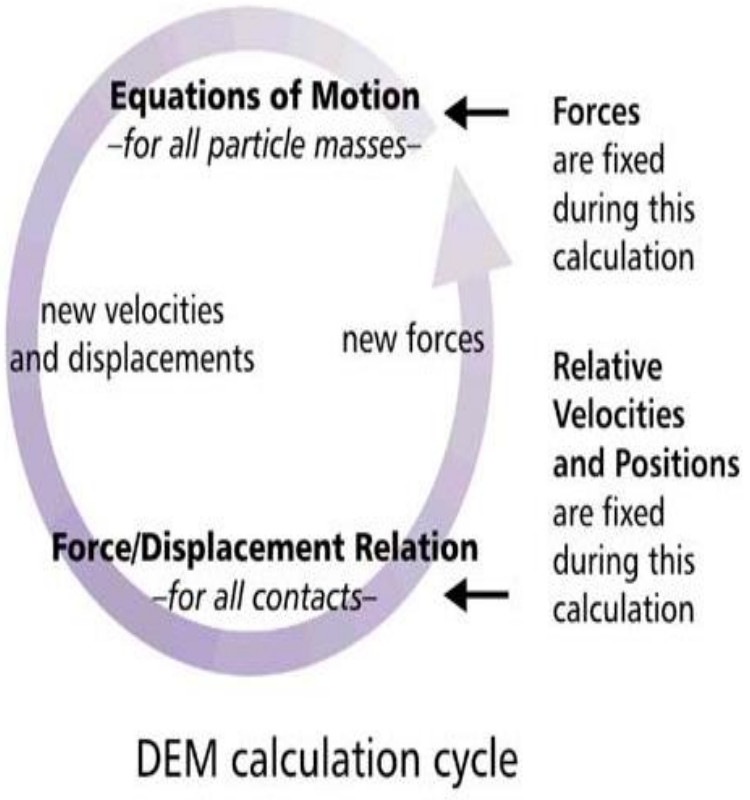

Figure 3-2 Components of the explicit, dynamic solution scheme in DEM(Hart, 2003)

3.5 General formulation in the PFC 3D

The program used in this research is distinct element based program called PFC/ 3D by Itasca Company. As it was pointed out previously. The key belongs to the University of Leeds. In the program the models is composed of particles which are spherical rigid bodies in the case of (3D) with predetermined mass. These particles can move independently of one another and can overlap and rotate.

Furthermore, the particles can be connected together with bonds like a cement. Having microscopic parameters, as input for particle and the bonds between them. This will make it possible to control the macroscopic behaviour of physical specimens, like young modulus, Poisson ratio, tensile strength and UCS. The

boundaries of the particles are walls that acts as boundary to the particles. It is used to create a synthetic force on the particles. In addition, the walls can move in any specified velocity to impose pressure on the particles, or could be removed if the desired stress or pressure is fulfilled. In the code, the contacts are assigned by commands with different value. It could break automatically during the process of a simulation, when the stress overcome the value of the contacts.

Moreover, the interaction between particles are computed repeatedly. Then updated by a time-stepping algorithm at the start of each time-step. Contacts are updated from the known particle and wall positions. The force-displacement law updates contact according to the relative motion between particles and the contact constitutive model .Particle accelerations are computed according to the resulted force and the moment acts one it. It is worthy of mentioning that the units used in PFC/3D is SI units [kg/m3] for density, particle stiffness in [N/m], the parallel-bond stiffness contact-bond strength [N/m3] and [N] for and [N/m2] in the parallel-bond strength measurements (Hazzard, 1998) see figure 3-3.

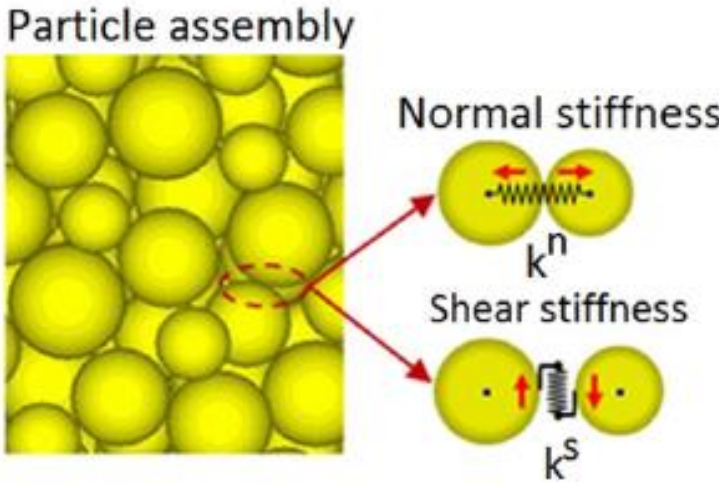

Figure 3-3 Particles collection and relative normal to tangential forces modified from (Fatahi and Hossain, 2015)

3.6 Calibration of the model

As it was mentioned in the previous section . There are bonds between particles that connects the particles together. These bonds stiffness's and strength (micro-properties) controls the model Marco properties. These micro-properties like micro-stiffness and micro-strength of particles and bonds, can be adjusted to reproduce real macro properties of the rock sample. The micro-parameters are required to model a specific rock sample properties are listed in Table 3-3. That are generated in which the particle specified stiffness influences the macro stiffness (Young's modulus) of the rock being modelled. It must be clear that calibration means changing the micro parameters. Then doing the uniaxial tests, biaxial test, or Brazilian test, or any other needed test to get the desired parameters. If the parameter was not correct, then going on with the selected tests, again and again until the desired macro parameter is achieved. This means repeating the calibration process several times until all the macro parameters measured in the model is equal or near the parameters(Young modulus, Poisson ratio, tensile strength and UCS) of the real sample.

The macroscopic strength can be calibrated either to unconfined compressive strength, tensile strength, Young modulus, and Poisson ratio (Itasca Consulting Group, 2005).

Table 3-1 Micro parameters and Units of PFC3D code

Parameter	Unit	Discerption
ρ	Kg/m^2	Particle density
r	m	Minimum particle radius
r_g		Particle size ratio
E_c	GPa	Particle Young modulus
k_n/k_s		Particle stiffness ratio
μ		Particle friction coefficient
σ_c^-	MPa	Particle bond tensile strength Mean and standard deviation
t_c^-	MPa	Particles bond shear strength Mean and standard deviation
γ^-		Parallel-bond radius multiplier
E_c^-	GPa	Parallel-bond young modulus
k_n^-/k_s^-		Parallel-bond stiffness ratio

3.7 DEM modelling of fluid flow in the synthetic sample.

In the PFC code, the fluid flow is simulated by creating a small reservoir that is called "domain" between every four balls. And these domains will be connected to each other by "pipes". The length of the pipes is calculated for each neighbouring domain (Itasca Consulting Group, 2004). As far as the fluid is concerned, the cylindrical pipe has the length (l) and cubic pipe aperture a^3.

The flow rate q is calculated by

$$q = k\ a^3\left(\frac{p_2 - p_{21}}{i}\right) \quad (15)$$

Where $(p_2 - p_{21})$ is the pressure difference between the two adjacent domains, i is the length of the pipe, and k is the conductivity factor and could be defined as

$$k = \pi a/(16\mu) \quad (16)$$

Where,

μ is the fluid viscosity.

Fluid pressure in the reservoirs are updated over each time step, and act on the surrounding particles as equivalent body forces. The change in fluid pressure, *ΔP*, within each reservoir, resulting from the flow from the surrounding pipes ∑Q in one time step, Δt , can then be calculated from the fluid bulk modulus K_f and the apparent volume of the reservoir V_d by application of the continuity equation in the form of

$$\Delta p = \frac{K_f}{V_d}(\sum q\, \Delta t - \Delta V_d) \quad (17)$$

In order to enable hydro-mechanical interaction to occur between particles and the force resulted from the pressure the pipe aperture decrease by the effect of force on it according to

$$a = \frac{a_0 * f_0}{f + f_0} \quad (18)$$

Wheref_0 is the value of normal force *F*, at which the pipe aperture decreases to a_0/2.

When the calculation starts every domain receives flows from the enamouring pipes, which will cause increase in fluid pressure given by Eq.16. then the effect of pressure on the walls of pipes and domains will cause the mechanical interactions or coupling .

In order to calculate the initial pipe aperture, it is necessary to either run a Darcy flow test or use the relation between permeability of the sample and pipe aperture. If the permeability of the real sample was known, and if we assume

that all apertures are the same which is possible in a statistically uniform model, then the initial pipe aperture before starting fluid movement can then be calculated. This an important step to insure that model will have the same permeability as it in the real sample see 3.7. (AL-busaidi, 2004; Jung et al., 2014; Zhao, 2010).

3.7.1 simulation of an injection test

In the simulation of an injection test, an anisotropic stress state is produced by moving fixed balls in the synthetic sample at the side boundaries of the sample, toward the central axis of the column. Then these boundaries are fixed to make sure that the largest compressive stress will be in the horizontal direction. The apparent aperture therefore depends on normal force (when the contact is in compression) and the gap between the particles (when the contact is in tension). The strength of this dependency is not great, but is sufficient to give rise to a mechanism similar to hydro-fracturing (Itasca Consulting Group, 2005). The fluid flow through a pipe is considered as a laminar flow through two parallel plates that has the same aperture between the walls of the pipes. The fluid flow will be calculated according to equation 13.

Fluid flow through a pipe is considered a laminar flow through parallel plates. That has the aperture ($Aper$) between the walls of the (pipes), with pipe length (i), Then the rate of volumetric flow (Q) in each pipe is determined by;

$$q_p = a\text{^}4(dp/12 * u * i) \quad (19)$$

Where,

a is the aperture of the pipe

q_p is the fluid flow in the pipe

And regarding the time step calculation equation

$$\Delta t = S_f * (\frac{12*u*i*V_d}{N*K_f*Aa^4}) \quad (20)$$

Where,

S_f is the safety factor

u is the viscosity of the injected fluid

V_d is the domain volume

n is the number of pipes connected to the domain

a is the aperture of the pipe

K_f is the bulk density of fluid

In addition, in each time step the aperture of the pipes is updated.

3.7.2 Calculating the aperture

Before starting the calculation, the initial aperture of the pipes has to be calculated so that the model will have the permeability of the real rock sample through using this initial in the calculation. This could be done through the relation below (Al-Busaidi et al., 2005; Zhao, 2010);

$$k = \frac{\sum_p La^3}{12\,\pi \sum_b R^2} \quad (21)$$

Where,

$\sum_p La^3$ is the cubic summation of the length of the pipes.

$\sum_b R^2$ is the square of the radius of the balls in the model..

$$a_0 = \sqrt[3]{\frac{12*k*3.14*\sum_{balls} R^2}{\sum_{Nt} i}} \quad (22)$$

Where,

k is the true permeability of the sample in metres square.

$\sum_{balls} R^2$ is the square of all ball radiuses summation in the sample.

$\sum_{Nt} i$ is the summation of all the pipe radiuses in the sample.

To validate the calculated aperture, it is possible to a run permeability test. Then when a steady flow is achieved, it is possible to calculate the permeability of the synthetic sample. This calculation could be easily done using a developed code in the PFC or it is possible to do it manually. In addition it is possible to calculate the initial aperture using calibration process but unfittingly it is time consuming.

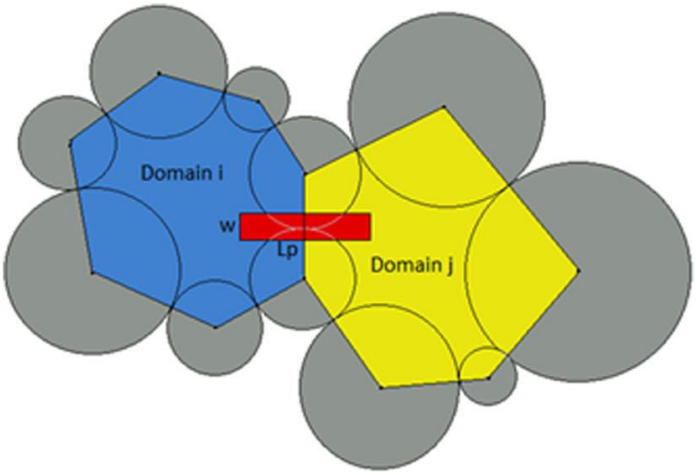

Figure 3-4 Two domains, in blue and yellow, are created between the balls and the pipe that connects each of them is shown in red (Fatahi and Hossain, 2015)

3.8 Modelling the acoustic properties of rocks using PFC code

It is possible to use the vertical or horizontal movement of particles to simulate the movement of particles under mechanical force. This will cause the generation of mechanical waves. It is possible to use the particles that produce the wave as the source and the particles that are used to measure the displacement as geophones or receivers, then use the relative movement between the particles as a measure of the velocity of the waves, assuming that the particle string is equivalent to a continuous bar. An example of this case is in a string of pearls that has been generated. A wave was generated, then the three curves correspond to the left-hand end, the middle and the right-hand end of the bar. The time interval between each peak is 0.25 seconds, which means that the velocity is 100 m/sec. The time history for the right-hand end shows a peak velocity of double the input velocity. In this example, circular cross-r which is the particle radius too, in this case. The Young's modulus is expressed

$$E = \frac{f}{3.14(r^2)} \frac{2r}{U} \tag{23}$$

f is the contact force

U is the contact displacement

And because $\frac{f}{u} = \frac{kn}{2}$ where kn is the normal stiffness;

$$E = k_n /3.14r \tag{24}$$

And the particle mass is equal to a third of bar relent mass;

$$P_b = (3/2)p \tag{25}$$

The P_wave $P_{w.ve}$ is

$$P_{w.ve} = \sqrt{E/p} \tag{26}$$

To create a wave pulse that is double the equivalent force at the boundary is applied, then a graph of the relative movement is created between the source and any particle that represents the receiver.

This model was developed by Hazzard (1998) to measure in an efficient way the velocity of the p-wave in a granite model. The PFC string model was a string made up of 640 particles. The string was created so that the particles were just touching such that zero normal force existed at the contacts prior to testing. The particle diameter 10m, Particle density 2000 kg/m3, and the Contact Young's modulus was 55GPa. Now notice that these microparameters are the same as granite micro Properties. Then in order to test the wave velocity in the model, he assumed that the string of particles actually represents a continuum bar with a square cross. The particle's linear normal stiffness's (in N/m) are given. Then a displacement force (double the equivalent force at the first particle) is placed at the beginning of the string of particles. The displacement of a few chosen particles was measured, then the time difference was used to calculate the velocity.

In the Hazzard model, which represented the granite model, the measured velocity was an average of (7215) m/s, which represents an error of less than 0.5% from the analytical value. Note that a sample was taken every 0.1 ms; therefore an error of one sample point is approximately equal to 10 m/s at 500 m from the source.

3.9 Setting particle density

The density of the particles is determined based on the material bulk density, so the mass of one particle in PFC must be the same as the mass of the volume of the PFC balls that they represent in the real sample. The mass depends on the porosity so that;

$$P * V_t = m \tag{27}$$

Where P is the density

V_t is the total volume and m is the mass. If it was assumed that the mass of the model is the same mass as in the real sample, then

$$P_d * V_p = m \tag{28}$$

Where P_b and V_p are the density and volume of the PFC balls respectively. Because, since the program used here is the DEM program that means that the model is not a continuum. Then, incorrect wave propagation will be noticed if the density was not correct. Then this equations becomes;

$$P_b * V_t(1 - \emptyset) = m \tag{29}$$

where $\emptyset$ is the porosity

$$P_b = p/(1 - \emptyset) \tag{30}$$

Now in the modelling of the wave propagation, in order to get the accurate P-wave velocity, the density needs to be adjusted.

In the case of modelling wave propagation as pointed out, the velocity of the P-wave could be determined by creating a string of particles, then applying a

frequent double horizontal force on the beginning of the particles, then receiving the displacements in several particles that work as sensors. By calculating the displacement time, and comparing them with the displacement in the first particle, it is possible to get the velocity of the wave in the string, which must have the same micromechanical properties as the model. Then, by changing the different density in each test, it is possible to get the right particle density that gives the desired p-wave velocity. After getting that specific density that gave the model the exact p-wave velocity, it will be used in the modelling process.

Knowing that the effect of density on the mechanical properties is very small, it is desired to achieve the uniaxial and biaxial tests first till the appropriate micromechanical properties are achieved (Young modulus, Poisson ratio). then create the string and measure the p-wave velocity to get the desired density, which will be used when creating the model.

3.10 Dynamic simulation for acoustic emissions.

It is possible to assume that each break of bonds in PFC is a microcrack. The crack direction is perpendicular to the line joining the two centres of the balls in the PFC model. Furthermore, if more than one crack is formed at one time, it is possible to join them in one event, which is a measure of the energy loss of the acoustic waves' propagation in the rock. Now, in PFC, if the model was run dynamically with a low level of numerical damping, it will be possible in the code to achieve a realistic level of attenuations. The units that measure attenuation in rocks are quality factor Q., where Q is defined as 2 π times the ratio of stored energy to dissipated energy in one wavelength and if W is the peak strain energy

during the cycle. The larger the Q, the lower the attenuation. Then, for a single degree of freedom system, according to (Hazzard, 1998)

$$Q = 2\pi * W/\Delta W \tag{31}$$

Where,

Q is the attenuation

W peak strain energy during the cycle

ΔW dissipated energy in one wavelength

α is the damping value which could be assigned through the code.

In reality, it is difficult to calculate Q directly and instead it is usually calculated by propagating waves through the medium and determining the changes in energy of the waves $R_j M_o$ with distance or time (Hazzard, 1998):

3.11 Predicting the deformation of the surface and curvature of the surface.

In 2009, Hautmann et al. (2009) simulated the deformation of the surface resulting from a dyke and Cho et al. (2004) modelled the dilatation in a rock sample under stress, while Le Guen et al. (2007) simulated surface deformation using PFC and stated that the accuracy of this procedure depends on the accuracy of the model parameters. On the other hand, Hunt et al. (2003) simulated the Kaiser effect and the deformation of sandstone using PFC in a uniaxial test and cyclic loading.

It is possible to choose two balls and measure the displacement between them in order to predict the surface curvature. Additionally it is also possible to measure the deformation of the surface of the model by picking a ball and measuring the displacement alone in the model boarder. This technique could work side by side with the acoustic emission results in order, to get the surface curvature and the deformation, which will help in the future development of the model to study hydraulic fracturing in a real field case. Although PFC code has been used to measure surface deformation as a result of injection, however, this is the first time, to the author's knowledge, that the surface curvature and the displacement have been measured combined with acoustic emissions by this technique.

3.12 Summary

It is concluded from all of the studies presented in the previous sections that the PFC program has the capability to be used as a simulation program to create a model for rocks and other materials. It uses balls as discrete bodies connected by bonds, with predetermined density and micro-mechanical properties that control the macro-mechanical characteristics (Young modules, Poisson ratio and UCS) of the modelled rock. In addition, the program has the capability to adjust the macro-parameters with the micro-parameters between the bonds and to create models of different particles, having different mechanical properties which will make the rock model act in a realistic way.

In addition, these models can actually represent the reality of the original materials' behaviour. This characteristic makes it very accurate in simulating rock behaviour under stress.

Furthermore, it is possible to produce acoustic emission (micro-seismic) events in the case of failure and to reproduce the source mechanic, seismic magnitude and to plot the b-value.

Chapter 4 Preliminary models of induced seismicity in a rock sample

4.1 Introduction

Studying hydraulic fracturing is necessary in gas and oil production from unconventional reservoirs to meet the global demand for oil and gas, in order to achieve efficient production and predict potential seismicity problems. Additionally modelling the fracturing process and the resulting microseismicity can also help to understand and interpret the recorded microseismic data. Moreover, the microseismic models could be used to study the relation between microseismicity and the fracturing process itself (Raziperchikolaee et al., 2014; Zhang and Bian, 2015; Zhao, 2010).

A review of the existing computational models (see Chapter 2) indicated that the Distinct Element Method (DEM) had the capability to create dynamic models for accurately reproducing fracture events. Potyondy et al. (1996) described the use of DEM/PFC code to reproduce and model elastic deformation, and fractures of the rock samples under stress, and pointed out that this code could be used to capture the mechanical characteristic properties of Lac du Bonnet granite, such as elasticity, failure, and peak stress. Additionally, Hazzard (1998) created a model for simulating acoustic emissions using the DEM program PFC by Itasca. The model reproduced a synthetic acoustic emission resulting from a Springwell sandstone under triaxial test. The model was able to produce a similar b_value and acoustic emission number beside the position of the events (Hazzard, 1998; Hazzard and Young, 2004).

Although there were many applications of the DEM code initially developed by Hazzard (Al‐Busaidi et al., 2005; Wanne and Young, 2007; Zang et al., 2013), this code still had some fundamental weaknesses in simulating seismic events, such as using a fixed rupture speed to control the combination of events to form clusters, that influences the accuracy of the b_value and T.K. plot from the modelling results. The recent developments in DEM simulations of seismic events focused on the domain creation and the injection of fluids algorithms, but not on improving the seismic code itself (Zhao, 2010; Zhao et al., 2012; Zhao and Young, 2009).

The aim of this research is to develop a modified modelling scheme based on the existing codes to adopt changing combination factors, instead of fixed ones, to improve our understanding about the relation between microseismicity and hydraulic fracturing, For validation purposes, the developed model was first used to recreate some simple acoustic emission cases. The modelling results were compared to the real tests. The equation used in the model were initially developed for earthquakes, as they are similar in size distribution, stress drop and source characteristics (Lei and Ma, 2014; McLaskey et al., 2014).Then, the developed model is used to study two simple hydraulic fracturing cases from a lab test, one of them on granite and the other on sandstone (Matsunaga et al., 1993; Stanchits et al., 2011).

Moreover, the used values in the all models in this study are the default values unless otherwise stated, any changed value from the default will be mentioned.

4.2 DEM modelling of seismicity

When a bond breaks as a result of stress, it releases energy and a crack is formed in that position. The direction of the crack should be perpendicular to the bond between the two particles. The amount of released energy is proportional to the strength of the bond which is determined by the aforementioned calibration tests. Furthermore, with numerical damping, a DEM model of a synthetic rock sample can produce realistic levels of attenuation, and thus every crack causes a release of stored energy as an acoustic wave. The space/time distribution can be monitored in a DEM model, which means that, when a crack is formed, the program will record the position and properties of the crack. After the bond breaks, the displacement of the particles and the moment tensor produced from such movement can also be calculated. Then it is possible to determine other seismic parameters produced from the crack, such the type of fracture: either a shear or tensile fracture.

The seismic moment is calculated by using the following equation at the contacts surrounding the source:

$$M_{IJ} = \sum_S \Delta F_i \; R_i \tag{32}$$

Where,

ΔF_i is the change in contact force, and R_i is the distance between the contact point and the event centroid.

The sum is performed over the surface *S* enclosing the event. The moment tensor is a result of all forces affecting the fracture (Hazzard and Young 2002; Potyondy and Cundall, 2004; Zhao, 2010).

Furthermore, the relative contributions of different source types from the recorded event can be shown in a T-K plot (Hazzard, 1998; Hudson et al., 1989).

4.3 Multiple cracks joining to create seismic clusters.

It was assumed in Hazzard's model that a fracture propagates at half of the shear wave velocity in the rock, in this way the duration of the event is determined by the time it would take a shear wave to propagate to the edge of the source area, equation 33 is the imperial equation that was used in the previous model to determine the duration of events (Hazzard, 1998) which refer to as ae_mkes

$$ae\_mkes = 2 \times (md\_ravg) \,/\, (com\_fac * AE\_SVEL) \quad (33)$$

Where,

com_fac is the combination factor which is equal to 0.5 in the original code which will be refer to as C.F.

md_ravg is the average particle radius

AE_SVEL is the shear wave velocity at each time step.

In addition to that, the moments are calculated for all active events each time step, from the time of breaking the bond to double the time it would take a shear wave to propagate to the edge of the source area. During this time the crack will be considered as an active crack. Or If a crack is formed around one particle diameter from the source area of another crack, then it will be considered active too.

Furthermore, active cracks could be combined with other active cracks and none active ones in the model. If any crack in the model was formed next to the active

crack in a way that the source areas of both cracks overlapped, or If any other crack formed in the same duration time of another active crack. Then the two cracks will be considered part of the same event. In this way, events made up of the cluster of cracks could be combined, and more realistic b_value with acceptable magnitude distributions results could be achieved (Hazzard and Young 2002).

In this research, the duration of the event are not fixed and it could be twice the shear wave or half of the shear wave. That means the duration of the event is controlled by the user and it is changed around the simulation test, which means more controlling on the number of events that are produced in any stage. Varying the duration of event would allow the model to achieve more accurate results for the number of events and hence better b_value. This process opens a door for more applications, because If we can determine when and how many cracks are forming in an event in a specific time it will be possible to mimic the resolution power of the geophones. Moreover, Hazzard (1998) Stated that in his model no consideration has been made for the movements of surrounding particles close to the cracks. Because, the moment tensors were calculated based on the moments of balls involved in each crack only. Not all the particles that moves around the crack and cause reversal of the value of T and K in the case of shear vents . In order, to remove the effect of this moving particles a correction factor (-1) was multiplied by the value of T, and the results were acceptable see 4.4.

4.4 Acoustic emission monitoring in PFC

There are two ways of monitoring seismic events during the fracturing process: internal monitoring by recording the crack information by the code itself, when a crack is formed and external monitoring through choosing a ball that will simulate the work of the sensors. In this research, the results of the acoustic emissions in the model are monitored internally by recoding the forces applied on the particles around the fracture, not by using external balls because the developed program will be used in future studies to study the crack characteristics of the source that form the acoustic emission events. Additionally, the internal monitoring was not accurate in the original Hazzard's code so some modifications will be made.

4.5 The simulated lab test and modelling procedures

A triaxial test on cubic 58.8 mm thickness Springwell sandstone, as reported by (Pettitt, 1998), is chosen to be simulated to validate the developed model. The model was then generated and the results were compared with Hazard's code and with real test too, in order to prove the validity of the developments in the code.

4.5.1 The lab test

A tri-axial test on cubic 58.8 mm thickness Springwell sandstone was chosen to be simulated. as reported by (Pettitt, 1998). The rock sample is composed of particles sized between 0.75-1.27 *mm* with porosity of about 35%. In addition, a uniaxial and tri-axial test was performed on the sample to get the mechanical properties of the rock sample. The rock parameters are listed in table 4-1. The

test was carried out under a confined stress of 2 MPs. Then a direct load was applied, till it reached about 70 MPs, and then the sample was unloaded directly before failure. In this test, there were 8 sensors all around the sample registering the acoustic emission recorded as a result of cracking in the sample. During the test, about 1175 events were recorded a T.K. plot was plotted to study the events' source type. This was explained in more detail in chapter one. In addition to that, the b-values were plotted during the test (Pettitt, 1998).

4.6 Model generation

It was decided to generate a model with parameters as close as possible to the real test. Therefore, a model was generated with a DEM/ PFC 3D program.

The synthetic rock sample is composed of particles sized between 0.75-1.27 *mm*, as in the real rock sample. The particles were connected using parallel bonds. The porosity of the synthetic rock sample is 35%. A calibration process was carried out to match the mechanical properties of the real sandstone sample and the synthetic model, as listed in Table 4-1. Knowing that default values for the properties were used unless otherwise stated, and the stress strain curve is in figure 4-1 in which the balls are yellow and the cracks are red for tensile and blue for shear type while the walls are in top and bottom are dark blue.

After the material calibrations the model was modified to the dimension used in the real AE test. The cubic synthetic sample was subjected to a triaxial loading and the loading was stopped before final failure, as in the laboratory test. The test was under confined stress of 2 MPa. Then a direct load was applied until it reached about 70 MPa. Finally, the sample was unloaded directly before failure.

In the real lab tests, there were 8 sensors placed all around the sample to record the acoustic emission as a result of cracking in the sample. During the experimental test, about 1175 events were recorded and the b-values were plotted during the test. The T.K. plot was plotted to study the event's source type but, in the plotting of the b_value and the T.K. plot, the clearest 87 events from the 1175 events were used only. These results will be used to compare with the modelling results later. In this research, the results of acoustic emissions in the model are monitored internally by recoding the forces applied on the particles around the fracture. Additionally, the internal monitoring was not accurate in the original Hazzard's code, so some modifications were made. Now the hypocentre of the position of the events in the simulation test is as shown below in Figure 4-2 A, with real the hypocentre in the real test Figure 4-2 B.

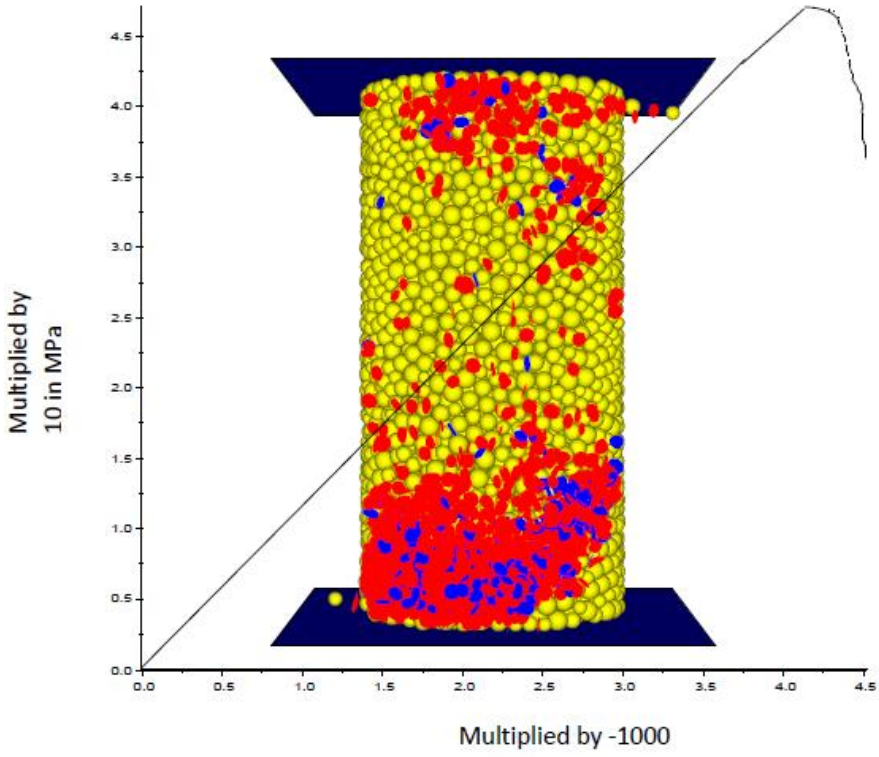

Figure 4-1 The synthetic uniaxial test on the cylindrical Springwell sandstone the vertical axes is stress in Pa while the horizontal is in strain.

Table 4-1 The mechanical properties of the Springwell sandstone synthetic and real sample

Type of experiment	Young modulus / GPa	Poisson Ratio	UCS MPa
Real confined lab test	14.1	0.294	64.3
Real unconfined lab test	12.2	0.355	46.7
PFC3d parallel bonded model/unconfined	11.37-13.03	0.372 -0.3287	47 - 4.9
Pfc 3D parallel bonded Model /confined	11.752-13.03	0.2899-0.2978	55.87-59.50

The hypocentre of the acoustic emissions from the DEM modelling is plotted Figure 4-2. Compared with the laboratory results, the distribution of the acoustic emission events from the DEM model seems to be similar to that of the lab recordings.

The number of acoustic emissions that were recorded during our simulation test using the modified code was about 1220 acoustic emission events, while the number of acoustic emissions in the real lab test were about 1175 events. In the original code, however, the number of acoustic events recorded during the simulation test was about 995 events in the test. It is clear from the numerical tests that the combination factor plays an important role in DEM models. In order, to obtain accurate results in terms of event population and distributions by controlling the number of events that could be combined in clusters. In Figure 4-2 C the particles or balls are presented the red and blue spots are the places of the bonds that represent the induced fractures that were broken and it clear that

there is similarity between the positions of the fractures and the positions of the acoustic emissions which is a good indication about the accuracy of the model.

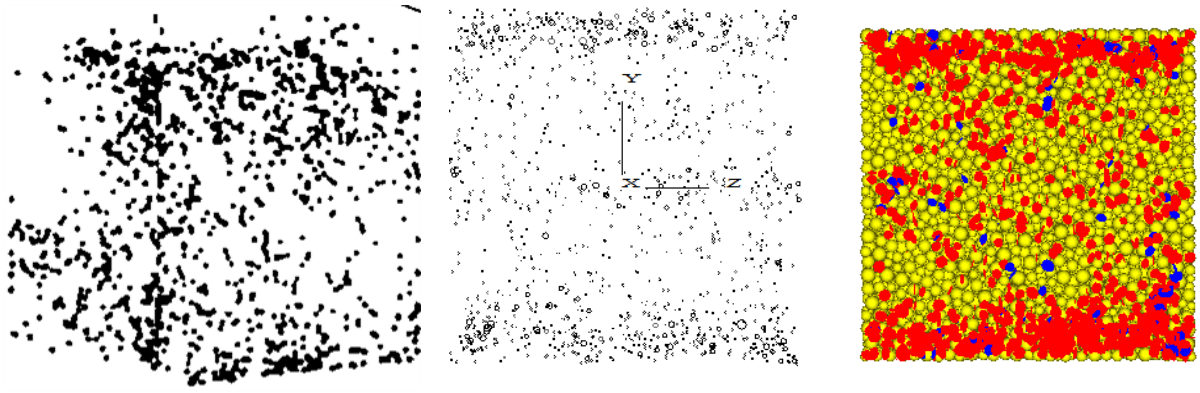

A B C

Figure 4-2 The acoustic emission event distribution. A, in a real rock sample . (Pettitt, 1998) B, in the synthetic sample, C the fractures red blue and particles yellow in the synthetic sample

The b-value in the laboratory test was about 2.36, the continuous yellow line in Figure 4-2. On the other hand, in the DEM model, the b_value was about 2.28 wich is the slope of the continuous green line in Figure 4-3, when changing the combination factor in an asecnding way, as mentioned earlier but, when keeping the combination factor 0.5 constant, the b_value is about 1.66 (the blue line in Figure 4-3). The main diffrence in Figure 4-2 is the number of events in the real test that were used to plot the b_value were only 87 events, not the entire 1175 events. It is clear from all of the dashed parts of the curves that represent the unused part of the curve to calculate the b_value in Figure 4-3, that we were able to retrieve all of the missed data in the test. In addtion, the better slope or the b_value improvement indicates that it is possible to improve the b_value by changing the combination factor. It is also noticed from the above results that the

technique of changing the combination factor can lead to more realistic results, in terms of the number of events and the b_value. The T.K. plots from the DEM modelling and laboratory test are compared in Figure 4-4 A and B.

It shows that most of cracks have a complex cracking mechanism which is some mixture of opening and shear mechanism, and there are hardly any pure shear or pure tensile fractures. The only difference between the T.K plot in the real and the model results is that, in the real test, they only plotted 87 of the events, while in the simulation test, we plotted all of the events. Moreover, it is clear from the length of the curve in the b_value curve and the number of events plotted in the T.K. plot chart that modelling can be used for the sake of recovering missing data.

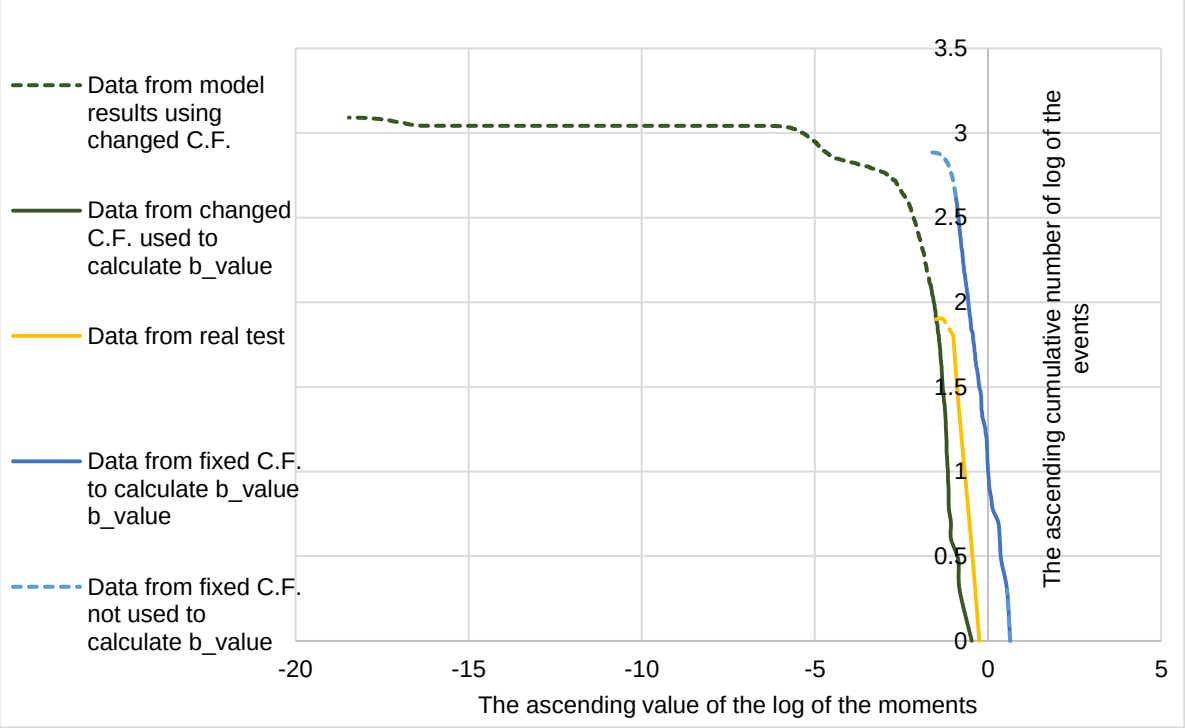

Figure 4-3 The b_value from the modelling experiment, changed C.F. the com_fac in equation 34. green line, real case yellow, the blue line is using a constant combination factor.

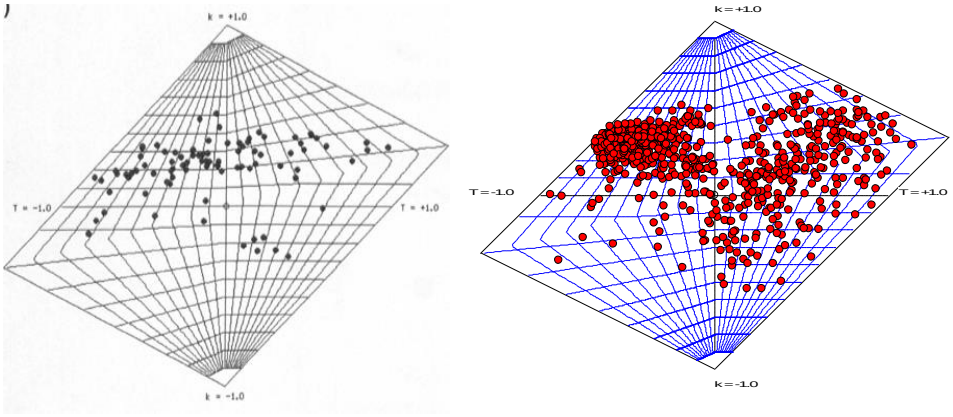

A **B**

Figure 4-4 . The T.K. plot resulting from A synthetic test B real test (Pettitt, 1998)

As it was pointed out in Chapter 1 and chapter 2, since the seismic moment and magnitudes can be computed from the modelling results. Then in the present DEM model it is possible to calculate the ruptured area and length of the fracture can be obtained. therefore it is possible to predict the resulted aperture of each fracture in the model Olson (2003); Wells and Coppersmith (1994b) Klimczak et al. (2010) Olson (2003) see 2.3.

The calculated aperture of the fractures in the model are shown in Figure 4-5. The predicted aperture is acceptable and it varies between (1e-5*m*--1e-6*m*) which is in good agreement with other studies in granite under stress, as observed by Zang et al. (2000).

It is obvious now that the model could be used to simulate more complicated situations as it is the case in the fluid injection tests.

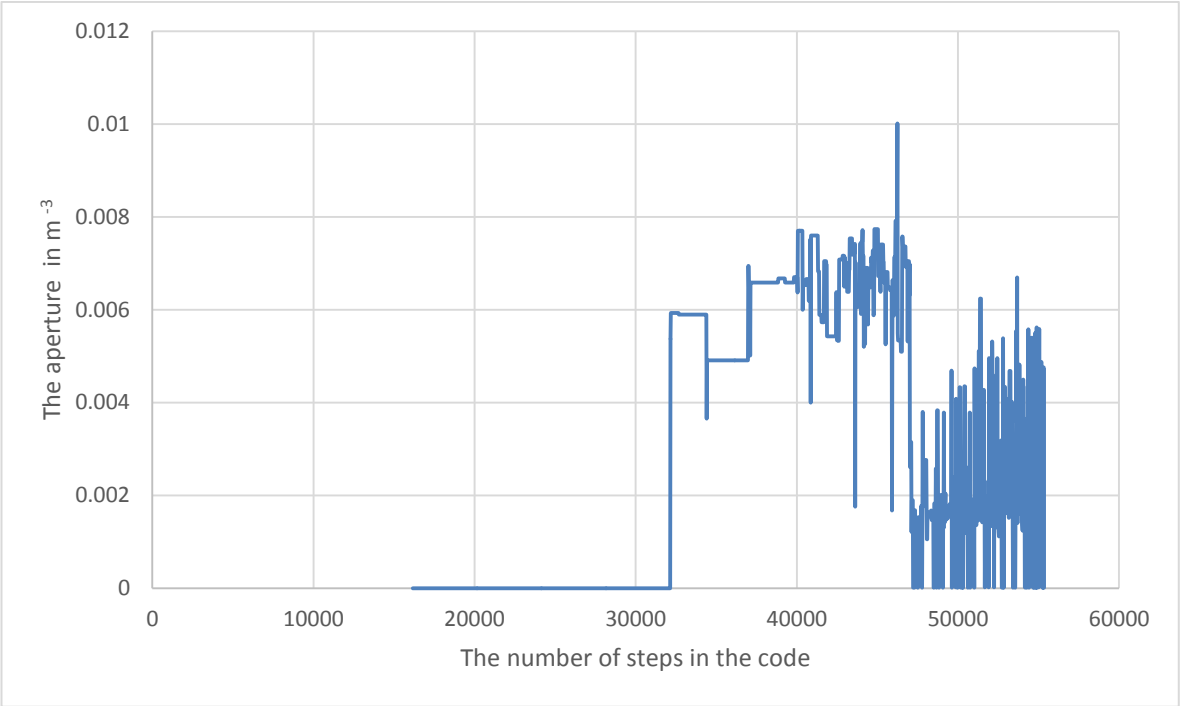

Figure 4-5 The resulting aperture from the triaxial test as predicted by the DEM

4.7 DEM modelling of the fluid injection test

A small injection test, as reported in Matsunaga et al. (1993), is used to validate the DEM model for predicting microseismic events caused by hydraulic fracturing. The experiment to be simulated is the injection test on a granite sample using water. In the injection test, a cubic granite sample with dimensions of about 20 cm was bi-axially loaded using flat jacks to 12.2 MPa and 6 MPa. The material properties of the Inada granite sample are listed in Table 4-2 (Lin, 2002).

In the real sample, the injection test with water started at the centre of the sample, and stopped when the fracture appeared on the surface. The pressure of the injected water was measured during the process, as shown in Figure 4-6.

The total number of recorded acoustic emissions that were possible to determine their location in the granite sample were 446 events. Unfortunately the were no figure that represent the hypocentre distribution of the events in the sample.

Table 4-2 The macro mechanical properties of the real granite sample (Lin, 2002)

Parameter	Value range
Poisson's Ratio	0.30
Elastic Modulus, (in GPa)	62
Unconfined Compressive Strength, UCS , (in MPa)	200
Tensile Strength (Direct and Brazilian)(MPa)	6.7 - 13.5
Porosity	>10%
Permeability m^2	$1.08 * 10^{-16}$

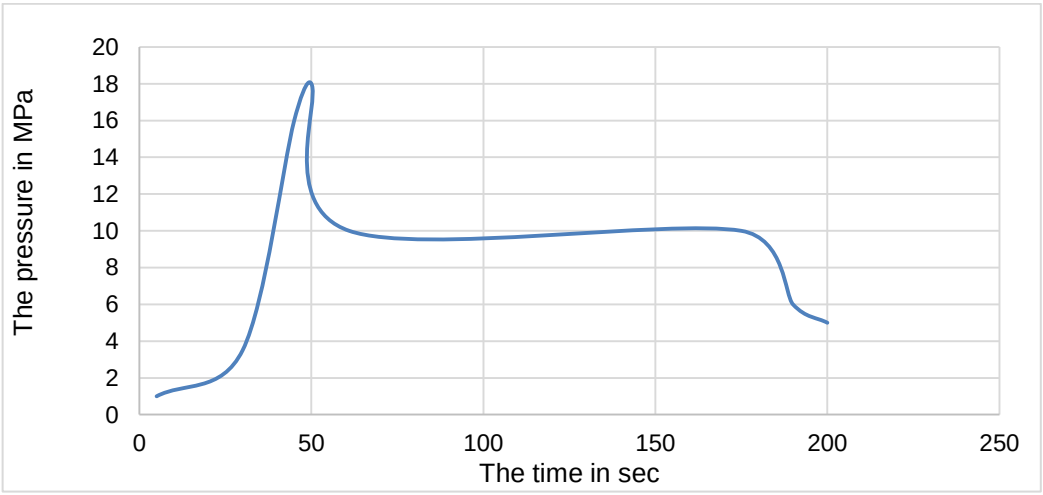

Figure 4-6 The measured pressure of the fluid in the injection test (Matsunaga et al., 1993)

A synthetic sample was created using DEM with a porosity of 10% which is close to the real sample, and then, through the same calibration process described in 3.1, to ensure that the synthetic model has the same mechanical properties as the real granite sample, the corresponding micromechanical properties of the synthetic sample are listed in Table 4-3.

After creating the synthetic sample and the domains between the particles, Then a fish in the PFC calculated the pipe aperture using equation 21 that give the simulated granite sample a permeability similar to the real one which was about $1.5965 * 10^{-5}$The injection process was simulated in DEM by applying a pressure to the centre of the sample similar to that in the real test Figure 4-7 . The modelling experiment stopped when fractures and events reached the surface of the sample.

At the end of the simulation test, the number of acoustic emissions was recorded as 550 events while in the lab test it was about 446. It is obvious that, in the simulation, it is not expected to get the exact number resulting from the lab test, because not all events in the lab test were recorded due to the limitations of the sensitivity and accuracy of the recording instruments, so it is possible to say that the number of events is acceptable

Anyway, it is important in comparing the results of the model with the lab test not to depend on the number of events, but also to compare other parameters produced from the model with the real test besides the number of events, such as the shape of the seismic cloud, the b_value if available, and any other measured parameters to be compared with real test. In the process of the model validation as done by other authors such as (AL-busaidi, 2004; Shimizu, 2010).

Because of a lack of any figure that represents the seismic cloud shape in the injection test on the granite, another model was created to mimic an injection of water into a Flechtingen sandstone see chapter 5 (Stanchits et al., 2011).

Table 4-3 The micromechanical properties of the synthetic granite sample and the Springwell sandstone

Micro parameter	Magnitudes in the synthetic Granite sample	Magnitudes in the synthetic Springwell sandstone sample
Particle Young's Modulus, (in GPa)	62	15
Particle stiffness ratio (k" / ks	2.5	2.5
Particle Friction Coefficient	0.5	0.5
Minimum grain radius (in mm)	2.5	0.75
Grain size ratio, Uniform	2.5	1.66
pb_sn_mean, (in MPa)	330	40
pb_sn_mean , (in MPa)	270	40

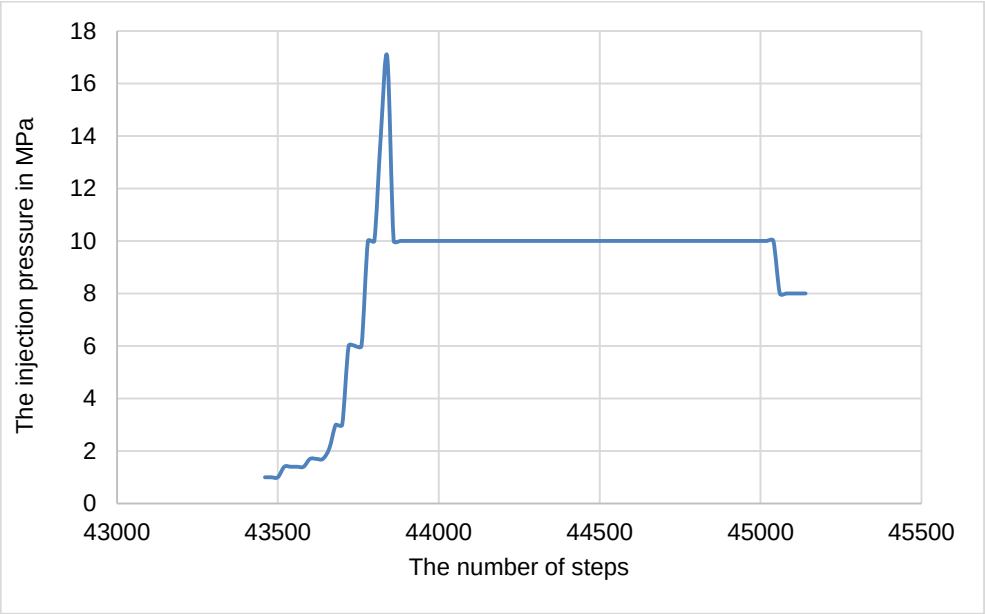

Figure 4-7 The measured pressure applied on the sample in the synthetic fracturing test

Now, based on the results of the simulation test on the Flechtingen sandstone see 4.9 and chapter five it is possible to conclude that the DEM has the capability to mimic the seismic cloud shape, using the same equations (10 and 11). The

aperture of the resulting fracture is predicted to range between 0.00001*m*-0.0001*m*, as shown in Figure 4-8. There is no record of the aperture caused by water injection in the lab test, and the DEM modelling results are compared with other studies of the same materials (Frash et al., 2014). In their fracturing test on a 300×300×300 *m* cubical specimen of granite, the resulting aperture was about 0.00015 *mm*. It is possible to say that the predicted aperture was acceptable.

Regarding the TK plot in Figure 4-9, unfortunately, there were no TK plot from the real sample to compare with it but it is obvious that most of the resulting fractures are tensile with an opening mode component. Regarding the b_value, in Figure 4-10, it was found that it is equal to 0.92 the slope of the red part of the curve, compared to the b_value in the natural state that is the b_value equal to 1. This small difference could be due to the inverse relation between differential pressure and the b_value, which makes the b_value smaller. Also, the b-value was found to be a function of grain size, and a finer grain size could lead to a higher b-value In this test, the particle size was adopted between 2.5*mm* and 6.25 *mm*, which is bigger than the real grain size of granite rocks, due to the limitations of the computer capacity. This can be improved in the future by using more powerful computers.

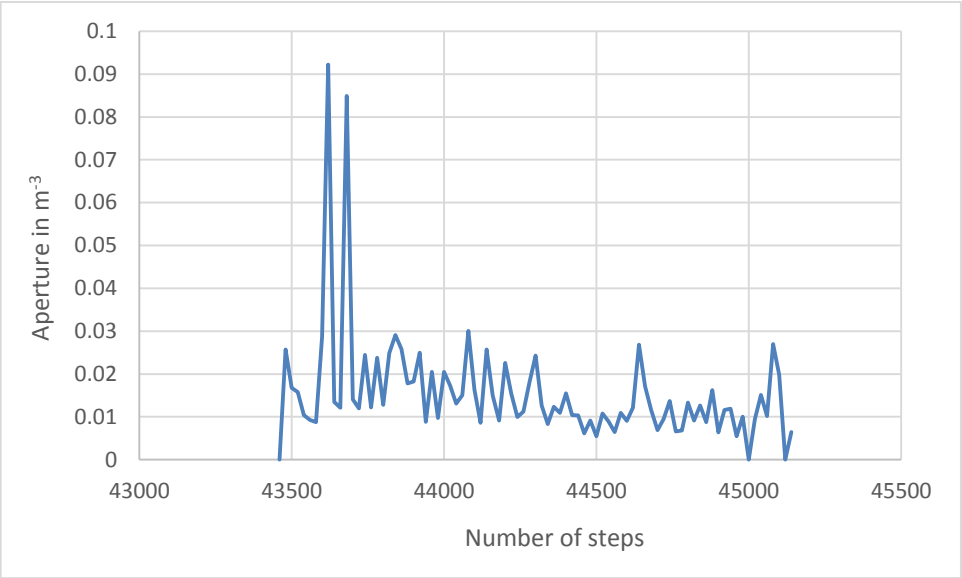

Figure 4-8 The aperture of the fractures resulting from the injection test in metres

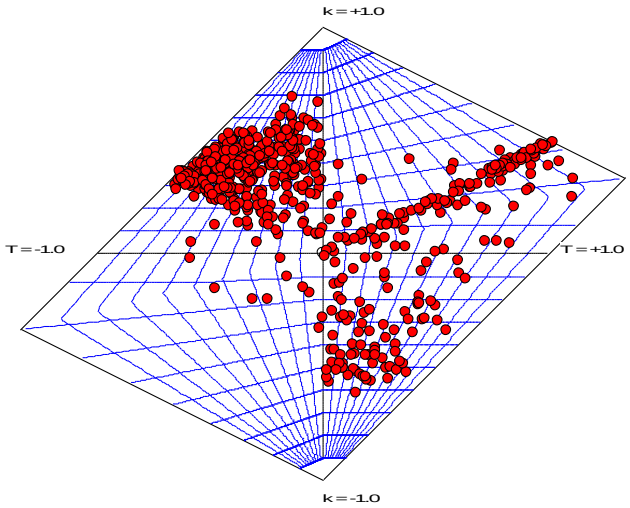

Figure 4-9 The TK plot resulting from the injection test

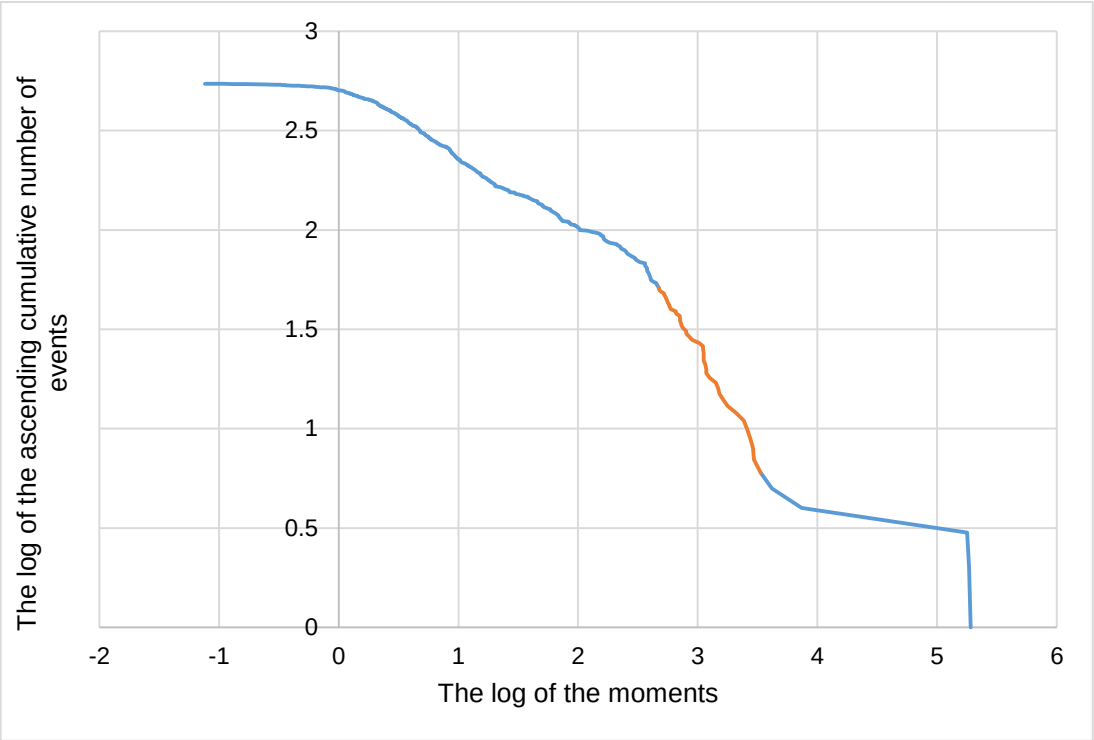

Figure 4-10 The b_value from the model which is the slope of the red part of the curve that equals 0.92

4.8 Modelling the seismic cloud shape

Stanchits et al. (2011) conducted six experiments on the acoustic emissions caused by fluid injection on Flechtingen sandstone. The mechanical properties are listed in table 4-4. Two tests were simulated only. One of them contains a test on fluid injection through a hole drilled into the centre of the sample (Figure 4-10). In the other, the hole penetrates the entire sample (Figure 4-11). These tests were simulated using the PFC 3D to test the accuracy of the model in producing the seismic cloud shape only .Because of using a much bigger particle size to save time, it would be expected to get fewer acoustic emissions. Table 4-4 below contains the mechanical properties of the real and the synthetic sample used in both the real injection and the simulation test.

Table 4-4 The mechanical properties of the real sandstone and the synthetic model

The property	The Average of real sandstone sample properties		The average of modelled one create using PFC 3D	
Peak confining strength	$27 * 10^6$	Pa	$27 * 10^6$	Pa
Young modulus	$28.6 * 10^{10}$	Pa	$31 * 10^{10}$	Pa
Poisson ratio	0.25		0.27	
Minimum Particle size	0.1	mm	1	mm

4.8.1 The first test

The first simulation test was on a cylindrical sandstone sample, with properties listed in Table 4-4. The particle size was about 0.1 *mm*, drilled into the middle and then injected with water. The model has the same mechanical properties but, with a bigger particle size of about 1 *mm*, the shape of the seismic cloud was acceptable (Figure 4-11), but with fewer events, because of the size of the particles and the fact that particles are not breakable in the code. Anyway, in the acoustic emissions induced by fluid injection into sandstone in (Figure 4-11) the red, blue and yellow dots are the acoustic events in real sample (Stanchits, et. al. 2011). A and B are vertical and horizontal section of the real sample and C is the vertical D is the horizontal section of the modelling results of the injected sample into the middle of the model, (red dots and circles for shear cracks, black for tensile cracks in the model only) the size of the circles is proportional linked to the moment of the events.

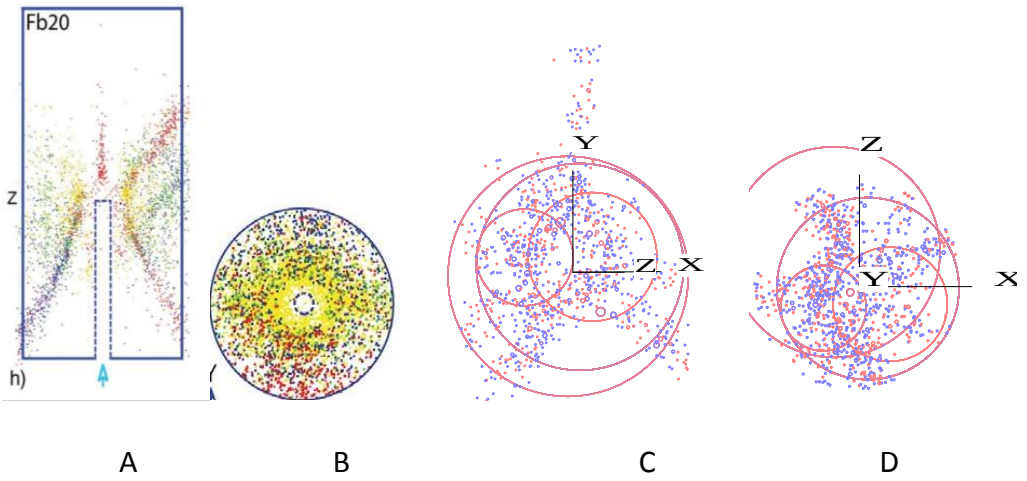

Figure 4-11 A comparison between the acoustic emissions induced by fluid injection in to sand stone A vertical and B horizontal sections (Stanchits, et. al. 2011) and modelling results are both C is the vertical D is the horizontal section

4.8.2 The second test

The second test was carried out on the same rock type, but the hole was drilled to penetrate the entire sample, and then injected with water. The model has the same mechanical properties. The results are presented in Figure 4-11, where the acoustic emissions induced by fluid injection into real sandstone A is the horizontal and B is the vertical. The events are the red, blue and yellow dots (Stanchits, et. al. 2011). The modelling results of the injected sample into hole C is the horizontal, and D is the vertical. Please note that both verticals in the model do not has a bedding plane but a bigger particle size of about 1 mm, as in the first model. The shape of the seismic cloud was acceptable. The difference is attributed to the anisotropy of the rock sample, which causes the shape of the cloud to look more oval in the real sample than in the model (Figure 11 B and 11 D), and the exact length of the drilled hole was not clear in Figure 4-12, but with

fewer events only because of the size of the particles and the fact that particles are not breakable in the code.

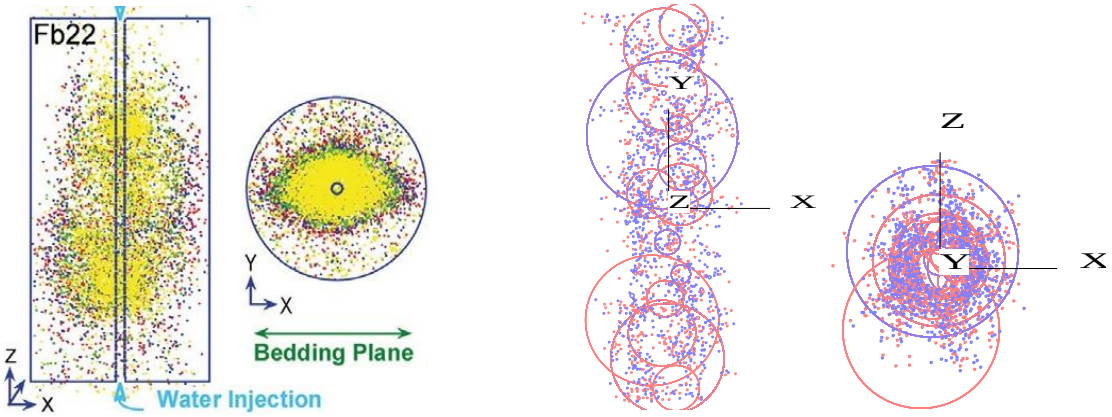

Figure 4-12 The acoustic emissions induced by fluid injection into real sandstone (Stanchits, et. al. 2011) and the modelling results

The shape of the seismic cloud in both cases was acceptable. The number of events were less than the real sample, because, of using a much bigger particle size in the model than the real particle size in the real sample, where the minimum particle size was about 0.1mm, while in the modelling test it was about 1 mm, and the fact that, in the modelling test, particles are breakable while in the real sample they are breakable.

One of the advantage of the DEM model is that it can distinguish tensile and shear events which is very difficult to achieve in a lab test. As could be found in Figure 4-11 and Figure 4-12, the red dots and circles stand for seismic events due to tensile cracks, and the blue dots and circles represent events induced by shear cracks as in the lab test. As in the lab tests, there were fewer tensile events, as the tensile failures has less energy release and might get lost in noise and so not be recorded (Falls et al., 1992; Shimizu et al., 2009). In addition, other

factors determine the fracture type like the fracture roughness of the material, as proven by (Raziperchikolaee et al., 2014). This proves that the developed DEM model could be used to reveal important data that are difficult to retrieve in lab studies like real fracture types.

It must be mentioned here, however, that the initial model was incapable of predicting the pore sources type of acoustic emissions in this stage. To overcome this problem, another modification was needed (see Chapter five).

4.9 Prediction of surface deformation and curvature

In most hydraulic fracturing field operations, microseismic monitoring is used to monitor the operations, but there other methods such as Tiltmetere which is used to monitor fracturing operations too. It was thought that a model that can simulate the deformation of the injected mass will be more beneficial in future studies (Arop, 2013; Coulson, 2009; Evans and Columbia, 1983; Warpinski et al., 2012b).

In 2009, Hautmann et al. (2009) simulated the deformation of the surface resulting from a dyke and Cho et al. (2004) modelled the dilatation in a rock sample under stress, while it was Le Guen et al. (2007) who simulated surface deformation using PFC and stated that the accuracy of this procedure depends on the accuracy of the model parameters. On the other hand, Hunt et al. (2003) simulated the Kaiser effect and the deformation of sandstone using PFC in a uniaxial test and cyclic loading. Although a PFC code has been used to measure surface deformation as a result of injection, measuring the surface curvature and

the displacement combined with modelling acoustic emissions, as far as the researcher is aware, has not been reported before, using the same techniques.

The curvature of the surface in one exact place between the particles (Figure 4-12). Regarding the shape of the resulting curve, it is noticed that the value goes up and then stops for a period of time then decreases again, which means that the angle of the surface deformation increases at the beginning and deceases later. This means that the elevation of the two particles becomes close and the surface is no more inclined.

In order to predict, the surface deformation associated with the hydraulic fracturing operations, a displacement of one particle was measured and plotted (Figure 4-13) but, in order to determine the curvature of the surface, two particles were allocated. The difference in the displacement was measured and plotted in Figure 4-13. The curve in Figure 4-13 indicated that there are measures of the surface displacement and the displacement increases with time but it goes back after stopping the injection test.

These two curves indicated that it is possible to use the PFC code to simulate the tilt metre readings and to predict the surface deformation combined with fluid injection. Since there were no real data to compare with, however, there will be no more comments on the readings.

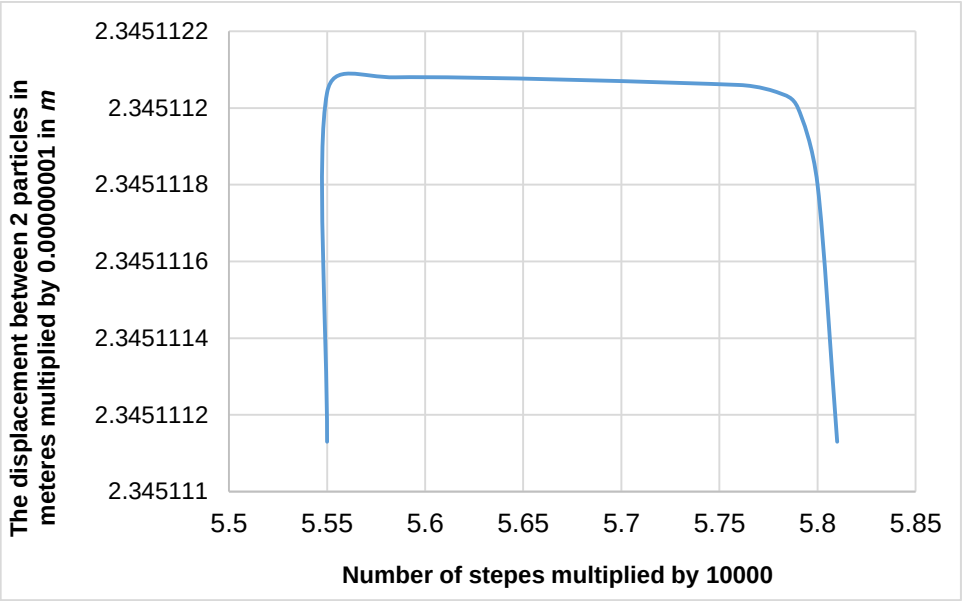

Figure 4-13 the curvature of the surface during the injection process

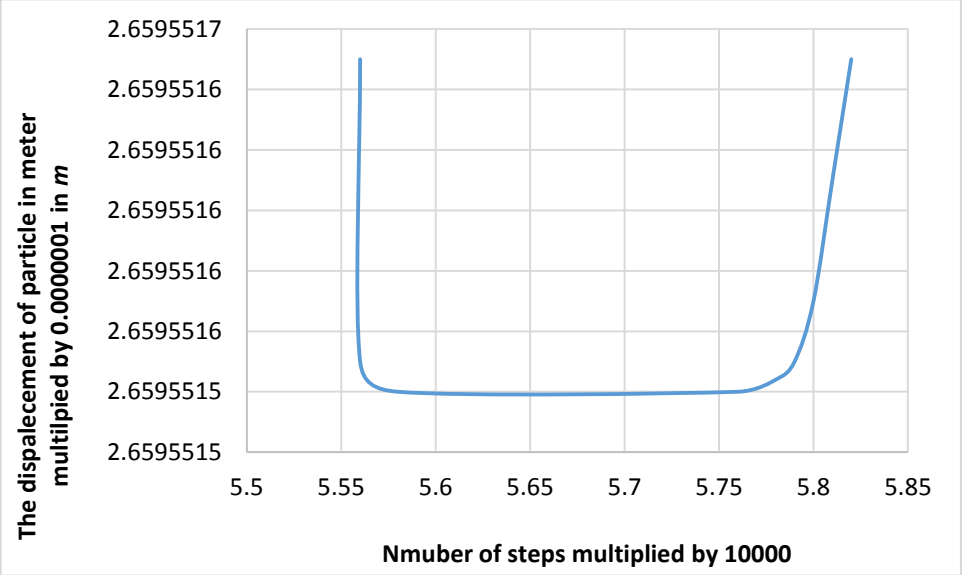

Figure 4-14 the change in the surface displacement in the Z direction associated with the injection process

4.10 Summary

The acoustic emission in a rock sample caused by triaxial stress and fluid injection is modelled using DEM/PFC code. The original Hazzard's code was modified to overcome some of its main limitations and the T.K. plot, number of events and b_ value are improved to be more compatible with real values. It is also found that controlling the b-value through varying the velocity rupture in the DEM model leads to a more realistic prediction of rupture velocity in the fractures and hence more applications in hydraulic fracturing. Moreover, the DEM model predicts the range of resulting apertures of the fractures and measures the surface deformation and curvature of the sample during the fracturing test, which may make the approach more useful in modelling the Tiltmetere readings in the fracturing process. It is also noticed that there are still some improvements needed in the model to predict the pore sources of the events.

Chapter 5 The relationship between the seismic clusters and the resulting fractures

5.1 Introduction

It was thought that creating or modelling microseismic events, induced by fluid injection from one of the tests that was conducted by Stanchits et al. (2011), in an acceptable way (see chapter four). In addition, simulating this test will provide another good validation. Further, it is possible to use the modelling results (microseismic cloud shape) and their relation to induced permeability to perform a parametrical study, then it will be possible to use the results to draw valid conclusions about the relation or indication of the components of the microseismic cloud that could be monitored in the field (shape of the cloud, types and magnitudes of the events) and the resulting permeability.

Furthermore, it will be possible to conclude the permeability resulted from the fracturing test from direct observation of the induced microseismicity, which could be a good indication of the effectiveness of the fracturing process. Such an indication could help in planning or changing the schemes of the fracturing operations, to obtain better results. This parametrical study will be conducted to gain a better understanding, and to conclude any probable relationship between microseismic events and fractures properties, such as permeability or the measured aperture of the fractures. The parametrical study consists of studying the effect of changing pressure, and the effect of changing the injection radius of the injection pipe only.

5.2 The injection test

Stanchits et al. (2011) experimentally conducted a hydraulic fracturing test, on a 25 *mm* radius and 105-125 *mm* length cylinder Flechtingen sandstone, from Flechtingen quarry, NE Germany. The rock sample was aged Lower Permian. The mineral composition of this sandstone is quartz (65-75%) and a cement of Elite and Calcite (15%). The measured permeability is of the order of ($0.2 * 10^{-16}\ m^2$ - $0.8 * 10^{-16}\ m^2$) The grain size is between 0.1*mm* and 0.5 *mm*, with porosity between 5.5% and 9% (Stanchits et al., 2011).

In this test, water was injected till fracture appeared on the surface. The resulting acoustic emission cloud was plotted, the type of source was determined. After completing the injection, a picture of some of the injected samples was taken, which can give a good idea about the fracture direction and the aperture. Two experiments were simulated in this research, as pointed out in the fourth chapter, but one only will be used in the parametrical study in this chapter. The main reasons for choosing this test for the simulation and conducting the parametrical study were the fact that sand is composed of particles which make it physically closer to the PFC modelling program (Pettitt, 1998), the fact that the seismic cloud shape was available see 4.10, and the permeability was measured after injection which makes it suitable for comparison with our results. One of the experiments only will be used here for the sake of devising a simple parametrical study

A cylindrical sample of Flechtingen sandstone was placed under confining pressure of about 40 MPa, and Vertical stress of about 240 MPa. The results of the real test are shown in Figure 5-1 which includes a sketch representing the

horizontal sample and the injection pipe (A), while B is the vertical cross of the sample (Stanchits et al., 2011). The coloured circles or dots indicate the time sequence of AE events, starting with yellow through to green, blue and finally, red hypocentres. The direction of the X-axis is aligned in the bedding plane direction.

The real sample was injected with water of viscosity of about 0.001 Pa.Sec through a hole that penetrates the sample. The pressure of the injected fluid was 5 MPa as plotted in Figure 5-2, which is the fluid pressure on one of these tests. It is noticed that the horizontal of the plotted acoustic emissions in the sample (Figure 5-1) B is elliptical because of the anisotropy of the sample, as pointed out by the author (Stanchits et al., 2011).

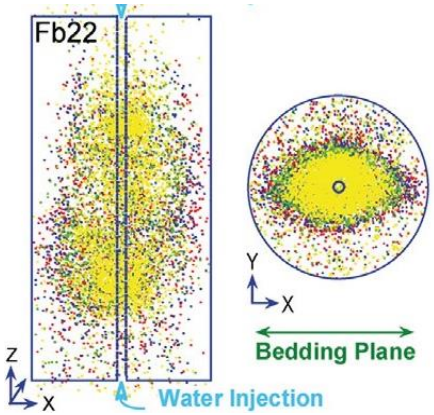

Figure 5-1 A sketch representing the acoustic emission in both horizontal sample S, while B is the vertical cross (Stanchits et al., 2011)

One of problems was that the real number of events were unavailable, so it was decided to depend on the approximation by drawing an ellipsoid around the seismic cloud and calculating the number of events by hand in one unit then

multiplying that number with the area of the episodes. The results indicated that there were about 11052 events in the test.

5.3 Modelling procedure

A PFC model was created to represent the Flechtingen sandstone. The two main problems in this procedure were that the real Flechtingen sample has a particle radius of about 0.1*mm*. It is computational expensive to conduct an experiment with such a small particle radius because it will be time consuming so it was decided to create a model, with particles with a minimum of 1 *mm* radius. The second expected problem was the anisotropy of the real sample, as it was pointed out previously that this will be hard to simulate in order to mimic the effect of the bedding plane, which causes the anisotropy of the real sample. Although these two differences may affect the simulation results, it will still capture the general features of the test results (Potyondy and Cundall, 2004).

5.3.1 Sample creation

The real sample's properties are listed in Table 5-1, which are the mechanical properties of the real Flechtingen sample. A synthetic sample was created with a porosity of 8%. After the creation of the synthetic sample using the method explained in chapter four and three, the synthetic sample was subjected to a uniaxial test, in order to obtain its properties. The resulting mechanical properties of the synthetic sample are listed in Table 5-1, which is very close to the real sample Table 5-1. Then, by using the micromechanical properties that give the model these properties, a new cylindrical sample was created.

Table 5-1 The mechanical properties of the real sandstone and the synthetic sandstone

The property	The Average of real sandstone sample properties	The average of the modelled one created using PFC 3D
Peak confining strength at confining pressure 40 MPa	$270 * 10^6$ Pa	$270 * 10^6$ Pa
Young modulus	$28.6 * 10^{10}$ Pa	$31 * 10^{10}$ Pa
Poisson ratio	0.25	0.27
Minimum Particle size	0.1 *mm*	1 *mm*

The new sample that was created had the dimensions of about 105 mm in length and 50mm in diameter, and the macro-mechanical properties of the Flechtingen sample that was used in the test are listed in Table 5-1. Then, it was subjected to confining stress as in the real test of 40 MPa, with a vertical stress of about 247 MPa, close to the real test. Then it was possible to create the domains and pipes between particles by calling a subroutine in PFC called Domain fish. This fish connects every four balls to each other to create domains, and then creates pipes between these domains to prepare the sample for the injection test (see 3.4).

Now, since the true permeability of the Flechtingen sample was about ($0.2 * 10^{-16}$-- $0.8 * 10^{-16}$) m^2 (Stanchits et al., 2011), it was necessary to calculate the expected initial aperture of the pipes that connect the small reservoirs in the models. This initial aperture will give the synthetic rock sample the same permeability as the real Flechtingen sandstone (Al-Busaidi et al., 2005; Zhao, 2010). A fish in PFC can calculate the initial aperture sing equation 33 which was

$a_0 = \sqrt[3]{\frac{12*k*3.14*\sum_{balls} R^2}{\sum_{Nt} i}}$. Where, k is the true permeability of the sample in m^2. $\sum_{balls} R^2$ is the square of all ball radiuses' summation in the sample, and is equal to $1.67667e-2m^2$. $\sum_{Nt} i$ is the summation of all of the pipe radiuses in the sample.

Now. Since the summation of the square radiuses of all balls is already given by the code, which was equal to 470.394 , the summation of the pipe radius was equal to 1.3822e2 m provided by the program too. By substituting these values in equation 20:

$$a_0 = \sqrt[3]{\frac{12*k*3.14*470.394}{\sum_{Nt} i}} = \sqrt[3]{\frac{12*0.5*10^{-16}*3.14*470.394}{1.3822*10^2}} = 4.4*10^{-5}$$

Which is the initial aperture of the pipes in the synthetic sample. That gives the synthetic sample the mentioned permeability.

5.3.2 The injection test

After the creation of the synthetic sample, and determining the aperture of the pipes, the injection simulation begun, using water as fluid injection with a viscosity of (0.001 Pa.Sec) and bulk modulus of about (2.18 GPa). The injection pressure during the simulation process see Figure 5-2 changed by the same ratio of values as in the other real tests see Figure 5-3. The radius of the injection fluid in the model was about 1.25 millimetres, the same as the on the real model. The injection stopped when the acoustic emissions reached the surface of the sample (Figure 5-4).

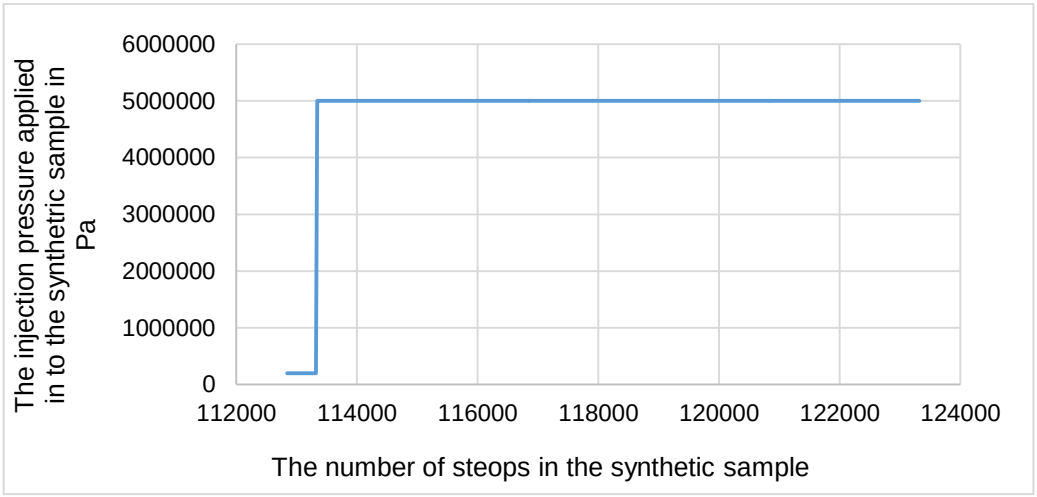

Figure 5-2 The injection pressure during the simulation test

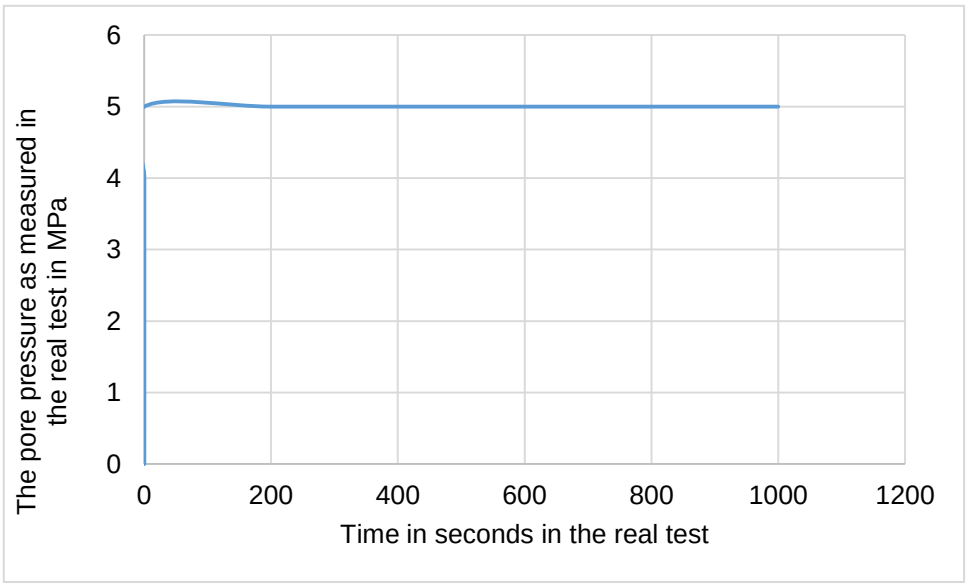

Figure 5-3 The injection pressure during the real test

5.3.3 Simulation results of the lab test

The results of the modelling were not entirely compatible with the lab test because of the big particles radius, as mentioned earlier in 5.3. The results could be better if the size, size distribution, and size ratio of the particles were similar to the real Flechtingen sandstone. Regarding the distribution of the seismic

cloud, it was similar to the real test if we considered that it was hard to simulate the effect of anisotropy which caused the oval shape of the cloud (Stanchits et al., 2011) Figure 5-4 A and B both are vertical and horizontal in the real sample. The acoustic emission induced by fluid injection into sand stone (the red, blue and yellow dots) are the acoustic events according to time (Stanchits et. al., 2011).

C and D are the vertical and horizontals in the modelling. The small dots and circles are the events according to their magnitude. The red small circles are the tensile, the blue ones are the shear source, and the green ones are the pore collapse sources) the area of the circles is proportional to the magnitudes of the events not to the moments. Additionally, the aperture source type of events will be compared. Unfortunately, there were no TK or b_value for comparison, so these will not be studied since they were studied before.

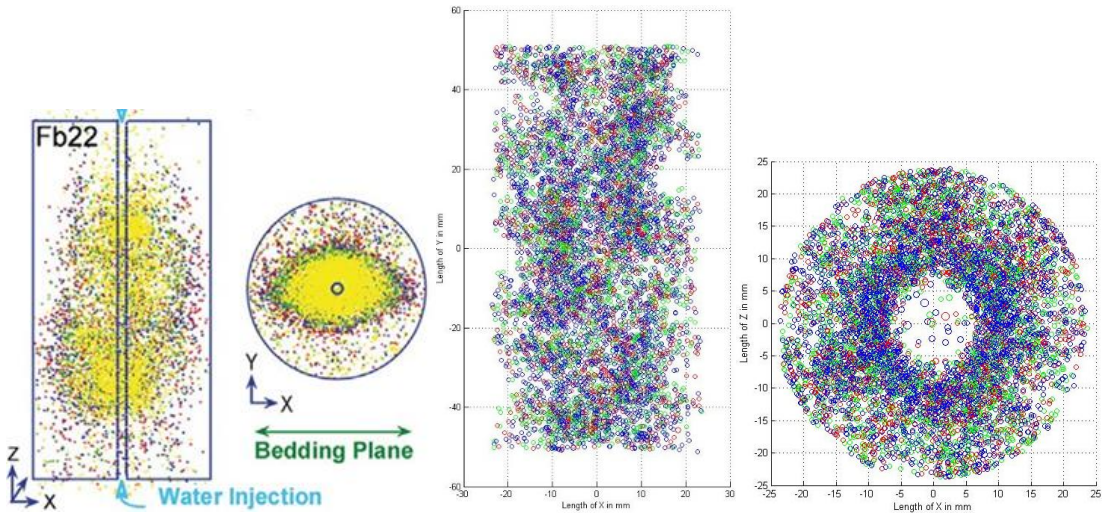

A B C D

Figure 5-4 The induced acoustic emission induced a real sand stone A and b (Stanchits et al., 2011), while the C and D are the acoustic emissions of the modelling results

5.4 The Predicted fracture aperture and number of events

It was possible, by using the same procedure mentioned in 2.3, to predict the aperture of the resulting fracture. The results are presented in Figure 5-5, and lie in the range of 0.000005*m*-0.000018 *m*, which is acceptable as observed in injected Flechtingen in other samples (Stanchits et al., 2011).

While the number of events was about 7014, which is less than the estimated original number of events. This could be caused by the particle size that was used in the model, which is bigger than the real particle size in the real sample, which affects the number of fractures (Hunt et al., 2003) and hence the number of acoustic emissions. Besides, the particles are not breakable in the model as is the case in the real sample (Wong, 1982). The explanation for the effect of these two characters are that more bonds mean more…

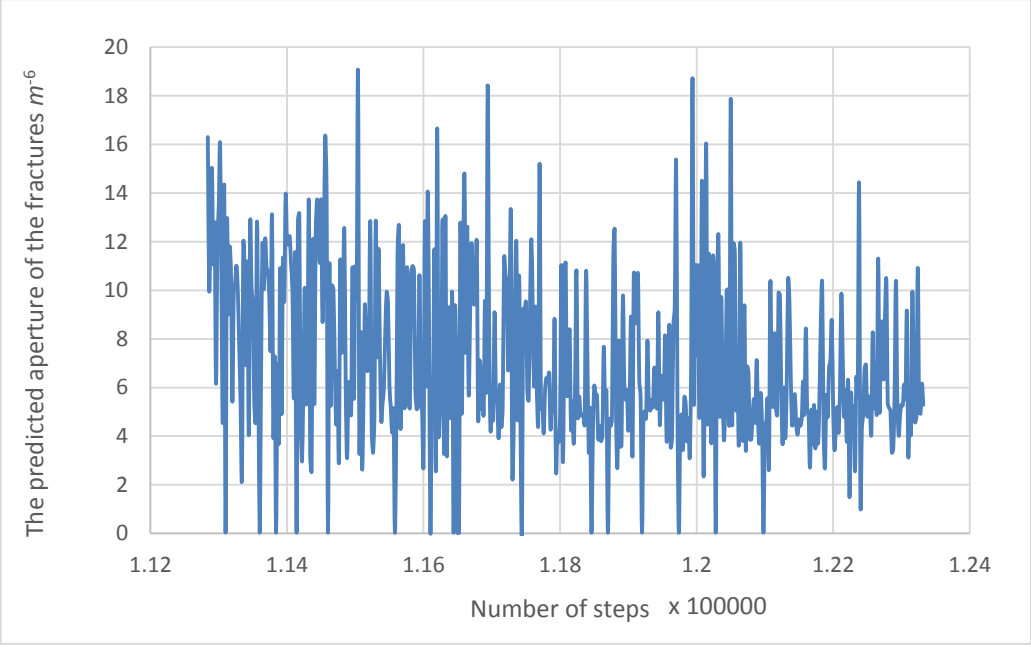

Figure 5-5 the predicted aperture of the fractures in the modelling of the injection test in meters

5.5 Acoustic emission source type and seismic cloud

It is clear from Figure 5-6 that represents the ratio of source type of events during the simulation time, that the average of the tensile is 28%, while the average shear events were about 49% and that for the pore collapse was about 23%. Although one of the advantages of the DEM/PFC code is its ability to distinguish between the shear and tensile events source of acoustic emissions. However, this type was not recognized in the granite sample because of the low porosity, as suggested by (Hazzard et al., 1998) but, as this type was monitored in the injection test, it has to be modelled, so the challenge was to model the pore collapse source of the acoustic emission for use in the paramedical study, in addition, to the important role of pore collapse in the reservoir studies (Economides and Nolte, 2000).

5.5.1 Pore collapse source type determination

Eshiet (2012) suggested that pore collapse happens when the stress applied to the rock volume leads to changes in the volume of the pores, which may be caused by the depletion of the reservoir's pressure, adding that an immediate large deformation of the formation occurred with the pore collapse. In addition, (Nouri et al., 2002a) suggested that "not only do effective hydrostatic stresses increase as a result of the depletion, but the shear stresses are also elevated. Shear failure of the formation as a result of the depletion causes pore collapse".

Additionally Grosse et al. (2003) suggested that pore collapse source type could be studied better, if we used explosion source type but with negative sign, which means that pore collapse could be modelled using, implosion source type of acoustic emission. In the other hand (Alassi, 2008) suggested to model this type

source of emission using DEM/ PFC by reducing the particles radius. When the compressive mean stress on that balls reaches a pre-specified value. Although he suggested to do that in future studies.

In this research it was thought that since pore collapse source type is companied by change in volume, and since the domains between particles are, the closest thing to pore spaces in any real sample. Additionally, since that any change in the volume of domains, that leads to distraction of the domains, will cause bond breakages which leads to emission of waves, either as tensile or shear type, and it is best described using model close to implosion type of acoustic emission source type as suggested by (Grosse et al., 2003). But it is possible to calculate the deformation accompanied in any acoustic emission type, using the K value see chapter four and one. Because, this value determines the amount of deformation accompanied the source types, as suggested by (Hudson et al., 1989) and. Therefore, using the calibration process to decide, what will be the value of the K that could be distinguished in the real test as a pore collapse type. That gives the best ratio of the pore collapse acoustic emission type, to the amount of all calculated events, so, by changing the K to give the appropriate ratio of close to 23%. That means, trying to find what will be the value of K that makes 23% recoded events be registered as pore collapse source type.

Any way it was found, if we considered the emissions that has K values less than 0.1 of K value, as pore collapse source. Then the ratio of pore collapse sources to the amount of all recoded events would be about 26%. So for every fracture the value of K was calculated, then if it was less 0.1 it would be considered as pore collapse source. After applying this results, 89 of the results

of the type of rations of the emission in the model are listed in Table . It was found that 56% of the events were shear, while 20% were tensile and 26% were of the pore collapse source type, if compared with the source type distribution in Figure 5-6, which is the source type distribution of the fracture in the real injection test. The colour of the dots corresponds to the different types of AE event: pink is the tensile source, green is the shear source, and yellow is the pore collapse type of AE events (Stanchits et al., 2011). It was found that 56% of the events were shear, while 20% were tensile and 26% were of the pore collapse source type. If compared with the source type distribution in Figure 5-5, it is clear that the results are almost compatible. Additionally, the increase in the number of shear events could be related to the bigger particles used in the model (Ishida, 2001). The distribution of the sources types of the acoustic events are explained in more detail in Table 5-10.

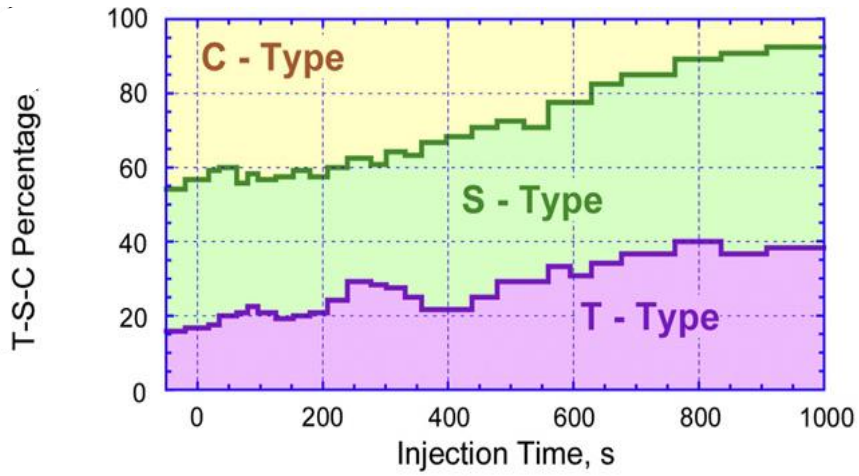

Figure 5-6 the source type of the fracture in the real injection test (Stanchits et al., 2011)

5.6 The calculated permeability of the injected Flechtingen sample

The permeability of the injected sample was measured using the inversion method (Grechka et al., 2010; Moreno, 2011) that was outlined in 1.6.5 in detail, because this method was proven to produce acceptable results if it was used to determine the induced permeability (Moreno, 2011). The values of the seismic cloud dimensions were determined using ellipsoids to determine the approximate boarder of the seismic cloud, and then the length of the axis of the clouds was used as the dimension of the seismic cloud to be used in equation 10 (Moreno, 2011). See Figure 5-7, that represents the acoustic emission clouds in the simulation test of the real sample of the injected water in the sandstone. The ellipsoids were used to determine the approximate border of the cloud and the length of the clouds are shown by the brown line while the green line indicates the length and the yellow the cloud. The small blue circles are the shear events and the red ones are tensile, while the green ones are pore-collapse sources. Shows the seismic cloud dimension in the model that represents the real test. The radius of the circles is proportional to the magnitudes of the events. The border of the clouds are shown by a blue line, while the brown line is the height, the yellow line the length and the green line the width of the cloud. The other parameters and the resulting permeability are listed in Table5-2. The permeability results from the injection test using the inversion method show that it is equal to 0.7e-16 m^2, which means that the measured permeability is close to the real measured permeability in the real sample, which was about 0.2-0.8e-16 m^2, in both real samples with the same dimensions and fluid injection.

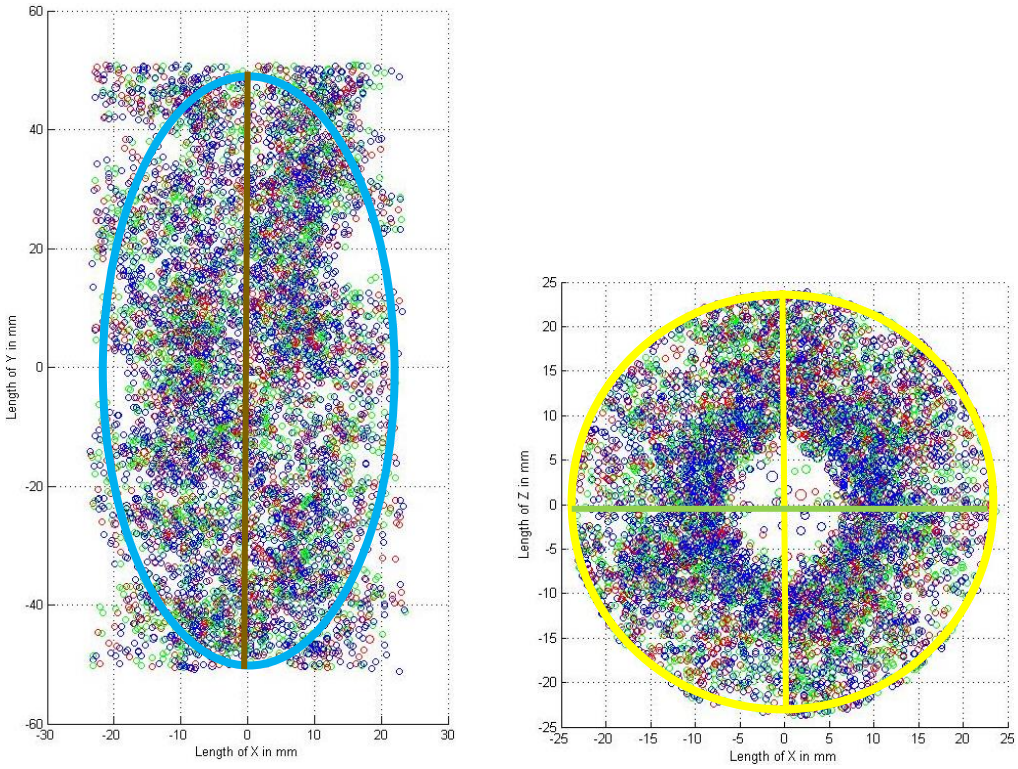

A B

Figure 5-7 The acoustic emission clouds in the simulation test of the real sample of the injected water in the sandstone

5.7 The simulation results for several hypothetical models

In order to study the resulting acoustic emissions, in terms of the number of events, the acoustic emission cloud shape, aperture of the resulting fracture, and the resulting permeability, but this time from different hypothetical injection tests, it was decided to study the effect of changing the pressure, then the effect of changing the injection radius. The first hypothetical model was designed for a simulation test of double the pressure than that used in the real test. The second was for a 3 *mm* radius of the drilled injection pipe.

5.7.1 The simulation test for higher injection pressure values

The simulation was for hypothetical test with 2 pressure values see Figure 5-10. The acoustic emission was enclosed in ellipsoids to make the calculation easier. The small red circles are the tensile source while the shear is represented by blue circles, while the green circles show the pore collapse source. In this test, the injection was about twice the pressure of the real test but, by keeping the rest of the parameters fixed, the results indicated that there will be fewer events (about 4560), which may means that fewer fractures are produced, but the aperture ($5 * 10^{-6}m$ - $1.4 * 10^{-6}m$) is similar to real test, even though there is less pressure. Regarding the shape of the seismic cloud see Figure 5-8, it still keeps the same general direction, but with the shear type more dominant in the centre of the cloud. Now, regarding the resulting permeability, it was about $7.42 * 10^{15}\ m^2$. It is a higher value than the permeability induced in the real case. In addition, the changes in the percentage of shear tensile events and pore collapse are about 1%, possibly because of the small size of the sample, but generally more tensile events and more permeability are produced.

Although the changes in the permeability is not too much but that's probably because of using very small sample this could be verified by doing more experiments or simulation on bigger samples or even field case studies.

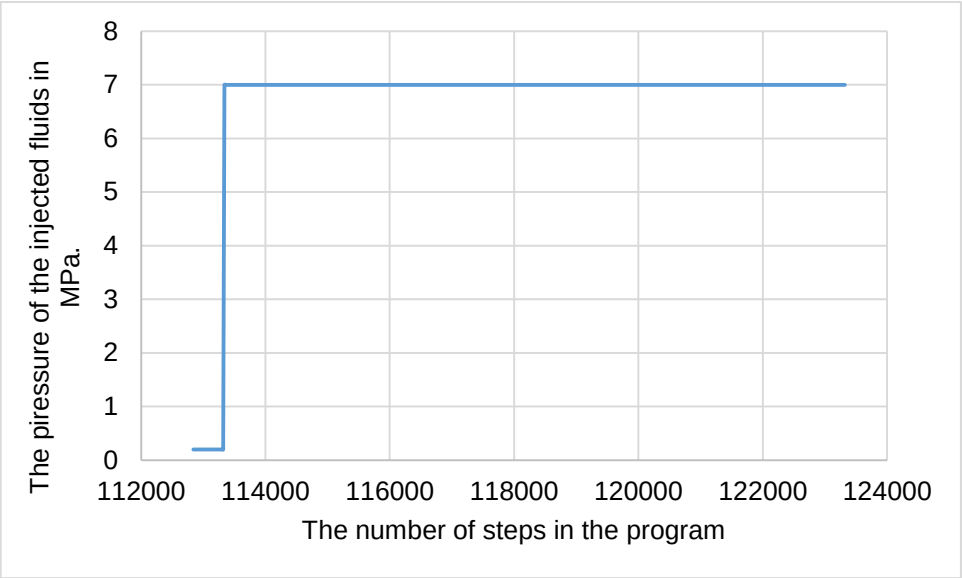

Figure 5-8 The pressure curve. In the first hypothetical situation, the pressure is about twice that during the real test

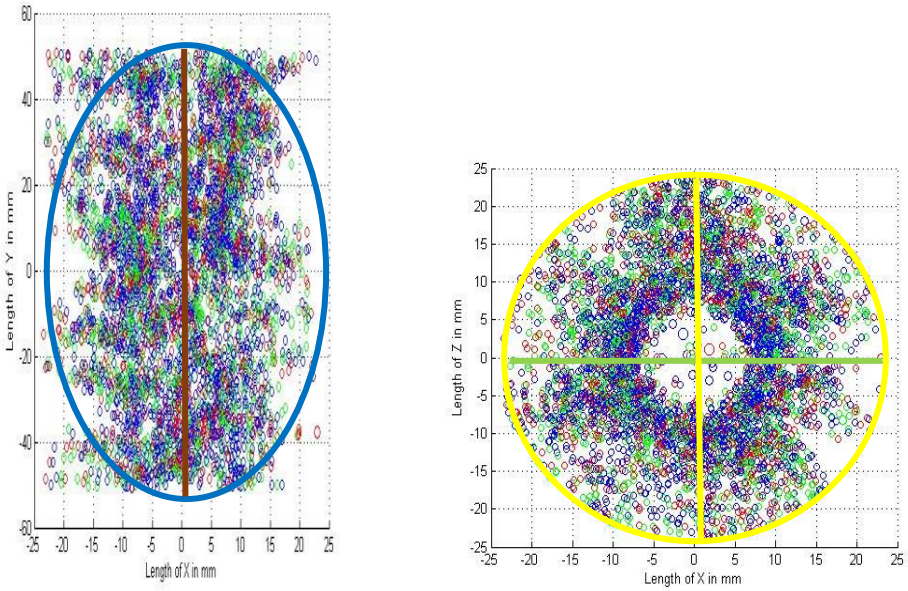

A B

Figure 5-9 The seismic cloud of the injection test with double injection pressure

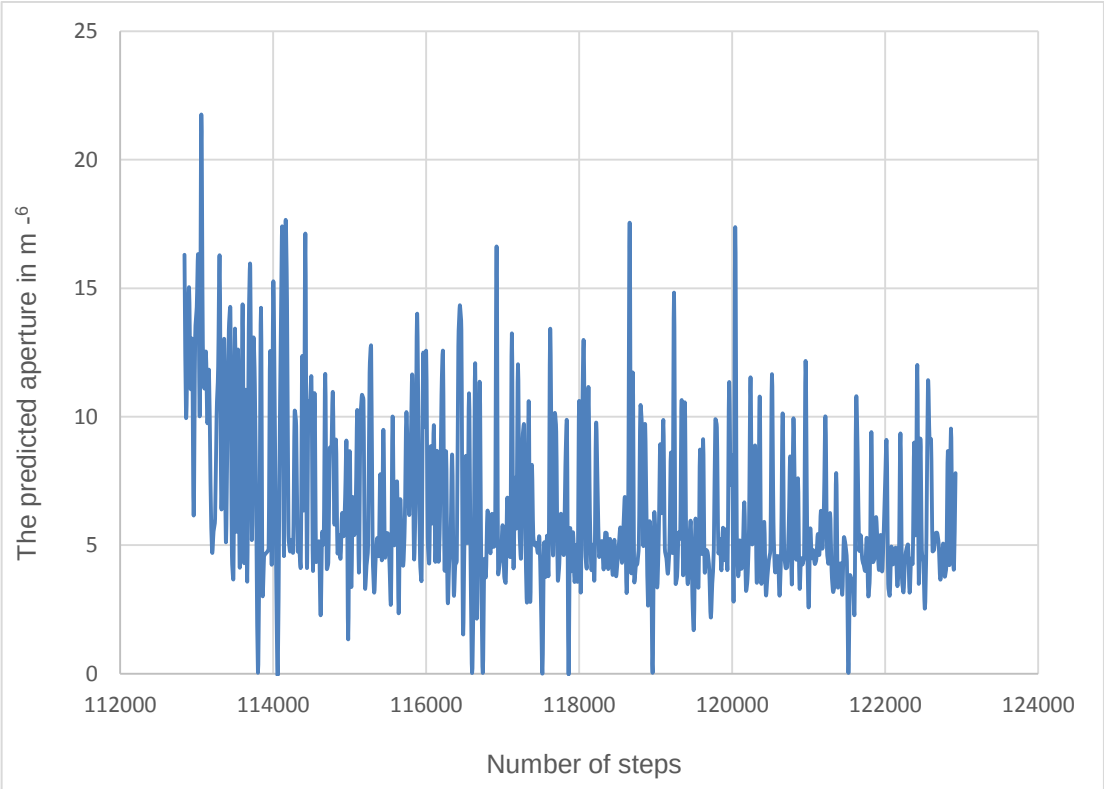

Figure 5-10 The predicted aperture in the case of using double injection pressure with oil as the injection fluid

5.7.2 A simulation test using a bigger radius for the injection

The simulation test was tested for a condition where the injection pipe was 3*mm*, but the pressure curve was kept constant. The results of the injection test see Figure 5-12 show the shape of the seismic cloud when using a bigger radius for the injection pipe but keeping the same pressure curve, the acoustic emissions are plotted in Figure 5-12 where A is the vertical and, in Figure 5-12, B the horizontal one. The green line is the length of the seismic cloud and the brown line is the width of the seismic cloud, while the yellow line is the length of the cloud. The red circles show the tensile events, the blue circles the shear events, and the pore collapse sources are the green ones, the radius of the events is proportional to the magnitudes of the events. Showing the seismic cloud's shape.

The number of events was less than 1541, which may be because the radius was increased but the pressure was kept the same, as the effect became less as the area of the well became bigger, which means less pressure on each particle. The resulting permeability was about $3.47 * 10^{15}\ m^2$, less than for the other two tests. The resulting aperture (0.000006*m*-0.000016*m*) was much less than with the previous models. It is noticed that there are fewer tensile events than with the other models (see Table 5-2 and Table 5-3).

The expected reason for the low induced permeability may be the low number of fractures, the lower value of the fracture aperture, and the lower extent of the induced fracture. Or all of these combined together cased low induced permeability Of the synthetic sample

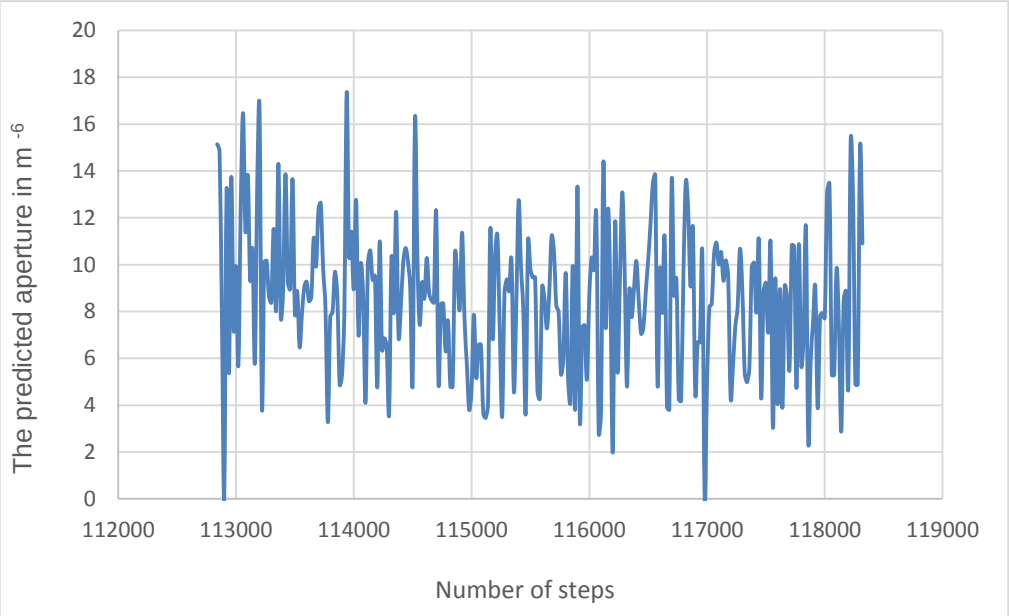

Figure 5-11 The predicted aperture in the case of using a 3 *cm* radius for the injection pipe as predicted by the code

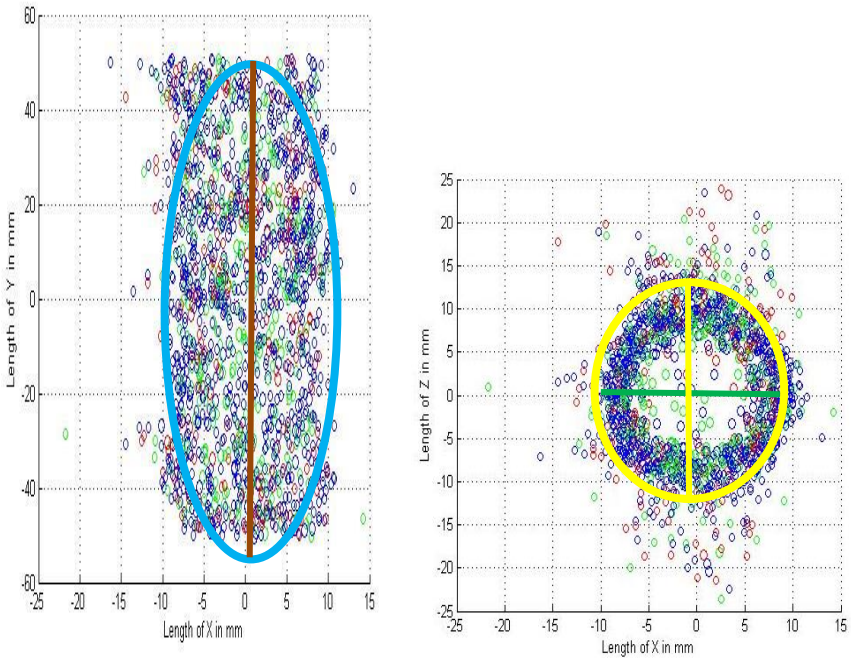

A B

Figure 5-12 The shape of the seismic cloud when using a bigger radius for the injection pipe but keeping the same pressure curve . A is the vertical and B the horizontal one

5.8 The predicted permeability of the real test and the three hypothetical models

The permeability of the injected sample was measured using the inversion method (Grechka et al., 2010) and was tested in the lab by (Moreno, 2011), as explained in 1.6.5 in detail.

Now, according to (Fatahi and Hossain, 2015), the radial in the flow from the well bore in a steady state case is equal to:

$$Q = 0.00708\, k\, h(p_e - p_w)/(u * lin\left(\frac{R_e}{R_w}\right)) \qquad (34)$$

Where,

k Permeability in *md*

h Sample height in *ft*

R_e External radius in ft

R_w Wellbore Radius in *ft*

u Fluid viscosity in *Pa.Sec*

p_w Well-bore pressure in *Pa*

p_e External pressure in *Pa*

It is clear from this equation that doubling the pressure difference will increase the flow rate to double, while increasing the well bore will increase the flow by about 1.4 times, then the flow rate in the case of double pressure is about $2.11936 * 10^{-5} m^3/sec$.

The values of the seismic cloud dimensions and the other parameters are listed in Table 5-2. These were substituted in equation 10 to calculate the value of the in-situ permeability

The results indicate that the permeability increased more when using higher fluid pressure in the fracturing operations. In addition, it is noticed that the increase in permeability is combined by an increase in the tensile events too. This phenomenon was noticed by (Raziperchikolaee et al., 2014).

Table 5-2 The permeability results from the injection test using the inversion method

Parameters used in the calculation	Value in real test simulation (1.25 radius and 5MPA injection pressure	10 MPa pressure simulation (double the pressure used in the real test)	3 mm radius pipe simulation test values
Length of the cloud *m*	$48.538 * 10^{-2}$	$4.76 * 10^{-2}$	$2.66 * 10^{-2}$
Width of the cloud *m*	$47.811 * 10^{-2}$	$4.75 * 10^{-2}$	$2.12 * 10^{-2}$
Height of the cloud *m*	$1.03157 * 10^{-1}$	$1.01 * 10^{-1}$	$1.02 * 10^{-1}$
α (alfa)	$9.85022045 * 10^{-1}$	$9.99 * 10^{-1}$	$7.97 * 10^{-1}$
Pressure *Pa*	$5 * 10^{6}$	$1.00 * 10^{7}$	$5 * 10^{6}$
Viscosity *Pa.Sec*	$1.00 * 10^{-3}$	$1.00 * 10^{-3}$	$1.00 * 10^{-3}$
Injection flow rate $m^3/sec.$	$1.5 * 10^{-5}$	$3.00 * 10^{-5}$	$2.12 * 10^{-5}$
Permeability in m^2	$7.16157 * 10^{-15}$	$7.42 * 10^{-15}$	$4.14 * 10^{-15}$
Permeability in Darcy	$7.256465 * 10^{-3}$	$7.51 * 10^{-3}$	$4.19 * 10^{-3}$

5.9 The types of events in all models

Since the DEM/PFC in its initial state predicts only tensile and shear events, so it has to be developed to predict the pore collapse source of emission. As explained previously, after using Mat lab, it became possible to change some events to the pore collapse source, depending on the K value. As explained in 5.5.1, by using Mat lab, it became possible to predict the tensile, shear, and pore collapse sources of events and to count the number of events that were initially recorded as tensile or shear. In addition, the events that were changed from

tensile sources or shear to pore collapse sources and those that were not changed. All of these are listed in Table 5-3.

It is clear that twice as many events were changed from shear events sources to pore collapse sources than were recoded as tensile. This result leads to the conclusion that a link exists between shear events and pore collapse sources (Nouri et al., 2002b).

Table 5-3 The number and types of all events with their ratios

The measured unit	real test	10 MPa injection pressure	bigger radius (3*mm*)
Total number of events	*7014*	*4560*	*1541*
Number of events that were not changed	*5164*	*3297*	*1186*
Changed tensile events	*468*	*361*	*85*
Changed shear events	*1382*	*902*	*270*
Percentage of events that were not changed	*73.6242*	*72.302*	*76.96*
Percentage Changed tensile events	*6.6724*	*7.1346*	*5.5*
Percentage Changed shear events	*19.7035*	*19.4581*	*17*
Percentage original tensile events	*27.4309*	*31.4693*	*21*
Percentage original shear events	*72.5691*	*68.5307*	*78.9*
Percentage of tensile events	*20.7585*	*23.5526*	*15.5743*
Percentage of shear events	*52.8657*	*48.7500*	*61.388*
Percentage of pore collapse source	*26.3758*	*27.6974*	*23.037*

In the real lab test, the number of events was estimated to be about 11052. There were double the number of shear events sources than tensile events in the real lab. On the other hand, there was a bigger ratio for tensile events, probably because of the big particle size (Ishida, 2001). It is also shown in Figure 5-7 that

the radius of the shear events is greater and that they are likely to be dominant in the inner region, while the aperture is between 0.000005- 0.00005 m and the permeability is equal to $0.7 * 10^{-16} m^2$.

Now, if the injection test using higher pressure is studied (see Figure 5-9), there are fewer events (about 4560 events), and the number of shear events is increased in the inner circles. Furthermore, it is noticed that there is an increased number of shear events in the near wellbore in the case of higher injection pressure. Jung et al. (2014) explain that this is because, when the injection rate is higher, the fluid cannot penetrate the pores so the fractures actually happen before the fluid reaches them. The fractures will propagate, forming brunches. When the sample reaches break down pressure, the tensile cracks generated around the borehole rapidly, as the existing cracks grow. The shear cracks occur as the existing cracks connect to each other, which connection between fractures produces tensile fractures. Regarding permeability, it was about $7.42 * 10^{-15} m^2$ and the aperture was between 0.00006 *m* to 0.00001 *m* but the increase in the tensile source of emissions was greater. This may be because tensile events need more energy to be formed (Shimizu, 2010) than was available when using higher pressure. This may be because of the infiltration of fluid into the pores near the borehole, that causes additional pore pressure near the borehole. This pore pressure minimizes the effect of stress on the sample (Shimizu et al., 2011).

Furthermore, in the case of a bigger radius of injection, the number of events is 1541. The predicted apertures were between (0.000006*m*-0.000016*m*), see Figure 5-11. Regarding the ratio of the different types of events in the case of a bigger radius of injection Figure 5-12, the tensile events and shear events

increase in width and the cloud is not as dense as the other clouds because of the fewer number of events, while the permeability is about $4.14 * 10^{-15}\ m^2$.

The main conclusion is that the increase in permeability is combined with an increase in the number of tensile events, and a similar phenomenon has been noticed by (Raziperchikolaee et al., 2014). In addition, it is noticed that the tensile events lie mainly at the border of the cloud, in the case of higher pressure and real test conditions. Moreover, the increase in the density of the acoustic emissions and the number of events are accompanied with higher permeability because of the higher number of fractures, which means more pathways for the fluids.

5.10 Criticizing the test and the modelling results

The first critical point is the big ball size that was used in this study. Had smaller sized particles been used, it would have been time consuming. The first effect of using a bigger particle radius is that the number of acoustic emission events becomes smaller than in the real test because of the reduced contact between the particles, and this certainly effects the type of acoustic emissions too, as the shear fracturing would increase with larger grains whereas the tensile fracturing increases in the case of smaller grains (Ishida, 2001). Regarding any conclusions drawn previously, these are based on the fact that all models use the same range of particle sizes. Which will make any conclusion about the increase or decrease event type valid. The other point is that it is possible that the results may be better if breakable clump particles were used instead of non-breakable ones.

5.11 Properties of the synthetic seismic cloud

The seismic clouds, in all cases, are similar to some degree to the real test cloud, and it seems that the shape of the seismic cloud is most likely to be changed by the amount of injected fluids into the rock material because it enables the seismic cloud to cover more space. In addition, the general shape of the seismic cloud is mainly affected by the length of the injection pipe too, as is obvious from Chapter Four. In long injection pipes, the cloud covers the entire injected sample from the inside like a cylinder shape, but in the case of focused injection in the centre, the cloud looks like a star with a central point in the centre of the injection.

Although, it was not possible to simulate the effect of anisotropy, it is still clear (Stanchits et al., 2011) that anisotropy of the fractured rock sample could affect the shape of the seismic cloud.

It is noticed that there are more tensile events at the border of the seismic cloud accompanied by higher induced permeability. Moreover, this research again proves, regarding the accuracy of using microseismic cloud shape, that the inversion method can predict the permeability of the induced sample.

5.12 Summary

It is concluded that injection with higher pressure could be effective in our model, because it produces higher values of permeability in the fractured rock sample. These fractures are bigger in terms of aperture, which means that it is possible to use bigger proppants and hence obtain better results from hydraulic fracturing operations. This conclusion is valid for this model. In order to be applied to other models, many more models must be created, so this conclusion could be applied

in the real field process, when the results of the fracturing operations are ineffective and it is desired to gain better permeability results.

Additionally, since one phenomenon that could be measured during the fracturing process is evidence from microseismic events, through monitoring during hydraulic fracturing, it is possible to say that, in the case of this rock sample, the creation of tensile events, when changing the injection conditions for example pressure or fluid type, could mean the increase in the permeability, resulted from hydraulic fracturing. Creating more tensile events and their presence in the seismic cloud, especially in the borders of seismic clouds, is a good indication of the increasing efficiency of hydraulic fracturing. In addition, the increase in the density of the acoustic emission and number of events could mean higher induced permeability.

Moreover, the presence of the shear sources type of events near the wellbore proved that the empirical method used to distinguish the pore collapse sources of emissions could give acceptable results, but still needs further development.

Chapter 6 Conclusions and recommendations

6.1 The validity of the model

Based on the results of the simulation tests on Springwell sandstone, Granite and Flechtingen sandstone, the DEM/ PFC model captures the main features of the fracturing process of the rock sample under stress, and can mimic the elastic deformation of the injected sample. Additionally, it is possible to model the mechanical characteristic of the rock samples, like failure, elasticity, cracking peak stress, and many other observations that could be reported in any of the traditional laboratory tests that have been mentioned throughout the thesis.

In addition, the DEM/ PFC model produced a comparable seismic moment range. This is obvious through comparing the b_value curves, with an acceptable T.K. plot, that could be used to study the source mechanisms of the fractures. Additionally, the DEM/ PFC proved to be capable of creating a similar pattern of pressure scheme for the injected fluid into the synthetic sample. Furthermore, it captures the main features of the hydraulic fracturing process, the resulting microseismicity induced by hydraulic fracturing operations. These main features are: number of induced microseismic events, the fracture type and the source type of the emissions, as well as the mechanics of the hydraulic fracturing process, in addition to the characteristics of the microseismic cloud itself, like the shape, the ratio of each source type inside the cloud, and the aperture, length and surface area of the fracture caused by the hydraulic fracturing process.

Moreover, the program can be used through modelling to identify the effect of different parameters on the seismic emissions properties, and on the parameters

that affect the acoustic emission cloud. Moreover, the program can be used to identify the efficiency of the fracturing operation, through measuring the induced permeability and aperture of the fractures, and it could be used to plan the fracturing process when using different pressure schemes.

It must be mentioned here, however, that using this code to solve field cases may need better and much faster equipment then that used in the research.

6.2 Conclusions about the properties of acoustic emissions and fractures.

It is concluded from the literature review and the modelling results that the microseismic emissions could be used to study the hydraulic fracturing operations, the induced fracture positions within the rock sample and in field, and to determine fracturing efficiency in an acceptable manner. The acoustic emissions and microseismic events could give the properties of the fractures that were induced by the hydraulic fracturing. These include the fracture length, fracture aperture, and fracture surface area.

The seismic cloud or the acoustic emission cloud can give certain limits of accuracy, the resulted permeability. This means that using the general shape of the seismic cloud to determine the efficiency of the fracturing process could be valid, and the results may be acceptable. The measured permeability from the fracturing process and the shape of the seismic cloud are affected by the shape of the injection pipe and the pressure of the injected fluids, so it possible to change these parameters to gain the desired results.

The use of certain types of acoustic emission sources to determine the efficiency of the fracturing process needs more study. Anyway, in the rock type that was simulated in this study, it is possible to say that the presence of more tensile events in one stage, more than the other, could mean better results, more permeability and bigger apertures of the fractures. Additionally, the existence of tensile events in the front or boarder of the seismic cloud, and its absence in another seismic cloud, may reflect the efficiency of the fracturing process, so it is possible to use the ratio or the existence of the tensile emission sources to monitor the fracturing process and to decide what scheme gives better results.

Moreover, it is proven again in this research that the accuracy of using a microseismic cloud shapes the inversion method to predict the permeability of the induced sample. Additionally, the increase in the density of the acoustic emission means higher permeability, because it means more pathways for the fluids to move through it.

6.3 The original contributions

The scientific contribution in this research can be divided into two types of development. The first one is related to the development of the DEM/ PFC code itself, while the second is related to the development in the field of microseismic events application.

6.3.1 The developments in the DEM

Regarding the development of the code, the code was developed to use a changed combination factor during modelling. In the developed code, it is

possible to mimic the resolution power of the sensors that record the seismic emissions; in other words, calibrating the resolution power of recording in the monitoring process because some times more than one event is recoded as one big cluster. Now it is possible to create the cluster of events in the code, to mimic the combination of microseismic events in the real cases, because the DEM models need to be calibrated fundamentally to match the recorded events in the real test. This widens the application of the code in the field of modelling seismic activities and makes the results more acceptable. Furthermore, to the author's knowledge, this is the first time that it was possible to create a model to simulate the work of the Tiltmetere, by using the technique of choosing two balls to represent the work of bubbles in the Tiltmetere, to model the deformation of the sample surface.

Additionally, it is possible to predict the pore collapse source type of microseismic emissions, from the information gained from the DEM model results using the Mat-lab program.

6.3.2 The developments in the field of microseismic applications

The development in the field of microseismic applications is the second type of development which includes the use of microseismic event magnitudes or moments to predict the aperture of the resulting fractures. To the author's knowledge, this is the first time that the aperture of the fracture has been determined directly from the magnitude of the seismic event in an acceptable way, which could have many applications in the oil industry. Furthermore, a simple analogue relation between the existence of the tensile events in the boarder of the seismic cloud, and the ratio of the tensile events source from one

side and the permeability was established. That could be widened in future to determine the effectiveness of hydraulic fracturing through microseismic events recording.

6.4 Recommendations for future work

The recommendations for the future works and developments can be classified into two groups. The first class is related to the code itself while the second class of developments is related to the field of microseismic applications.

Firstly, it is recommended to develop the domain and pipe fish to construct more than four balls, may be five or six balls, or even to include a set of parallel balls, to be able to model the fluid flow in the faults and fracture. Additionally, it is highly recommended to develop the program to be able to construct the domains, and the pipes in a more natural way; for example, using the information about pore volume and throat radius from the x-ray scan of particles in the rock sample to construct the domains and pipes in a more natural way to mimic the natural situation. Because, it is possible by using x-ray scan, to gain number of pipes, number of pores that could be equivalent to domains, pipe length and pores radius too. Then using these data to construct a model in a way that the number of domain and pipes with their radiuses and length close to the real sample. Furthermore, the equation that controls the fluid flow in the domains and pipes needs to be developed too, in order to give better results.

It is better to develop the seismic code to model the acoustic emissions caused by fracture surface movements, sliding and even friction between balls. In

addition to that, it is better to develop the code to mimic the acoustic activities caused by the effect of chemical changes that causes acoustic emissions.

It is possible to use alternative methods, in the case of simulating the fluid flow in the DEM environment. An example of this is developing the fluid flow model to be more realistic, perhaps by using small particles with special bonds between them to represent the fluids that flow between the domains and pipes. Moreover, it is believed that creating rock models, with clumps of particles, or breakable particles that have the same properties of the particles and sub particles in the real rock sample. That means creating synthetic grains with properties similar to the grain properties in the real rock. For example creating grains to represent Quartz and grains to represent Feldspar then forming the entire sample. These have to be packed in a similar size and size distribution to the real rock sample, in order to mimic the behaviour of a real rock sample, subjected to stress or fluid injection. The use of crack able clumps of particles may give better results because, in these cases, the particles will have the ability to divide into smaller particles, as in the real cases.

It is highly recommended to develop the program to distinguish between pore collapse sources of emissions, using the change in domain size during hydraulic fracturing. This could be done by creating a data block for each domain, then using the number of breakable bonds in the domains as the potential sources of the acoustic emissions. Additionally, if the pore-elastic parameters for the simulated rock sample were studied and available, the DEM/ PFC code could then be capable of predicting pore-elastic constants, such as the drained and undrained bulk compressibility.

Regarding the developments suggested regarding the field of seismic application, it is believed that in order to predict the average aperture of the induced fractures from microseismic data, to give much more accurate results, that could be comparable with the real induced fractures and give better accuracy, in an acceptable was. Instead of using average values of alpha to represent the alpha value in the equation, to calculate the aperture from magnitudes see chapters two, three and four. Additionally, it is better to use or to develop better equations that control the relation between the magnitude of the events and the length or surface area of the fractures, which may give much more accurate results.

It is recommended to study the combination of microseismic events in clusters, and the effect of combination factors, the sensor resolution and rapture velocity on the clustering process, and what are the best values that could be used by the program, to gain more understanding of the process of clustering the events and the factors that control it.

References

Abercrombie, R. E., 1995, Earthquake source scaling relationships from −1 to 5MLusing seismograms recorded at 2.5-km depth: Journal of geophysical research, v. 100, no. B12, p. 24015.

Adejuyigbe, O. J., 2013, Correlation between the volumes of slurry and the volumes of fracturing in the Barnet Shale [Master: University of Houston, 96 p.

Aker, E., Kühn, D., Vavryčuk, V., Soldal, M., and Oye, V., 2014, Experimental investigation of acoustic emissions and their moment tensors in rock during failure: International journal of rock mechanics and mining sciences, v. 70, p. 286-295.

Aki, K., 1967, Scaling law of seismic spectrum,: Journal of geophysical research solid earth, v. 72, no. 4.

AL-busaidi, A., 2004, Distinct element modelling of hydraulically-induced fracture and associated seismicity [PhD. : The university of liverpool.

Al-Fattah, S. M., and Startzman, R. A., 2000, Forecasting world natural gas supply.

Al-Harrasi, O. H., Kendall, J. M., and Chapman, M., 2011, Fracture characterization using frequency-dependent shear wave anisotropy analysis of microseismic data: Geophysical journal international, v. 185, no. 2, p. 1059-1070.

Al-Busaidi, A., Hazzard, J., and Young, R., 2005, Distinct element modeling of hydraulically fractured Lac du Bonnet granite: Journal of geophysical research: solid earth (1978–2012), v. 110, no. B6.

Alassi, H. T., 2008, Modeling reservoir geomechanics using discrete element method: Application to reservoir monitoring [PHD: PHD thesis, Norwegian university of science and technology (NTNU), 144 p.

Ali, A., 2011, Correlations between the effective permeability and seismic anisotropy of fractured reservoirs: University of Bergen,Norway.

Arop, J. B., 2013, Geomechanical review of hydraulic fracturing technology [Master: Massachusetts institute of technology

Aslam, T., 2011, Review on hydraulic fracturing technique [master: Dalhousie university, Halifax, Nova Scotia.

Bachmann, C. E., Wiemer, S., Goertz-Allmann, B. P., and Woessner, J., 2012, Influence of pore-pressure on the event-size distribution of induced earthquakes: Geophysical research letters, v. 39, no. 9, p. n/a-n/a.

Barker, W., 2009, Increased Production Through Microseismic Monitoring of Hydraulic Fracturing Over a Multiwell Program, SPE Annual Technical Conference and Exhibition: New Orleans, Louisiana, USA, Society of Petroleum Engineers.

Bazan, L. W., Lattibeaudiere, M. G., and Palisch, T., 2012, Hydraulic fracture design and well production results in the Eagle ford shale: one operator's perspective, Americas unconventional resources conference . Pittsburgh, Pennsylvania, USA, 5–7 June 2012, Society of Petroleum engineers.

Biglarbigi, K., Dammer, A., Cusimano, J., and Mohan, H., 2007, Potential for oil shale development in the United states, SPE annual technical conference and exhibition Anaheim, California, U.S.A., 11–14 November Society of petroleum engineers.

Bizzarri, A., 2012, Rupture speed and slip velocity: What can we learn from simulated earthquakes?: Earth and planetary science letters, v. 317-318, p. 196-203.

Busetti, S., Jiao, W., and Reches, Z. e., 2014, Geomechanics of hydrolic fracturing microseismicity: Part 2. Stress state determination: AAPG Bulletin, v. 98, no. 11, p. 2459-2476.

Cai, M., Kaiser, P. K., Morioka, H., Minami, M., Maejima, T., Tasaka, Y., and Kurose, H., 2007, FLAC/PFC coupled numerical simulation of AE in large-scale underground excavations: International journal of rock mechanics and mining sciences, v. 44, no. 4, p. 550-564.

Caia, M., Kaisera, P. K., and Martinb, C. D., 2001, Quantification of rock mass damage in underground excavationsfrom microseismic event monitoring: International journal of rock mechanics & sining sciences v. 38 p. 1135–1145.

Castillo, D., Hunterl, S., Wright, C. A., Conant, R., and Davis, E., 1997, Deep hydraulic fracturing imaging; recent advances in tiltmerter technilogy D. ; S.; P. Harben l; C. ; R. ; E. 2: Int. ,I. Rock Mech. Min. Sci. & Geomech. Abstr., v. 34, no. 3-4.

Chang, S. H., and Lee, C. I., 2004, Estimation of cracking and damage mechanisms in rock under triaxial compression by moment tensor analysis of acoustic emission: International journal of rock mechanics and mining sciences, v. 41, no. 7, p. 1069-1086.

Cheng, Y., 2010, Impacts of the number of perforation clusters and cluster spacing on production performance of horizontal hale-gas wells, SPE

Eastern regional meeting, morgantown,: West Virginia, USA, Society of petroleum engineers.

Cho, N., Martin , C. D., Sego, D. C., and Christiansson, R., 2004, Modelling Dilation in Brittle Rocks, the 6th North America Rock Mechanics Symposium (NARMS): Rock Mechanics Across Borders and Disciplines: Houston, Texas,.

Cipolla, C. L., Mack, M. G., Maxwell, S. C., and Downie, R. C., 2011, A practical guide to nterpreting microseismic measurements, SPE North american unconventional gas conference and exhibition . Woodlands, Texas, USA, 14–16 June 2011, Society of petroleum engineers.

Cipolla, C. L., Maxwell, S. C., and Mack, M. G., 2012, Engineering guide to the application of microseismic interpretations, SPE hydraulic fracturing technology conference: The Woodlands, Texas, USA, 6–8 February Society of petroleum engineers.

Cipolla, C. L., and Wright, C. A., 2000a, Diagnostic techniques to understand hydraulic fracturing: what? why? and how?, Society of petroleum engineers.

-, 2000b, State-of-the-art in hydraulic fracture diagnostics, SPE Asia pacific oil and gas conference and exhibition: Brisbane, Australia, Society of petroleum engineers.

Colombo, I. S., Main, I. G., and Forde, M. C. F., 2003, Assessing damage of reinforced concrete beam using ‘‘b-value’’ analysis of acoustic emission: Journal of material in civil engineering.

Coulson, A. L., 2009, Invistigation opf the pst peak strength state and behaviour of confined rock mass using indiced microseismicity [PhD: University of Toronto.

Crampin, S., and Gao, Y., 2015, The physics underlying Gutenberg-Richter in the earth and in the moon: Journal of Earth Science, v. 26, no. 1, p. 134-139.

Cundall, P. A., and Starck, O. D. L., 1979, A Discrete numerical mode for granular assemblies: Geotechnique, v. 29, no. 1, p. 47-65.

Diederichs, M. S., 2000, Instability of hard rockmasses: The role of tensile damage and relaxation. Ph.D. [Master: University of Waterloo.

Duhault, J. L. J., 2012, Cardium formation hydraulic “frac” microseismic: observations and conclusions, SEG Las vegas 2012 annual meeting: las Vegas 2012, p. 1-5.

Economides, M. J., and Nolte, K. G., 2000, Reservoir stimulation.

Eshiet, K. I.-I., 2012, Modelling of hydraulic fracturing and its engineering applications [Doctor of Philosophy: University of Leeds.

Evans, K., and Columbia, U., 1983, On the development of shallow hydraulic fractures as viewed through the surface deformation field: Part I-Principles: Jounrnal of petroleum technology, p. 406-410.

Falls, S. D., Young, R. P., Carlson, S. R., and Chow, T., 1992, Ultrasonic tomography and acoustic emission in hydraulically fractured Lac du Bonnet Grey granite: Journal of Geophysical Research, v. 97, no. B5, p. 6867.

Fatahi, H., and Hossain, M. M., 2015, Fluid flow through porous media using distinct element based numerical method: Journal of petroleum exploration and production technology.

Fischer, T., and Guest, A., 2011, Shear and tensile earthquakes caused by fluid injection: Geophysical Research Letters, v. 38, no. 5, p. n/a-n/a.

Frash, L. P., Hood, J., and Gutierrez, M., 2014, Laboratory measurement of critical state hydraulic fracture geometry, 48th US rock mechanics / geomechanics symposium held in , MN, USA, 1-4 June: Minneapolis.

Geller, R. J., 1976, Scalling relations for earthquacke source parameteres and magnitude Bulletin of the seismological society of America. , v. 66, no. 5, p. 1501 1523.

Gil, I., 2005, Hydraulic fracturing of poorly cosildated formation cosideration on rock proerties failer mechanisms [Doctorate of phalsophy Ph.D. thesis]: The Uinversity of Oklahoma.

Goertz-Allmann, B. P., Goertz, A., and Wiemer, S., 2011, Stress drop variations of induced earthquakes at the Basel geothermal site: Geophysical research letters, v. 38, no. 9, p. n/a-n/a.

Gong, B., Qin, G., Towler, B. F., and Wang, H., 2011, Discrete modeling of natural and hydraulic fractures in shale-gas reservoirs, SPE annual technical conference and exhibition Denver, Colorado, USA, 30 October–2, Society of petroleum engineers.

Grechka, V., Mazumdar, P., and Shapiro, S. A., 2010, Case History Predicting permeability and gas production of hydraulically fractured tight sands from microseismic data: Geophysics, v. 1

Grosse, C. U., Reinhardt, H. W., and Finck, F., 2003, Signal-based acoustic emission techniques in civil engineering: Journal of material in civil engineering, v. 15, no. 3, p. 274-279.

Gutenberg, B., and Richter, C. F., 1956, Earthquacke magnitude , intensity, energy, and accelration(Second Paper): Bull. Seism. Soc.

Hanks, T. C., and Kanamori, H., 1979, A moment magnitude scale: Journal of geophysical research, v. 84, no. B5, p. 2348.

Harris , R. A., and Day, S. M., 1997, Effects of a low-velocity Zone on a dynamic rupture: Bulletin of the Seismological Society of America, v. 87, no. 5, p. 1267-1280.

Hart, R., 2003, Enhancing rock stress understanding through numerical analysis: International journal of rock mechanics and mining sciences, v. 40, no. 7-8, p. 1089-1097.

Hautmann, S., Gottsmann, J., Sparks, R. S. J., Costa, A., Melnik, O., and Voight, B., 2009, Modelling ground deformation caused by oscillating overpressure in a dyke conduit at Soufrière Hills Volcano, Montserrat: Tectonophysics, v. 471, no. 1-2, p. 87-95.

Hazzard, J. F., 1998, Numerical modelling of acoustic emissions and dynamic rock behaviour [Ph.D. : Keel university, 384 p.

Hazzard, J. F., Maxwell, S. C., and Young, R. P., 1998, Micromechanical Modelling of Acoustic Emissions, SPE/ISRM Eurock 98 confrence Norway, Society of Petroleum Engineers.

Hazzard , J. F., and Young , R. P., 2001, Seismic validation of micromechanical models: Rock mechanics in n the national interest.

Hazzard , J. F., and Young , R. P., 2002, Moment tensors and micromechanical models: Tectonophysics v. 356, p. 181–197.

Hazzard, J. F., and Young, R. P., 2004, Dynamic modelling of induced seismicity: International journal of rock mechanics and mining sciences, v. 41, no. 8, p. 1365-1376.

Hofmann, H., 2015, Development of enhanced geothermal systems (EGS) in Northern Alberta [Doctor of Philosophy: University of Alberta.

Holditch, S. A., and Madani, H., 2010, Global Unconventional Gas - It Is There, But Is It Profitable?, Managament, Society of Petroleum Engineers.

Hudson, J. A., PEARCE, R. G., and ROGERS, R. M., 1989, Source Type Plot for Inversion of the Moment Tensorinterpreted: Journal of geophysical research, v. 94, no. B1, p. 765-774.

Hummel, N., and Muller, T. M., 2009, Microseismic signatures of non-linear pore-fluid pressure diffusion: Geophysical journal international, v. 179, no. 3, p. 1558-1565.

Hunt, S. P., Meyers, A. G., and Louchnikov, V., 2003, Modelling the Kaiser effect and deformation rate analysis in sandstone using the discrete element method: Computers and geotechnics, v. 30, no. 7, p. 611-621.

Ishida, T., 2001, Acoustic emission monitoring of hydraulic fracturing in laboratory and field: construction and building materials v. 15, p. 283□295.

Itasca Consulting Group, 2005, Particle Flow Code PFC 3D user's manuals , version 4: Minneapolis, Minnesota.

Ivars, D. M., 2010, Bonded particle model for jointed rock mass: Royal Institute of Technology (KTH) in Sweden.

Jing, L., 2003, A review of techniques, advances and outstanding issues in numerical modelling for rock mechanics and rock engineering: International Journal of Rock Mechanics and Mining Sciences, v. 40, no. 3, p. 283-353.

Jung, J., Heo, C., and Jeon, S., 2014, Study on hydraulic fracturing evolution under various fluid viscosity and injection rate, 8th Asian sock sechanics symposium: Japan.

Kim, J., and Moridis, G. J., 2015, Numerical analysis of fracture propagation during hydraulic fracturing operations in shale gas systems: International Journal of Rock Mechanics and Mining Sciences, v. 76, p. 127-137.

Klimczak, C., Schultz, R. A., Parashar, R., and Reeves, D. M., 2010, Cubic law with aperture-length correlation: implications for network scale fluid flow: Hydrogeology Journal, v. 18, no. 4, p. 851-862.

Kwiatek, G., T. H. W. Goebel, and Georg Dresen, 2014, Seismic moment tensor and b value variations over successive seismic cycles in laboratory stick-slip experiments: Geophysical research letters, v. 41.

Le Guen, Y., Renard, F., Hellmann, R., Brosse, E., Collombet, M., Tisserand, D., and Gratier, J. P., 2007, Enhanced deformation of limestone and sandstone in the presence of high Pco2fluids: Journal of geophysical research, v. 112, no. B5.

Lee, W. H. K., International Association of Seismology and Physics of the Earth's Interior. Committee on Education., and International Association for

Earthquake Engineering., 2002, International Handbook of Earthquake & Engineering Seismology, Amsterdam ; London, Published by Academic Press for International Association of Seismology and Physics of the Earth's Interior, International geophysics series, xx, 933 p., 924 p. of plates p.:

Lei, X., Kusunose, K., Rao, M. V. M. S., Nishizawa, O., and Satoh, T., 2000, Quasi-static fault growth and cracking in homogeneous brittle rock under triaxial compression using acoustic emission monitoring: Journal of geophysical research, v. 105, no. B3, p. 6127.

Lei, X., Kusunose, K., Satoh, T., and Nishizawa, O., 2003, The hierarchical rupture process of a fault: an experimental study: Physics of the earth and planetary interiors, v. 137, no. 1-4, p. 213-228.

Lei, X., and Ma, S., 2014, Laboratory acoustic emission study for earthquake generation process: Earthquake science, v. 27, no. 6, p. 627-646.

Li, Q., Xing, H., Liu, J., and Liu, X., 2015, A review on hydraulic fracturing of unconventional reservoir: Petroleum, v. 1, no. 1, p. 8-15.

Likrama, F., 2008, Study of mechanical and flow properties of weakly cemented and uncemented sands using Discete Element method [Mater pdf]: The University of Texsas at Austen.

Lin, W., 2002, Permanent strain of thermal expansion and thermally induced microcracking in Inada granite: Journal of geophysical research, v. 107, no. B10.

Madariaga, R., 1976, Dynamics of an expanding circuler fault Bulletin of the seismological society of America, v. 66, no. 3, p. 639-665.

Majer, E. L., and Doe, T. W., 1986, Studying Hydrofractures by High Frequency Seismic Monitoring: International Journal of Rock Mechanics and Mining Sciences & Geomechanics Abstracts, v. 23, no. 3, p. 185-119.

Marina, S., Imo-Imo, E. K., Derek, I., Mohamed, P., and Yong, S., 2014, Modelling of hydraulic fracturing process by coupled discrete element and fluid dynamic methods: Environmental earth sciences, v. 72, no. 9, p. 3383-3399.

Matsunaga, I., Kobayashit, H., Sasaki, S., and Ishida, T. I., 1993, Studying hydraulic fracturing mechanism by laboratory experiments with Acoustic emission monitoring: Int. ,I. Rock Mech. Min. Sci. & Geomech. Abstr., v. 30, no. 7, p. 912, 1993.

Maxwell, S. C., 2012, Comparative microseismic interpretation of hydraulic fractures, SPE Canadian unconventional resources conference: Calgary, Alberta, Canada, 30 October–1 November Society of petroleum engineers.

Maxwell, S. C., Shemeta, J., Campbell, E., and Quirk, D., 2008, Microseismic deformation rate monitoring, e 2008 SPE annual technical conference and exhibition: Denver, Colorado, USA, 21–24 September 2008.

McLaskey, G. C., Kilgore, B. D., Lockner, D. A., and Beeler, N. M., 2014, Laboratory Generated M -6 Earthquakes: Pure and Applied Geophysics, v. 171, no. 10, p. 2601-2615.

Moreno, C., 2011, Microseismic mapping of fluid induced hydraulic fractures and analysis of location uncertanties [Master: University of Oklahoma

Morrill, J., and Miskimins, J. L., 2012, Optimization of Hydraulic Fracture Spacing in Unconventional Shales, SPE Hydraulic Fracturing Technology Conference The Woodlands, Texas, USA, 6–8 February Society of Petroleum Engineers.

Nouri, A., Al-Darbi, M. M., Vaziri, H., and Islam, M. R., 2002a, Deflection Criteria for Numerical Assessment of the Sand Production Potential in an Openhole Completion: Energy Sources, v. 24, no. 7, p. 685-702.

Nouri, A., Vaziri, H., Al-Darbi, M. M., and Islam, M. R., 2002b, A New Theory and Methodology for Modeling Sand During Oil Production: Energy Sources, v. 24, no. 11, p. 995-1007.

Nuannin, P., 2006, The potential of b-value variations as earthquake precursors for small and large events [Doctor of philosophy Uppsala university

Olson, J. E., 2003, Sublinear scaling of fracture aperture versus length: An exception or the rule?: Journal of geophysical research, v. 108, no. B9.

Palmer, I. D., Moschovidis, Z., and Schaefer, A. A., 2012, Microseismic clouds: modeling and implications, Americas unconventional resources conference: Pittsburgh, Pennsylvania, USA,, Society of Petroleum Engineers.

Pearson, C., 1981, The relationship between microseismicity and high pore pressures during hydraulic stimulation experiments in low permeability granitic rocks: Journal of geophysical research, v. 86, no. B9, p. 7855.

Pettitt, W. S., 1998, Acoustic emission source studies of microcrackingin rock [Ph.D.: Keel university

Phillips, W. S., Rutledge, J. T., House, L. S., and Fehler, M. C., 2002, Induced micro earthquake patterns in hydrocarbon and Geothermal reservoirs; sex case studies Pure and applied geophysics, v. 159, p. 345-369.

Potyondy, D., Cundall, P., and Lee, C. A., 1996, Modelling rock using bonded assemblieosf of circular particle: Rock mechamcs.

Potyondy, D. O., 2012, The bonded-particle model as a tool for rock mechanics research and application: current trends and future directions, Asian rock mechanic syposuem, Volume soal: South koria, International society for rock mechanics.

Potyondy, D. O., and Cundall, P. A., 2004, A bonded-particle model for rock: International journal of rock mechanics and mining sciences, v. 41, no. 8, p. 1329-1364.

Qin, S., Cheng, J., and Zhu, S., 2012, The application and prospect of microseismic technique in Coalmine: Procedia environmental sciences, v. 12, p. 218-224.

Raziperchikolaee, S., Alvarado, V., and Yin, S., 2014, Microscale modeling of fluid flow-geomechanics-seismicity: Relationship between permeability and seismic source response in deformed rock joints: Journal of geophysical research: solid earth, v. 119, no. 9, p. 6958-6975.

Richter, C. F., 1935, An instrumental earthquake magnitude scale: Bulletin of the Seismological Society of America v. 25, no. 1-2, p. 1–32.

Rutqvist, J., Rinaldi, A. P., Cappa, F., and Moridis, G. J., 2013, Modeling of fault reactivation and induced seismicity during hydraulic fracturing of shale-

gas reservoirs: Journal of petroleum science and engineering, v. 107, p. 31-44.

Sarmadivaleh, M., 2012 experimental and numerical study of interaction of a pre-existing natural interface and an induced hydraulic fracture [PhD. : Curtin university.

Sasaki, S., 1998, Characteristics of microseismic events during hydraulic fracturing experiments at the Hijiori hot dry rock geothermal energy site, Yamagata, Japan: Tectonophysics, v. 289.

Satoh, T., Nishizawa, O., and Kusunose, k., 1990, Fault development in Oshima granite under triaxial compression inferred from hypocenter distribution and focal mechanism of acoustic emission: Tohoku Geophys. Journ, v. 33, no. 3,4, p. 241-250.

Schmedes, J., Archuleta, R. J., and Lavallée, D., 2010, Correlation of earthquake source parameters inferred from dynamic rupture simulations: Journal of Geophysical Research, v. 115, no. B3.

Scholz, C. H., 1968, The frequency-magnitude relation of microfracturing in rock and its relation to earthquakes: Bulletin of the Seismological Society of America, v. 58, no. 1, p. 399-415.

Schubnel, A., Thompson, B. D., Fortin, J., Guéguen, Y., and Young, R. P., 2007, Fluid-induced rupture experiment on Fontainebleau sandstone: Premonitory activity, rupture propagation, and aftershocks: Geophysical research letters, v. 34, no. 19.

Shimizu, H., 2010, Distinct element modeling for fundamental rock fracturing and application to hydraulic fracturing [PhD.: Kyoto university, 178 p.

Shimizu, H., Murata, S., and Ishida, T., 2011, The distinct element analysis for hydraulic fracturing in hard rock considering fluid viscosity and particle size distribution: International journal of rock mechanics and mining sciences, v. 48, no. 5, p. 712-727.

Silas, M., Simiyu, S. C., and Malin., P., E., Avolcanoseismic approach to geothermal exploration and reservoir monitoring; Okaria, Kenya, and Casa *in* Proceedings USA. proceedings world geothermal congress 2000 Kyushu Tohoku, Japan, May 28 - June 10., 2000.

Silver, P. G., and Jordan, T. H., 1982, Optimal estimation of scalar seismic moment: Geophysical Journal of the Royal Astronomical Society, v. (1982) 70,755-787.

Simiyu, S. M., 2009, Application of micro-seismic methods to geothermal exploration: examples from the Kenya Rift: Short course IV on exploration for geothermal resources, Kenya.

Simiyu, S. M., and Malin , P. E., "Volcanoseismic " approach to geothermal exploration and reservoir mintoring ; Olkaria, Kenya casa diabloSilas M. Simiyu 1 and Peter E. Malin 2, *in* Proceedings world geothermal congress, Tokyo -japan, 2000.

Solberg , P., Lockner , D., and Byerlee , J. D., 1980, Hydraulic fracturing in granite under geothermal conditions: Int. J. Rock Mech. Min. Sci and Geomech, v. 17, no. 1, p. 25-23.

Stanchits, S., Mayr, S., Shapiro, S., and Dresen, G., 2011, Fracturing of porous rock induced by fluid injection: Tectonophysics, v. 503, no. 1-2, p. 129-145.

Talebi , S., and Cornet, F.-H., 1987 Analysis of microseismicity induced by a fluid injection in a granite rock mass: Geophysical rearch letters v. 14, no. 3, p. 227-230.

Tezuka, a., K. , and Niitsuma, b. H., 2000, Stress estimated using microseismic clusters and its relationship to the fracture system of the Hijiori hot dry rock reservoir: Engineering geology, v. 56 p. 47–62.

Tiab, D., and Donaldson, E. C., 2004, Petrophysics Theory and practice of measuring reservoir rock and fluid transport properties Elsevier, Golf professional publishing.

Tomac, I., 2014, Micro-mechanical aspetcs oh hydraulic fracture propagation and propppant flow and transprt for stimulation of enanced geothermal system [PhD. : Colorado school of mimens 210 p.

Verdon, J. P., 2010, Microseismic monitoring and geomechanical modelling of CO2 storage in subsurface reservoirs [Doctor of Philosophy: University of Bristol.

Volant , P., Grassol, J.-R., Chatelainl, J.-L., and Frogneux, m., 1992, b_value, aseismic deformation and brittle failure whithin an isolated geological object evedince from a dom structure loaded by fluid extractuions Geophysical rearch letteres, v. 19, no. 11.

Walter, J. I., Svetlizky, I., Fineberg, J., Brodsky, E. E., Tulaczyk, S., Grace Barcheck, C., and Carter, S. P., 2015, Rupture speed dependence on initial stress profiles: Insights from glacier and laboratory stick-slip: Earth and Planetary Science Letters, v. 411, p. 112-120.

Wang, H., Liao, X., and Ding, H., 2015, Monitoring and evaluating the volume fracturing effect of horizontal well: Journal of natural gas science and engineering, v. 22, p. 498-502.

Wang, T., Zhou, W., Chen, J., Xiao, X., Li, Y., and Zhao, X., 2014a, Simulation of hydraulic fracturing using particle flow method and application in a coal mine: International Journal of Coal Geology, v. 121, p. 1-13.

Wang, Z., Jin, J., Hang, Z., and Hu, X., 2014b, Influence of water injection fracturing on crack damage in soft coal and application in gas extraction: Journal of power and energy engineering, v. 02, no. 04, p. 1-6.

Wanne, T. S., and Young, R. P., 2007, Thermal modeling using particle clusters In PFC, 11th Congress of the International Society for Rock Mechanics London,, International society for rock mechanics.

Warpinski, N. R., Understanding Hydraulic Fracture Growth, Effectiveness, and Safety Through Microseismic Monitoring, *in* Proceedings Proceedings of the international conference for effective and sustainable hydraulic fracturing, Bunger, McLennan, and Jeffrey (editors).Brisbane, Australia, May, 2013/5/20/ 2013: ISRM, International society for rock mechanics.

Warpinski, N. R., 2014, A Review of hydraulic-fracture induced microseismicity, 48th rock mechanics/ geomechanics symposium: Minneapolis, MN, USA, American rock mechanics association.

Warpinski, N. R., Du, J., and Zimmer, U., 2012a, Measurements of hydraulic-fracture-Iinduced seismicity in gas shales, SPE hydraulic fracturing technology conference: The Woodlands, Texas, USA, 6–8 February 2012., Society of Petroleum Engineers.

-, 2012b, Measurements of hydraulic-fracture-induced seismicity in gas shales, SPE hydraulic fracturing technology conference The Woodlands, Texas, USA, 6–8 February, Society of petroleum engineers.

Warpinski, N. R., Waltman, C. K., Du, J., and Ma, Q., 2009, Anisotropy effects in microseismic monitoring, 2009 SPE Annual technical conference and exhibition: New Orleans, Louisiana, USA, 4–7 October SPE.

Warpinskil, N. R., Branagan , P. T., Engler , B. P. l., Wilmer, R., and Wolhart, S. L., 1997, Evaluation of downhole tiltmeter array for monitoring hydraulic fracturing International journal of rock mechanics and mon science v. 34, no. 3-4, p. 339.

Wells, D. L., and Coppersmith, K. J., 1994a, New empirical relationships among magnitude, rupture Length, rupture width, rupture area, and surface displacement: Bulletin of the seismological society of America., v. 84, no. 4, p. pp. 974-1002.

Wells, D. L. W., and Coppersmith, K. J., 1994b, New empirical relationships among magnitude, rupture length, rupture width, rupture area, and surface displacement: Bulletin of the seismological society of america, v. 84, no. 4, p. 974-1002.

Williams-Stroud, S., . Barker, B., and Smith, K., 2012, Distinguishing natural reactivated fractures from hydraulic induced fractures using microseismic event analysis: t CSPG/CSEG/CWLS GeoConvention 2012, (Vision) Calgary TELUS Convention Centre & ERCB Core Research Centre, Calgary, AB, Canada, 14-18 May 2012, AAPG/CSPG©2014.

Willis, R. B., Fontaine, J., Paugh, l., and Griffin, l., 2005, Geology and geometry: A review of factors affecting the effectiveness of hydraulic fractures, 5 SPE Eastern Regional Meeting Morgantown, SPE 97993.

Wilson, K. C., and Durlofsky, L. J., 2013, Optimization of shale gas field development using direct search techniques and reduced-physics models: Journal of Petroleum Science and Engineering, v. 108, p. 304-315.

Wong, T. F., 1982, 1982. Micromechanics of faulting in Westerly granite: , Int. J. Rock, Mech, Min, Sci & Geomech, v. 19.

Wuestefeld, A., Urbancic, T. I., Baig, A., and Prince, M., 2012, After a decade of microseismic wonitoring: Can we evaluate stimulation effectiveness and design better stimulations, SPE/EAGE european unconventional resources conference and exhibition Vienna, Austria, 20-22 March 2012., Society of Petroleum Engineers.

Zang, A., Wagner, F. C., Stanchits, S., Janssen, C., and Dresen, G., 2000, Fracture process zone in granite: Journal of geophysical research, v. 105, no. B10, p. 23651.

Zang, A., Yoon, J. S., Stephansson, O., and Heidbach, O., 2013, Fatigue hydraulic fracturing by cyclic reservoir treatment enhances permeability and reduces induced seismicity: Geophysical journal international, v. 195, no. 2, p. 1282-1287.

Zargari, S., Prasad, M., Mba, K. C., and Mattson, E., 2011, Organic maturity, hydrous pyrolysis, and Elastic property in shales, canadian

unconventional resources conference Calgary, Alberta, Canada, 15–17 November 2011., Society of petroleum engineers.

Zhang, J., and Bian, X., 2015, Numerical simulation of hydraulic fracturing coalbed methane reservoir with independent fracture grid: Fuel, v. 143, p. 543-546.

Zhao, X., 2010, Imaging the mechanics of hydraulic fracturing in naturally-fractured reservoirs using induced seismicity and numerical modeling [Doctor of philosophy: University of Toronto.

Zhao, X. P., Reyes-Montes, J. M., and Young, R. P., 2012, The role of pre-existing fracturing in enhanced reservoir treatments, 46th rock mechanics/ geomechanics symposium: Chicago, IL, USA, 24-27 June, American rock mechanics association.

Zhao, X. P., and Young, R. P., 2009, Numerical simulation of seismicity induced by hydraulic fracturing in naturally fractured reservoirs, 2009 SPE annual technical conference and exhibition New Orleans, Louisiana, USA, 4–7 Octobe, Society of Petroleum Engineers.

Zhou, X., and Burbey, T. J., 2014, Fluid effect on hydraulic fracture propagation behavior: a comparison between water and supercritical CO2-like fluid: Geofluids, v. 14, no. 2, p. 174-188.